Advances in Colloid and Interface Science 327 (2024) 103156

Contents lists available at ScienceDirect

Advances in Colloid and Interface Science

journal homepage: www.elsevier.com/locate/cis

Historical Perspective

Small-angle X-ray and neutron scattering applied to lipid-based nanoparticles: Recent advancements across different length scales

Lucrezia Caselli [a,**], Laura Conti [c], Ilaria De Santis [b], Debora Berti [b,c,*]

[a] Physical Chemistry 1, University of Lund, S-221 00 Lund, Sweden
[b] Department of Chemistry, University of Florence, Via della Lastruccia 3, Sesto Fiorentino, Florence 50019, Italy
[c] Consorzio Sistemi a Grande Interfase, Department of Chemistry, University of Florence, Sesto Fiorentino, Italy

ARTICLE INFO

Keywords:
Small-angle X-ray scattering
Small-angle neutron scattering
Lipid nanoparticles
Cubosomes
Lipid vesicles

ABSTRACT

Lipid-based nanoparticles (LNPs), ranging from nanovesicles to non-lamellar assemblies, have gained significant attention in recent years, as versatile carriers for delivering drugs, vaccines, and nutrients. Small-angle scattering methods, employing X-rays (SAXS) or neutrons (SANS), represent unique tools to unveil structure, dynamics, and interactions of such particles on different length scales, spanning from the nano to the molecular scale. This review explores the state-of-the-art on scattering methods applied to unveil the structure of lipid-based nanoparticles and their interactions with drugs and bioactive molecules, to inform their rational design and formulation for medical applications. We will focus on complementary information accessible with X-rays or neutrons, ranging from insights on the structure and colloidal processes at a nanoscale level (SAXS) to details on the lipid organization and molecular interactions of LNPs (SANS). In addition, we will review new opportunities offered by Time-resolved (TR)-SAXS and -SANS for the investigation of dynamic processes involving LNPs. These span from real-time monitoring of LNPs structural evolution in response to endogenous or external *stimuli* (TR-SANS), to the investigation of the kinetics of lipid diffusion and exchange upon interaction with biomolecules (TR-SANS). Finally, we will spotlight novel combinations of SAXS and SANS with complementary on-line techniques, recently enabled at Large Scale Facilities for X-rays and neutrons. This emerging technology enables synchronized multi-method investigation, offering exciting opportunities for the simultaneous characterization of the structure and chemical or mechanical properties of LNPs.

1. Introduction

Lipid-based NPs (LNPs) embrace a broad class of self-assembled nanomaterials with different levels of structural complexity (Fig. 1). These span from liposomes, where single or multiple lipid bilayer shells enclose an internal aqueous pool, to multicompartment nanostructured particles with exotic liquid-crystalline mesostructures, where the lipid bilayer assumes a non-lamellar arrangement [1–6]. Cubosomes represent a key example in the field [7–9], where a polymeric shell stabilizes an internal lipid cubic phase with 3-dimensional periodicity and coexistence of lipid and aqueous domains. The most common structures encountered in cubosomes include bicontinuous cubic phases with crystallographic space group symmetries Pn3m (Q [224]), Im3m (Q [229]), and Ia3d (Q [230]) or discrete micellar cubic phases with space groups Pm3n (Q [223]), Fm3m (Q [225]) and Fd3m (Q [227]) [10–13]. Other classes of non-lamellar LNPs include hexosomes [11,14], with internal direct (H_I) or inverse (H_{II}) hexagonal phase, or "spongeosomes" [15,16], featuring a bicontinuous fluid L_3 sponge phase core.

Additionally, nucleic acids-containing LNPs, recently employed to deliver antigen mRNA in COVID-19 vaccines, represent the state-of-the-art of non-viral gene delivery vectors [17,18]. These LNPs contain a mixture of nucleic acids, cationic ionizable lipids, helper lipids (such as phospholipids), cholesterol, and PEGylated lipids. Such systems typicallt exhibit a core–shell structure, featuring distinctive compositions of the core and of the inner and outer shell [17].

This structural versatility, coupled with the biocompatibility of the lipid matrix and ability to encapsulate hydrophilic and hydrophobic molecules, makes LNPs ideal candidates for application in different fields of Nanomedicine. In this respect, many excellent literature reviews summarize recent advancements in the design of lamellar and

* Corresponding author at: Department of Chemistry, University of Florence, Via della Lastruccia 3, Sesto Fiorentino, Florence 50019, Italy.
** Corresponding author.
E-mail addresses: lucrezia.caselli@fkem1.lu.se (L. Caselli), debora.berti@unifi.it (D. Berti).

https://doi.org/10.1016/j.cis.2024.103156
Received in revised form 28 February 2024;
Available online 12 April 2024

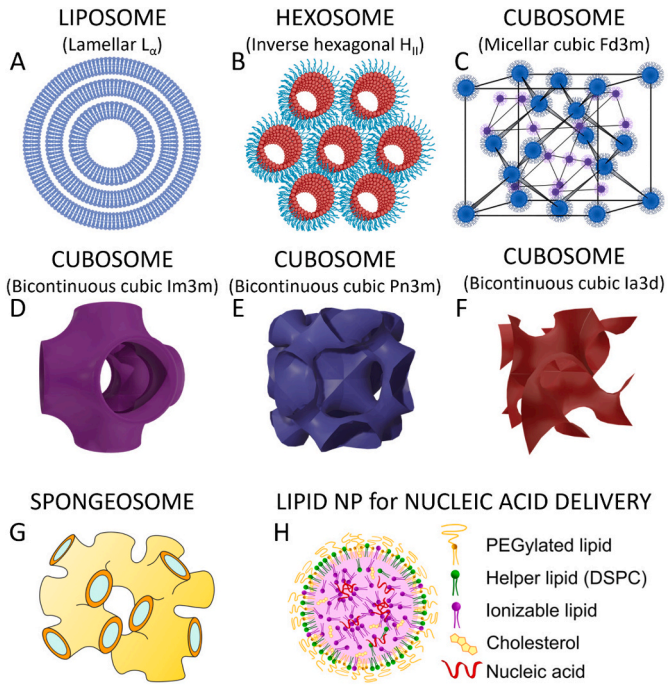

Fig. 1. Most common nanostructures found in LNPs: (A) Lamellar structure (liposomes); (B) H_{II} inverse hexagonal phase (hexosomes); (C) discontinuous micellar cubic phase Fd3m (cubosomes); (D) bicontinuous cubic Im3m phase (cubosomes); (E) bicontinuous cubic Pn3m phase (cubosomes); (F) bicontinuous cubic Ia3d phase (cubosomes); (G) L_3 sponge phase (spongeosomes); (H) Core-shell structure of LNPs for nucleic acid delivery.

non-lamellar LNPs for drug delivery [7,17,19–27], biomedical imaging [2,21] and biosensing [7,28,29]. In spite of this, the number of LNPs currently available on the market is surprisingly limited and primarily restricted to liposome-based formulations [19,30,31], or novel LNPs formulated with cationic ionizable lipids for gene transfection, recently employed in COVID-19 vaccines [17,18].

Elucidating the link between structure and biomedical functions in LNPs is key to bridge this translational gap and fully harness the medical potential of LNPs. The structure of LNPs has been found to control their stability under physiological conditions [32,33], encapsulation efficiency [34–36] and release kinetics of incorporated drugs [37,38]. For instance, the inherent nanostructure of cubosomes and hexosomes offers several benefits over liposomes, such as improved mechanical robustness and larger lipid bilayer-water interfacial area for enhanced drug loading capacity [11,21]. In addition, the tortuous nanostructure of non-lamellar LNPs ensures prolonged release of encapsulated molecules for sustained drug delivery applications [39,40]. In this respect, the structure of the lipid matrix controls the molecular diffusion and release kinetics of drugs [39,40]; for instance, inverse bicontinuous cubic phases promote a faster release than inverse hexagonal phases, due to the larger size of the water channels and enhanced surface area [38,41]. Similarly, micellar cubic phases of discontinuous nature exhibit slower release rates than bicontinuous cubic or hexagonal phases [37]. These differences may be harnessed to control the release of drugs through structural transitions in the lipid scaffold, potentially triggered by either external or endogenous *stimuli* [42]. Moreover, non-lamellar structures in LNPs proved to favor the conjugation with antibodies compared to liposomal analogues, making them more attractive for targeted delivery of chemotherapeutics [43]. Pioneering studies also reported that the lipid structure regulate cellular uptake [44,45], endosomal escape [46], biodistribution [47] and toxicity [48] of LNPs, shaping their biological fate and medical performance. Adding to the complexity, LNPs undergo dynamic structural alterations in biological environments, responding to natural pH gradients and/or interactions with biological molecules and interfaces [40,49]. When in biological fluids, the surface of LNPs gets readily covered with a layer of biomolecules, called "protein corona" [50,51]. This layer redefines the surface identity of LNPs, affecting their chemical and biological functions, such as blood circulation time, cellular uptake and endosomal escape ability [52–55]. Recent reports highlighted a mutual interplay between nanoparticles structure and protein corona formation, i.e., the morphology of nanoparticles may affect the composition and structure of the protein corona [56,57], while the adsorption of biomolecules can similarly modify the internal structure of LNPs [58,59]. Understanding such structural changes is key to predict the behavior of LNPs in living organisms and to improve their medical efficacy. Additionally, the structural responsiveness to endogenous *stimuli* (e.g., pH variations throughout the body) can be harnessed to design "smart" LNPs, able to deliver and release actives at specific locations or (sub)cellular compartments in living organisms [60–63]. Investigating the structure of LNPs is also instrumental to elucidate LNPs-drugs mutual interactions, impacting molecular loading and release [64], as well as to thrive the development of hybrid LNPs for controlled drug delivery, where incorporated inorganic nanomaterials introduce responsiveness to external *stimuli* (e.g., light, or magnetic fields) [65–70].

Small-angle X-ray scattering (SAXS) and small-angle neutron scattering (SANS) are excellent tools to investigate the structure of LNPs and their interactions at the nanoscale. These methods leverage X-ray or neutron probes and collect the scattering from the sample at small angles, which enables to resolve structures ranging from 1 nm to over 100 nm [71]. Compared to microscopic techniques with similar resolution, scattering methods allow sampling a vast number of scattering objects in a single experiment, leading to statistically significant ensemble-averaged structural information. In addition, no sample pre-treatment is required (e.g., drying, freezing or other invasive procedures, possibly leading to sample perturbation), and samples are conveniently characterized as particle dispersions in glass capillaries (SAXS) or quartz cuvettes (SANS). On the other side, background scattering and sample polydispersity may pose serious challenges in characterizing solution-based samples, which need to be addressed to generate reliable data. The signal recorded from a particle dispersion contains the scattering from LNPs, but also a scattering background originating from the solvent, sample holder and instrumental set-up. To remove this background, the scattering of the solvent (without the sample) must be acquired and subtracted from the signal of the sample, recorded within the same sample holder and under identical experimental conditions. The background subtraction is a critical step, especially for samples with a weak scattering signal [72]. For example, LNPs in water typically exhibit weak X-ray scattering intensities as compared to inorganic NPs, due to the small difference in the electron density between the lipids and the water medium. Such difference may decrease even more upon addition of components to the aqueous buffer of LNPs, inducing a further reduction in the scattering signal [72]. Under these circumstances, even small discrepancies in the composition of sample and control buffers may affect background subtraction and, in turn, the quality of data analysis. Ensuring a good match between the buffer for background subtraction and the sample solvent is thus a prerequisite for generating usable data. In addition, sample polydispersity may involve significant challenges for precise analysis of scattering data. When LNPs populations of different sizes coexist in the same sample, their signals sum-up inducing a smearing of the scattering profile, potentially causing a loss of the structural fingerprints of individual LNPs populations. The presence of aggregates is particularly crucial, as the scattering is proportional to the square of the NP volume [72]. Thus, even a relatively small number of aggregates might partially -or fully- cover the scattering features of single LNPs. Therefore, controlling LNPs polydispersity and limiting aggregation is essential to generate usable data and simplify their interpretation.

In the following, we will introduce the basic working principles of small-angle scattering, shared by SAXS and SANS (Section 1.1). A more

exhaustive description of these methods can be found in references [73–75]; then, we will focus on the main differences between SAXS and SANS (Section 1.2), including specific sample/probe interactions, experimental details and instruments availability, as well as different information accessible with the two methods. Next, we will provide recent examples of applications of SAXS to investigate the structure and interactions of LNPs at the nanoscale level (Section 2). A specific emphasis will be placed on Synchrotron SAXS, as a powerful tool for a fast readout of structural details of LNPs. We will then review recent literature on SANS applied to unveil lipid organization and molecular interactions of LNPs (Section 3). Finally, we will review recent advancements in the field of small-angle scattering applied to LNPs (Section 4), including the investigation of dynamic processes through Time-Resolved (TR)-SAXS and SANS. In this respect, TR-SAXS and TR-SANS provide complementary information at different length scales, i.e., from structural transformations at the nanoscale (SAXS) to alterations in molecular diffusion and exchange (SANS). Innovations in combined multi-technique approaches will be also discussed, enabling the simultaneous characterization of structural and physicochemical properties of samples.

1.1. Introduction to small-angle X-ray and neutron Scattering

In a small-angle scattering experiment, a collimated beam of X-rays (with wavelength 0.01–0.2 nm) or neutrons (0.1–2 nm) impinges on a sample, which will partially adsorb, transmit and scatter the beam (Fig. 2A). The scattering contribution arises from the interaction of the beam with the atoms in the sample; in particular, X-rays selectively interact with the *electrons* of an atom through electromagnetic forces [73,74], while neutrons interact with the *nucleus* through short-range nuclear forces [76]. Irrespective of the type of interaction, this results in the scattering of X-rays or neutrons from individual atoms. When the sample contains a nanoscale organization (1–1000 nm size), the waves scattered by different atoms form an interference pattern, which encloses structural information. Such pattern is collected on a 2-D detector, while the transmitted beam is blocked by a beam-stop (Fig. 2A). For a nanoparticle dispersion with a random distribution, the 2-D scattering pattern is isotropic and, thus, it can be radially averaged to obtain a 1-D curve (Fig. 2A), where the scattering intensity (I) is expressed as a function of the modulus of the momentum transfer, also called scattering vector (Q, $Å^{-1}$).

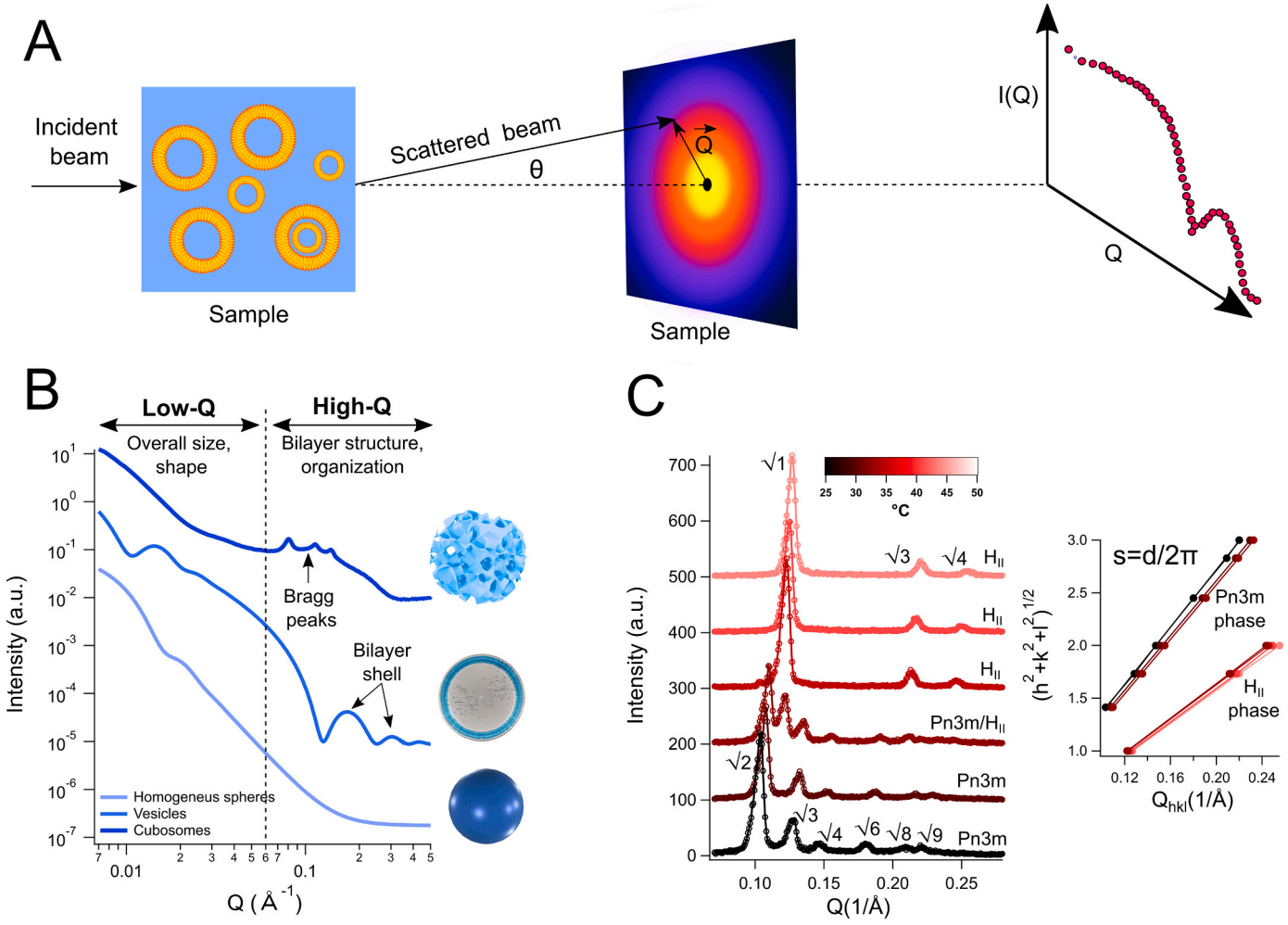

Fig. 2. (A) Scheme of a Small-angle scattering set-up, showing the interference pattern from the scattering of X-rays or neutrons by a lipid vesicles sample, collected on a 2D detector and radially averaged to obtain an I(Q) versus Q 1D profile. (B) Simulated Small-angle X-ray scattering curves from diluted homogeneous spheres (diameter = 500Å, polydispersity = 0.2 and SLD = $9{\cdot}10^{-6}$ $Å^{-2}$) and unilamellar vesicles (diameter = 500Å, polydispersity = 0.2 and shell SLD = $8.3{\cdot}10^{-6}$ $Å^{-2}$) in water (calculated with SasView), together with the experimental curve of glycerol monooleate cubosomes, functionalized with Pluronic F-127 (diam = 2300 ± 500 Å), with internal cubic Pn3m liquid crystalline phase (reprinted from [65]). Curves are shifted for the sake of clarity; (C) Small-angle X-ray scattering profiles of glycerol monooleate/oleic acid/oleylamine mesophases, showing different Bragg peak patterns as a function of temperature, corresponding to different liquid crystalline structures. The inset reports linear plots of $\left(h^2+k^2+l^2\right)^{1/2}$ versus experimental Q_{hkl} for the different Bragg reflections, whose slope relates to d through s = d/2π. Readapted from [66].

The latter represents the difference between the incident wave vector and the scattered wave vector for elastically scattered X-rays or neutrons, and its modulus is described as follows:

$$Q = \frac{4\pi}{\lambda} sin\left(\frac{\theta}{2}\right) \quad (1)$$

with λ wavelength of the probe and θ scattering angle.

Remarkably, Q is inversely proportional to the probed length scale (d), through the following relation (derived from the Bragg law [77]):

$$Q = \frac{2\pi}{d} \quad (2)$$

Thus, the lower-Q region of the scattering intensity curve yields information on the sample's larger length scales (e.g., particle size and overall shape), while the high-Q part captures structural details of smaller size (e.g., bilayer's arrangement and structure). This different structural information is contained in the scattering intensity curve as a function of Q, expressed as follows:

$$I(Q) - I_{background} = \nu(\Delta\rho)P(Q)_{NP}S(Q)_{NP} \quad (3)$$

where ν is the volume fraction of nanoparticles and $\Delta\rho$ (i.e., the contrast of the experiment) is a constant, represented by the difference in the scattering length density (ρ) between NPs and the solvent (discussed in Section 1.2). P(Q) and S(Q) describe the I(Q) functional dependency and are the so-called "intra-particle" form factor and "inter-particle" structure factor of the NPs, respectively. P(Q) describes the overall size and shape of LNPs, alongside smaller structural details, selectively resolved in different Q-regions. S(Q) is a dimensionless oscillatory function, which tends to 1 at high Q and describes inter-particle interactions (i.e., between different NPs in the systems), which can be attractive, repulsive, or excluded volume. A detailed description of S(Q) is beyond the scope of this review, and can be found elsewhere [73,74,78]. The S(Q) contribution to I(Q) is generally more pronounced at low-Q, as interparticle-interactions often occur at longer length scales compared to the size of the single particle. Thus, S(Q) can be normally neglected when $2\pi/d_{NP} \ll Q_{min}$, where d_{NP} is the particle diameter and Q_{min} the smallest Q measured [79]. In addition, for a sufficiently diluted dispersion of LNPs, inter-particle interactions are negligible (S(Q) = 1) and the I(Q) functional dependency is exclusively governed by P(Q). Unless there is a specific interest in measuring S(Q), this condition is normally the most convenient, as it strongly simplifies data analysis. The concentration threshold at which S(Q) = 1 depends on the strength of inter-particle interactions [79], e.g., it is lower for charged particles than for uncharged ones. A good strategy to find the highest concentration for which S(Q) = 1 is to probe the sample at varying concentrations, until the normalized scattering intensity as a function of Q becomes constant. Given that P(Q) does not depend on concentration, a constant normalized scattering intensity means S(Q) = 1 and, hence, negligible interactions between LNPs.

1.1.1. Scattering from lipid vesicles

Analytical expressions of P(Q) are known for a wide range of particle shapes, such as homogeneous spheres, cylinders, discs and spherical shells (e.g., lipid vesicles) [73,80,81], and can be combined with polydispersity functions accounting for particle's size distribution. Fig. 2B provides simple examples of P(Q), calculated for diluted dispersions of homogeneous spheres (light blue) and lipid vesicles (middle blue), of same size and polydispersity. The low-Q region the two profiles contain scattering features related to the size and the overall morphology of the particles. In contrast, the high-Q region highlights structural differences occurring at a smaller length-scale; here, the P(Q) of lipid vesicles features a series of bumps (absent for a homogeneous sphere), accounting for the vesicles' shell, i.e., the lipid bilayer, with thickness ~ 1/20 of the particle size.

Similar and more sophisticated models for P(Q) can be conveniently used to simulate LNPs systems, or fit experimental data to obtain information on real samples. Several open-source software packages are available for this, including SasView [82], SASfit [83], and the Igor-Pro based NCNR SANS (from the NIST Center for Neutron Research) [84] and *Irena* [85], each of them including comprehensive documentation on fitting models and useful guides to data analysis.

Additionally, Guinier and Porod model-free approaches can be applied across a limited range of Q [86]. The Guinier approximation [80] provides an estimation of particle size in terms of its radius of gyration (R_g), and it is defined as follows (only holding at small Q values, i.e., $QR_g < 1$ for spherical particles):

$$I(Q) = Ge^{\left(\frac{-Q^2R_g^2}{3}\right)} \quad (4)$$

where G is a scale factor.

Instead, the Porod law [86] provides an approximate shape and surface structure for the particles, through the following relation, holding at high Q values ($Q < \frac{2\pi}{d_{min}}$, with d_{min} smallest inhomogeneity present in the system):

$$I(Q) = \frac{C}{Q^p} \quad (5)$$

where C is the scale factor and p the Porod exponent. Different p values identify particles with varying physical forms, from spheres with a smooth surface, to spherical particles with a rough surface and rigid rods.

Beside these theoretical considerations, accessing simultaneous information on vesicles size, shape and bilayer's structure may be challenging in practice. As discussed above, these structural features correspond to different Q values, and the Q range required to capture all of them might not be accessible with standard instrumentation. Conventional SAXS and SANS instruments typically cover a Q range of approximately 0.006–0.6 $Å^{-1}$, which roughly corresponds to a probed length scale interval of 1–100 nm (Eq. (2)). While suitable for vesicles smaller than 100 nm, this Q range doesn't allow for probing the size and overall morphology of bigger particles. In this respect, recent advances in the instrumentations have opened new opportunities for LNPs investigation through Ultra-small angle X-ray and neutron scattering (USAXS and USANS, respectively). Such methods allow for accessing wider Q ranges and minimum Q values well below 0.001 $Å^{-1}$, to probe length scales from 100 nm to above 1 μm [87–89]. Remarkably, when used in combination with SAXS and SANS, they can cover the size range 1 nm-20μm [87–90]. Despite being less available than standard SAXS and SANS technology (see Section 1.2.2), USAXS and USANS offer several benefits for the field of LNPs, such as access to the whole form factor of large size LNPs or the possibility to investigate LNPs-LNPs interactions and aggregation processes occurring in the nano and micro size range.

1.1.2. Scattering from non-lamellar lipid NPs

LNPs of non-lamellar nature generate a characteristic fingerprint of the high-Q region, i.e., a pattern of sharp peaks called "Bragg peaks" (Fig. 2B, dark blue curve), associated to their ordered internal structure. In non-lamellar NPs, the lipid bilayer folds in the 2- or 3-D space originating complex arrangements with structural periodicity [91–94]. Resembling solid crystals, these systems consist in a unit cell repeated in the space, leading to a periodic lattice. The distribution of atoms in the unit cell dictates the symmetry of the lattice, which is identified by its crystallographic space-group. Each symmetry is associated with a series of parallel planes (lattice planes) of atomic arrangements, each indicated with the Miller indices $h\ k\ l$ [95]. The separation distance between different lattice planes is the characteristic spacing of the lattice, i.e., the lattice parameter (a). Importantly, since a size is comparable with the wavelength of X-rays and neutrons, the lattice planes act as diffraction

gratings, originating the characteristic pattern of Bragg peaks. In this pattern, each single reflection is associated with a specific set of Miller indices (*hkl),* identifying the lattice planes which generated it.

The pattern of Bragg peaks provides direct information on the structural arrangement in non-lamellar LNPs (i.e., their symmetry space group), through the reciprocal spacings between peaks (see Fig. 2C). For instance, LNPs with an internal hexagonal phase (hexosomes) have peaks spaced in the ratio of $\sqrt{1}$, $\sqrt{3}$, $\sqrt{4}$.., while bicontinuous cubic phase particles (cubosomes) show different spacings, depending on whether they belong to the Pn3m, Im3m or Ia3d space group. Table 1 provides characteristic spacing of Bragg peaks for the most common geometries found in non-lamellar LNPs, together with corresponding Miller indices and space groups.

Once the structure type has been identified, the lattice parameter (a) can be calculated from the maximum of each reflection (Q_{hkl}), through the following relations [95,96]:

$$\text{Multilamellar phases}: Q_l = \frac{l}{a} \tag{6}$$

$$\text{Hexagonal phases}: Q_{hk} = \frac{2\pi}{\sqrt{3}a}\left(h^2 + k^2 + hk\right)^{\frac{1}{2}} \tag{7}$$

$$\text{Cubic phases}: Q_{hkl} = \frac{2\pi}{a}\left(h^2 + k^2 + l^2\right)^{\frac{1}{2}} \tag{8}$$

with h k l the Miller indexes corresponding to the specific Bragg reflection with $Q_{max} = Q_{hkl}$.

In practice, for cubosomes and hexosomes, a is often obtained by plotting values of $\left(h^2 + k^2 + l^2\right)^{1/2}$ as a function of corresponding experimental Q_{hkl} for the different Bragg reflections (see right inset of Fig. 2C); the slope of the linear plot (s) directly provides a through Eqs. (6)–(8). Once determined, the lattice parameter can be used to calculate other structural features of non-lamellar LNPs, through simple geometrical models. For cubosomes with an internal bicontinuous cubic phase and hexosomes with a hexagonal phase, the lipid monolayer thickness (l), the area per lipid molecule at the lipid-water interface (A_l) and the radius of water channels (r_w) can be determined through the following equations [97,98]:

Bicontinuous cubic phase:

$$1 - \phi_w = 2A_0\left(\frac{l}{a}\right) + \frac{4}{3}\pi\chi\left(\frac{l}{a}\right)^3 \tag{9}$$

$$A_l = 2V_l\frac{A_o a^2 + 2\pi\chi l^2}{(1-\phi_w)a^3} \tag{10}$$

$$r_w = \left(-\frac{A_0}{2\pi\chi}\right)^{1/2} a - l \tag{11}$$

Hexagonal phase:

$$l = \left(\frac{1}{2}a - r_w\right)\left[1.1084 + 0.0572\left(\frac{r_w}{\frac{1}{2}a - r_w} - 1\right)\right] \tag{12}$$

$$A_l = \frac{4\pi r_w V_l}{\sqrt{3}a^2(1-\phi_w)} \tag{13}$$

$$r_w = \frac{1}{2}\sqrt{\left(\frac{2\sqrt{3}}{\pi}\right)\phi_w a^2} \tag{14}$$

where A_0 and χ are the surface area and the Euler-Poincaré characteristic per (cubic) unit cell of the lipid bilayer, both related to the topology of the cubic mesophase ($A_0 = 1.919$, $\chi = -2$ for a Pn3m, $A_0 = 2.345$, $\chi = -4$ for a Im3m and $A_0 = 3.091$, $\chi = -8$ for an Ia3d phase) [92], V_l is the lipid molecular volume and ϕ_w is the water volume fraction, calculated as follows:

$$V_l = \frac{m}{\rho_l} \tag{15}$$

Table 1
Main LNPs kinds, together with corresponding dimension, liquid crystalline phase and associated space group, spacings between characteristic Bragg peaks and Miller indices identifying Bragg reflexes in the scattering pattern [94,98,105–108].

Lipid-based NPs	Dimension	Phase	Space group	Peak Spacings	Miller indices
Multilamellar vesicles	1D	Gel (L_β) and fluid (L_α) lamellar	/	1: 2: 3: 4: 5: 6…	(100), (200), (300), (400), (500), (600)..
Hexosomes	2D	Direct (H_I) and inverse (H_{II}) hexagonal	p6m	1: √3: √4: √6: √9: √12: √16: √19…	(100), (110), (200), (210), (300), (220), (310), (400)…
Cubosomes	3D	Bicontinous cubic	Pn3m	√2: √3: √4: √6: √8: √9, √10: √11: √12: √14: √16…	(110), (111), (200), (211), (220), (221), (310), (311), (222), (321), (400)…
Cubosomes	3D	Bicontinous cubic	Im3m	√2: √4: √6: √8: √10: √12: √14: √16: √18…	(110), (200), (211), (220), (310), (222), (321), (400), (330)…
Cubosomes	3D	Bicontinous cubic	Ia3d	√6: √8: √14: √16: √20: √22: √24: √26…	(211), (220), (231), (400), (420), (332), (422), (431)…
Cubosomes	3D	Micellar cubic	Fd3m	√3: √8: √11: √12: √16: √19: √24…	(111), (220), (311), (222), (400), (331), (422)…
Cubosomes	3D	Micellar cubic	Pm3n	√2: √4: √5: √6: √8: √10: √12…	(110), (200), (210), (211), (220), (310), (222)…
Cubosomes	3D	Micellar cubic	Fm3m	√3: √4: √8: √11: √12: √16: √19...	(111), (200), (220), (311), (222), (400), (331)…

$$\phi_w = \frac{C_w}{C_w + (1 - C_w)\left(\frac{\rho_w}{\rho_l}\right)} \quad (16)$$

where, m is the mass of a lipid molecule (e.g., 5.92 10^{-22} g for glycerol monooleate (GMO)), C_w is the water weight fraction, ρ_w is the density of water and ρ_l is the density of the lipid (e.g., 0.942 ± 0.05 g cm^{-3} for GMO [99,100]).

Moreover, being based on periodic minimal surfaces, the Pn3m, Im3m and Ia3d cubic phases in cubosomes are related through the "Bonnet transformation", i.e., they can isometrically transform one into the other [101–103]. Consequently, the ratio of the lattice parameters of two coexisting bicontinuous cubic phases at the equilibrium, i.e., the so-called Bonnet ratio, is fixed and equal to 1.279 for a_{Im3m}/a_{Pn3m} and 1.576 for a_{Ia3d}/a_{Pn3m} [101–103].

Beside the internal nanostructure, the scattering profile of non-lamellar LNPs also contains information on their size and shape. Although theoretically possible, the simultaneous investigation of LNPs lattice structure and size/shape is practically challenging. Among the most significant issues, the size of non-lamellar LNPs such cubosomes is usually around 200–300 nm [8,21,26], while their lattice parameter is typically more than one order of magnitude smaller. The relatively narrow Q range of standard SAXS and SANS devices cannot simultaneously capture such a broad range of length scales. Moreover, as discussed in Section 1.1.1, the size of non-lamellar LNPs is typically bigger than the larger length scale accessible with these instruments. In this respect, USAXS and USANS represent a valuable alternative, enabling access to lower Q values. In addition, when used in combination with SAXS or SANS, USAXS and USANS can potentially provide simultaneous access to the whole form factor of non-lamellar LNPs and their lattice structure, yielding a complete structural and morphological fingerprint of particles. However, a major drawback of these methods is that they are currently less available in number than standard SAXS and SANS setup (see Section 1.2.2). Another issue is that the form factor of LNPs can partially overlap with lattice structure factor, i.e., the Bragg peaks pattern; this overlap can significantly complicate or even hinder the analysis of the particle form factor through model free approaches or fitting operations. Among the strategies to tackle this issue, Förster et al. [104] recently proposed a mathematical framework to model the scattering from a wide range of ordered meso- and nanoscale materials, including non-lamellar liquid crystalline particles. The model account for the lattice structure factor (comprising of expressions for the unit cell dimensions, finite domain sizes and peak shape) and for the particle form factor, including functional dependencies from particle size, size distribution and shape. The analytical expressions derived from this model could be potentially used to fit experimental data, enabling simultaneous analysis of morphology, size and internal structure of LNPs.

1.2. SAXS or SANS?

SAXS and SANS employ different probes, leading to diverse information achievable from a measurement, as well as experimental differences (e.g., experimental times and feasibility).

1.2.1. Probe-related differences

X-rays are electromagnetic waves (also referred to photons), while neutrons are subatomic particles. Both X-rays and neutrons have a spin and no charge. X-rays and neutrons interact with matter in a different way, i.e., either probing electrons via electromagnetic interactions (X-rays) or atomic nuclei through short-range nuclear forces (neutrons). Additionally, neutrons interact with unpaired electronic spins via magnetic dipole interactions [109]. A discussion on magnetic neutrons-electrons interactions is beyond the scope of this review and can be found elsewhere [110,111].

In simple mathematical terms, the difference in X-ray and neutrons interactions is encoded in ρ ($Å^{-2}$) (Eq. (3)), which, for a molecule, is expressed as [112]:

$$\rho = \frac{\sum_i^n b_i}{V_{mol}} = \frac{\delta N_A}{M}\sum_i^n b_i \quad (17)$$

where V_{mol} is the molecular volume ($Å^3$), δ the bulk physical density of the molecule (expressed in g/$Å^3$), M the molecular weight (g/mol), N_A is Avogadro's number (6.022•10^{23} mol^{-1}) and b_i is the X-ray or neutron scattering length of the -ith atom in the molecule (expressed in Å). The scattering length is connected to the cross section of the atom (σ), as follows [113]:

$$\sigma = 4\pi b^2 \quad (18)$$

σ represents the probability that the scattering process will occur and gives information on the "strength" of the interaction between the atom and the probe. X-rays and neutrons are associated with different cross-sections for the same atom, leading to different scattering lengths.

In addition, neutrons can discriminate between isotopes of the same element (e.g., hydrogenous and deuterium, Fig. 3A), which is a major advantage of SANS over SAXS. In SAXS experiments, Δρ is fixed for a specific sample/solvent combination, while, instead, it can be easily manipulated in SANS by varying the H_2O/D_2O ratio of the solvent ("contrast variation" approach) (Fig. 3B). This allows disentangling different scattering contributions in multicomponent systems, by selectively enhancing or matching the contrast of individual compartments. Contrast variation is often combined with deuteration (i.e., replacement of hydrogen with deuterium in selected molecules) to further enhance selectivity to specific molecular components [114,115]. These features make neutrons unique, able to provide structural information which cannot be obtained through other means. Recent studies benefiting from these approaches will be illustrated in Section 3.

Another important advantage of neutrons is that, interacting through short-range nuclear interactions, they can penetrate the matter far more than X-rays, without inducing sample damage and allowing for sample recovery after the measurement. On the other hand, matter scatters neutrons less than X-rays, determining intrinsically lower signal intensity. In addition, available neutron sources exhibit lower intensities than X-ray sources (i.e., typical flux of 10^4 neutrons/s/mm^2, against 10 [18] photons/s/mm^2 offered by Synchrotron X-ray sources [116]). Consequently, neutron scattering is a signal-limited technique, associated with significantly higher acquisition times (i.e., typically hours for neutrons versus minutes or seconds for X-rays).

1.2.2. X-ray and neutron sources availability

Finally, neutrons and X-rays are produced in different ways, which determines a different level of availability of the two probes. Neutrons are either produced in nuclear reactors through the fission process or in proton accelerator-based facilities, exploiting the spallation process [117]. Such neutron sources are only available at specific institutions, most of which are user facilities (i.e., open to external users), providing beamtime through a proposal evaluation system and a high level of support during experiments. In this context, Europe hosts two of the world-leading neutron sources, i.e., the reactor-based Institut Laue Langevin, ILL (Grenoble, France) and the accelerator-based ISIS Neutron and Muon Source (Oxfordshire, UK), together with several other large-, middle- and small-scale neutron facilities [118,119]. In addition, the European Spallation Source, ESS (Lund, Sweden), currently under construction, is expected to provide the next generation source of neutrons for Europe [119]. This consists of a spallation target station and a high-power proton accelerator, delivering a unique long-pulse source of slow neutrons. Leveraging the inherent high flux, flexible resolution, and large bandwidth of its long-pulse source, ESS will house a suite of 22 neutron beam instruments with breakthrough scientific capabilities,

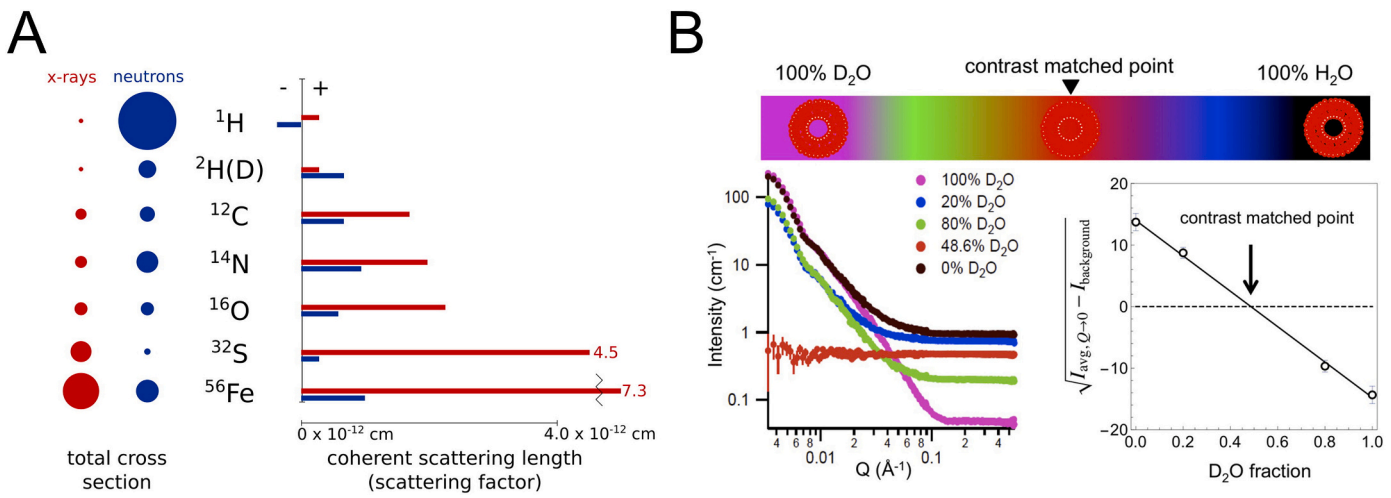

Fig. 3. (A) X-ray and neutron scattering cross sections for different elements, together with corresponding scattering lengths. Reprinted from [112]; B) Top: representative scheme of lipid vesicles in different solvents, determining a variation in the experimental contrast. Bottom left: Scattering from deuterated 1-palmitoyl-2-oleoyl-sn-glycero-3-phosphocholine vesicles in aqueous solvents with different D_2O/H_2O ratios, where vesicles are fully contrast-matched for 48.6/52.4 *v*/v % D_2O/H_2O. Bottom right: Square root of the background subtracted average low Q intensity vs D_2O/H_2O ratio. The linear fit identifies the contrast-matched point (0.486 D_2O fraction), where vesicles display a flat scattering intensity in this solvent condition (red curve on the left plot). Reprinted from [114], with permission from Elsevier. (For interpretation of the references to colour in this figure legend, the reader is referred to the web version of this article.)

currently unmatched at other facilities. Other key examples include the Spallation Neutron Source, SNS (Oak Ridge, Tennessee) and the NIST Center for Neutron Research (Gaithersburg, Maryland) in USA, the Australian Centre for Neutron Scattering, ACNS (ANSTO, Sydney) in Australia and Japan Spallation Neutron Source, JSNS (J-PARK, Tokai, Japan) in Asia. USANS and SANS combinations are available at some of these facilities, including the NIST Center for Neutron Research, the Oak Ridge National Laboratory, ANSTO, the Helmholtz-Zentrum Berlin (HZB), ILL and the Jülich Centre for Neutron Science (JCNS) [90].

X-ray sources are more easily accessible, as SAXS experiments can be conveniently performed in-house with commercially available SAXS laboratory instruments. However, LNPs characterization with lab instruments remains challenging, due to the relatively low difference in electron density between lipids and water media, yielding low experimental contrasts. For instance, the Bragg peak pattern of non-lamellar LNPs is only detectable with the state-of-the-art laboratory SAXS instruments, equipped with either a MetalJet source, or a rotating anode tube [87], providing X-ray fluxes up to 10^9 photons s^{-1} in a few hundreds of μm^2. Alternatively, Synchrotron X-ray sources provide a fast and high-resolution readout of LNPs structure and are available worldwide (http://www.lightsources.org/), accessible via project proposal mechanisms. These employ relativistic electrons to provide X-rays of high brilliance and flux (several order of magnitude more than for lab instruments) []. These sources offer unique possibilities, such as a high-throughput and high-resolution readout of LNPs structure (Section 2), analysis of samples of low concentrations and volumes, real-time monitoring of processes with very fast dynamics (Section 4), and extremely versatile sample environments (Section 4). Additionally, several Synchrotron facilities feature advanced USAXS set-up, such as the ID02 beamline at the European Synchrotron Radiation Facility (ESRF) [89].

2. SAXS applied to the investigation of lipid-based NPs

2.1. SAXS for the characterization of the nano-structure of LNPs

SAXS is among the most powerful methods for the characterization of lipid systems, providing structural information with high accuracy, in a label-free and high-throughput manner. Due to this unique features, SAXS is nowadays widely used to probe the shape and morphology of LNPs and the degree of their internal structure, aimed at guiding the rational design and development of lipid formulations for drug delivery, imaging, and many other applications in Nanomedicine [23,64].

Over the past decades, SAXS has found widespread use in the characterization of lipid vesicles [121–124], including structural effects of stabilizing agents [125,126] and embedded cargoes [64,125,127–130]. In addition, recent literature reviews collected the latest advancements in scattering data analysis from multilamellar liposomes [131–133] or compositionally complex unilamellar vesicles, mimicking relevant biological membranes [134]. The latter include models to analyze the scattering from lipid vesicles with an asymmetric distribution of lipids across inner and outer bilayer leaflets [134–136] or featuring the presence of nanosized compositional heterogeneities, i.e., “lipid rafts” [137,138].

In addition, SAXS was recently applied to investigate the structure of unilamellar or multilamellar vesicles prepared through innovative microfluidic approaches [139–143]. Other recent advancements feature the application of SAXS for the characterization of natural lipid vesicles, such as synaptic vesicles [144,145] and Extracellular vesicles derived from human erythrocytes [146], cord Mesenchymal Stem Cells [147], skeletal muscle cells [148], saliva [149] and bacteria [150].

On the other hand, X-ray scattering from non-lamellar LNPs is usually analyzed through model-free approaches, enabling the detection of their inner structure through the pattern of associated Bragg peaks (Section 1.1.2). Following this approach, the phase behavior of non-lamellar LNPs has been widely explored as a function of lipid composition [151–154], stabilizing agents [155–158], and embedded guest molecules [159–163]. In a recent example, Kulkarni et al. [164] described the self-assembly of Phytantriol and Dimodan U/J LNPs mixed with solubilized tetradecane (Fig. 4A). SAXS analysis revealed a rich polymorphism of such binary mixtures, featuring different liquid crystalline internal phases as a function of the tetradecane concentration. Authors also employed SAXS to investigate the structural response of such systems to hydrostatic pressure, aimed at assessing their robustness for technological applications involving high pressures.

Furthermore, SAXS is systematically applied to monitor the structural response of LNPs to different environmental conditions, such as pH [61,63,105,167–169], ionic strength [170] and solvents [171], temperature [65,66,172–174] and pressure [164].

In this context, Tyler et al. [61] recently engineered pH-responsive

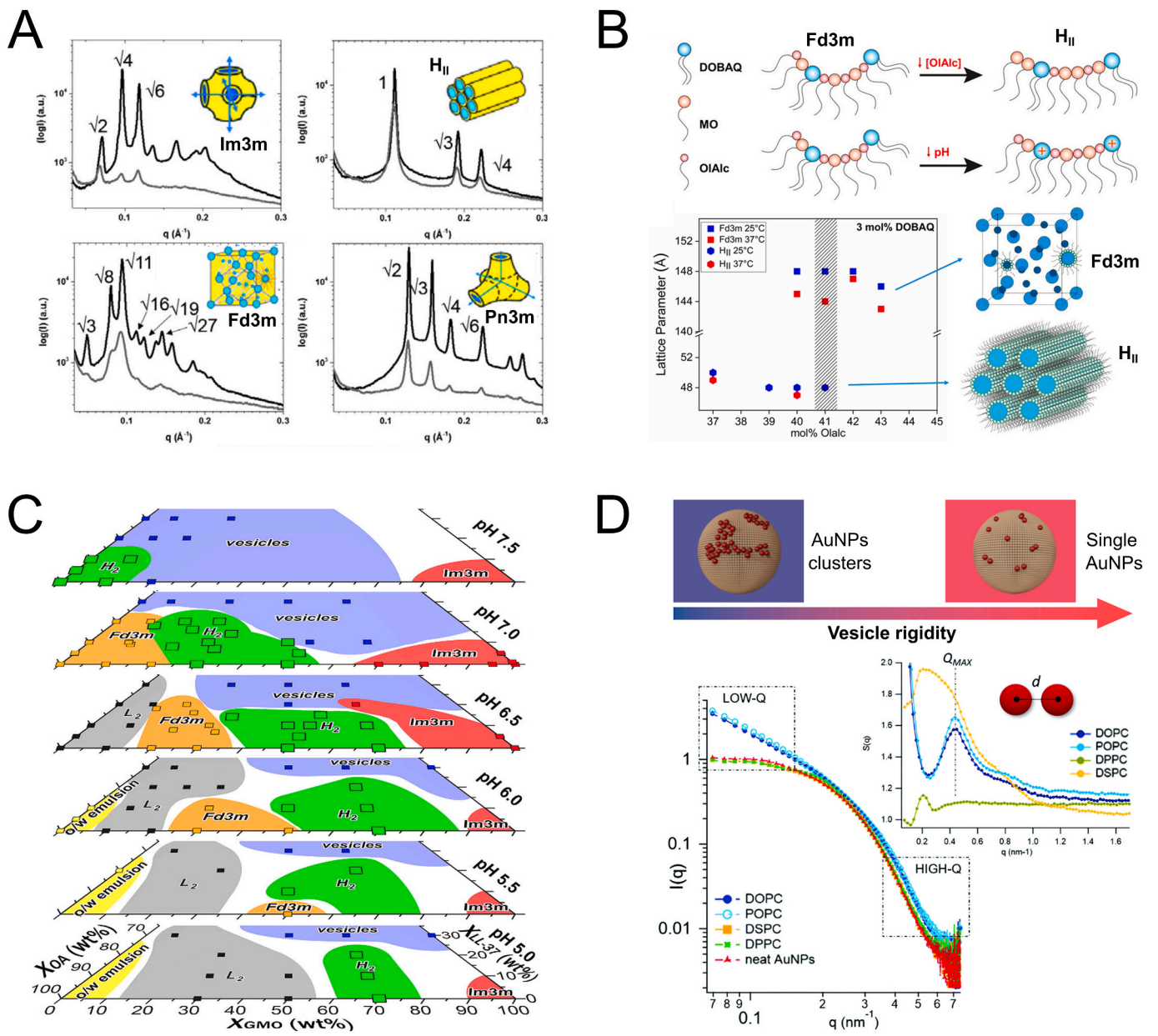

Fig. 4. A) SAXS profiles and identification of lipid-based bulk (black curves) and dispersed nanoparticles (gray curves) for Dimodan U/J or Phytantriol NPs mixed with solubilized tetradecane at different concentrations, at 25 °C and ambient pressure. The different lipid phases assumed by the ternary mixtures are sketched in the right insets, and spacings between corresponding Bragg reflections are indicated for each phase. Adapted with permission from [164]. Copyright {2016} American Chemical Society; (B) Phase behavior and lattice parameter GMO LNPs, mixed with 3 mol% of a pH-sensitive lipid, as a function of oleyl alcohol concentration, at pH 7.4. The dashed region highlights the composition explored in this study as a function of pH. The top inset sketches the effects of increasing amounts of oleyl alcohol or pH lowering on the lipid bilayer curvature, leading to the formation of different lipid mesophases. Reprinted from [61]; (C) Phase diagram for pH-sensitive oleic acid/GMO/LL-37 LNPs, extracted from SAXS measurements and reported as a stack of partial tertiary phase diagrams under different pH conditions. Black squares represent single SAXS measurements. Reprinted with permission from [165]. Copyright {2021} American Chemical Society; (D) SAXS profile of AuNPs with and without vesicles (1:8 vesicles/AuNPs molar ratio) of different composition, determining diverse membrane rigidities. The power law dependence at low-q is connected to the presence of AuNPs clusters and to their morphology, while the structure factor S(q), extracted from the high-q region, relates to AuNPs interparticle distance. The sketch on the top illustrates how the stiffness of lipid vesicles modulates AuNPs self-assembly onto their surface. Readapted from [166].

LNPs composed of glycerol monooleate (GMO), oleic acid, and an ionizable lipid. Through SAXS, authors determined the phase behavior of such ternary mixtures as a function of composition (Fig. 4B). In addition, SAXS investigation revealed that pH variations can trigger a reversible transition in the structural connectivity of the system from the inverse micellar cubic Fd3m phase (at neutral pH) to the inverse hexagonal H_{II} phase (at acidic pH). These findings pave the way to developing stimuli responsive LNPs that reversibly modify their structure at low pH, often connected to human diseases.

Other recent investigations employed SAXS to validate novel preparation methods for LNPs [175], often involving microfluidics [176–178], or to characterize innovative LNPs formulations incorporating specific functionalities [179–181]. The work by Jones et al. [180] is a relevant example in this field, where authors employed SAXS to characterize the first example of light-responsive cubosomes composed of mixtures of monoolein and photoswitchable amphiphiles. These authors showed that UV irradiation resulted in a fast squeezing of the cubic lattice induced by the isomerization of photoswitchable amphiphiles

within cubosomes. This squeezing enabled the release of guest molecules from cubosomes, highlighting the potential of such systems as carriers for photo triggerable drug release.

2.2. SAXS for the investigation of the interactions with biomolecules

SAXS can effectively investigate interactions between LNPs and various bioactive molecules, e.g., nucleic acids and peptides in Sections 2.2.1 and 2.2.2, respectively. Within this framework, SAXS demonstrated particularly valuable for investigating non-lamellar LNPs, whose structure is highly responsive to the interaction with biomolecules and encapsulation of guest species.

2.2.1. Interaction with nucleic acids

Recently, there has been a growing interest in developing novel non-viral vectors for gene therapy, specifically for the delivery of nucleic acids. Lipid-based vectors have emerged as highly promising in mRNA delivery, especially in the context of anti-SARS-CoV-2 vaccines [182]. While SAXS has been extensively employed to investigate lamellar vectors and their interaction with nucleic acids [183–188], non-lamellar LNPs have emerged as effective systems for encapsulating and transporting nucleic acids only recently. Recent studies addressed non-lamellar LNP interaction with nucleic acid cargoes through SAXS [177,189–192]. Among these, Kim et al. [190] prepared cubosomes of ~500 nm size based on GMO, 1,2-dioleoyl-3-trimethylammonium propane (DOTAP), and GMO-Polyethylene glycol (PEG) loaded with siRNA (referred to as "cuboplexes"). SAXS investigation demonstrated that cubosomes with an internal Im3m phase could encapsulate siRNA with higher efficiency compared to liposomal analogs. In a following study [177], the same authors developed a microfluidic platform to produce cuboplexes with smaller sizes (75 nm) and narrower distribution, to fulfill drug delivery requirements. Here, a combination of Synchrotron SAXS with Cryo-TEM revealed the mechanism of cubosomes' formation within the microfluidic device and how their size can be controlled by tuning the amount of PEG stabilizer. In addition, comparing the scattering of cuboplexes with the one exhibited by empty cubosomes, authors showed that the inclusion of siRNA shifted the Bragg peak pattern to higher Q, indicating a squeezing of the Im3m cubic phase unit cell due to siRNA-induced screening of the cationic lipid electrostatic repulsion. In another recent study, Sarkar et al. [191] systematically investigated the encapsulation and release of double-stranded (ds) DNA in cationic GMO-based cubosomes. Synchrotron SAXS was employed for a high-throughput characterization of GMO cubosomes formulated with six different cationic lipids at varying concentrations, and to investigate the structural effects of the encapsulation of different dsDNA ladders. This study showed that the Im3m phase was preserved upon the addition of cationic lipids in the 0–2 mol% concentration range. Moreover, a decrease in the lattice parameter was observed for pure GMO cubosomes with increasing dsDNA size due to the dehydration of the GMO hydroxyl groups induced by negatively charged dsDNA. Conversely, cationic cubosomes displayed a swelling of the lattice parameter with increasing dsDNA size, due to partial neutralization of their positive charge, which promoted hydration.

2.2.2. Interaction with peptides

In the last decades, LNPs have been widely investigated as potential carriers for peptides, aimed at increasing their bioavailability and achieving controlled delivery and release. In this context, antimicrobial peptides (AMPs) attracted significant interest, owing to their innate defence capabilities against bacterial infections. In particular, several works focused on the application of SAXS to develop liposomal carriers for AMPs [193–196]. Recent reports in this field include the work from Utterström et al. [194], where authors employed SAXS to investigate the structural destabilization of cholesterol-rich phosphatidylcholine (PC) vesicles induced by an AMP-mimetic peptide, as possible strategy to control and trigger the release of cargoes. They found that the binding to the liposomal surface, followed by peptide folding, triggered a lipid phase separation, involving high local peptide concentration at the bilayer surface, and abrupt release of cargo.

In latest years, pioneer researches also focused on the development of non-lamellar carriers and characterization of optimal structural features for peptides delivery [197–202]. Among these, Meikle et al. [159] investigated the incorporation of hydrophobic and amphiphilic AMPs within cubosomes of different compositions, i.e., from monoolein, to monopalmitolein, monovaccenin, and phytantriol. Authors employed SAXS to determine optimal peptide loading ranges over which cubic symmetry was retained, providing useful information for the future development of peptide carriers for drug delivery. Similarly, Zabara et al. [203] employed SAXS to validate new formulations of stabilizer-free cubosomes as carriers for the LL-37 AMP, while Gontsarik et al. [165] designed pH-responsive GMO/oleic acid cubosomes for the delivery of the same peptide. Aimed at targeting sites of bacterial infection with abnormal pH levels, authors employed SAXS to build-up a detailed pH-lipid composition phase diagram (Fig. 4C). Results showed that lipid composition controls the pH at which cubosomes undergo the structural transformations of interest for drug delivery, providing guidelines for the design of adaptable nanocarriers for patient-optimized pH-targeted AMP delivery.

2.3. SAXS applied to hybrid LNPs formulation

The combination of LNPs with engineered systems (from inorganic NPs to polymeric matrices and hydrogels) represents an innovative research area, where the biocompatibility and structural responsivity of lipids is combined with functional properties of inorganic or polymeric matrices, leading to versatile hybrid platforms for multiple biomedical purposes. In this respect, SAXS is instrumental in deciphering structure-functions relationships in hybrids LNPs, aimed at informing their rational design. In addition, SAXS can be applied to explore events occurring at the interface between engineered systems and LNPs as models for biological membranes, aimed at unravelling complex membrane-related phenomena [204–211].

In this field, recent reports employed SAXS to investigate the spontaneous clustering of citrated-gold nanoparticles (AuNPs) onto lipid vesicles [166,208]. In particular, Caselli et al. [166] focused on PC vesicles of varying membrane rigidity, to gain insights into the structure of AuNPs clusters adsorbed on their surface (Fig. 4D). For soft fluid-phase bilayer vesicles, the power-law dependence in the low-Q region of the double-logarithmic scattering plot relates to the presence of AuNPs aggregates with increasing fractal dimension as the stiffness of vesicles decreases. Conversely, the absence of such power-law for stiff gel-phase liposomes hints to non-aggregated AuNPs, preserving their original diameter. In addition, the analysis of the S(Q) structure factor vs Q, extracted from the high-Q region of SAXS profiles (right inset in Fig. 4D), revealed increasing AuNP center-to-center distances with enhancing membrane stiffness, highlighting that membrane rigidity controls the assembly of AuNPs.

Other studies employed SAXS to investigate the combination of lamellar and non-lamellar LNPs with different classes of inorganic nanoparticles, from metallic [179,212–215] to iron oxide [65–68,216] NPs. These investigations showed that, depending on their physico-chemical properties, inorganic NPs may preserve the structural integrity of the lipid assemblies or induce structural changes, ultimately controlling the properties and possible end-use of hybrid LNPs. In this respect, Meikle et al. [214] functionalized GMO- and Phytantriol cubosomes with a series of magnetite, copper oxide and silver nanocrystals. The SAXS investigation demonstrated that the lipid cubic phase can be retained up to 20 *w*/w % nanocrystals concentration, opening new possibilities for efficient dual delivery of nanocrystals and conventional drugs embedded within the same lipid nanocarrier. Other recent research employed SAXS to characterize zinc-functionalized LPNs, i.e., "metallo-cubosomes", for RNA delivery [179] and

cubosomes co-encapsulating inorganic up-converting Er^{3+} and Yb^{3+} co-doped NaYF4 NPs for photodynamic therapy [181]. In another key example, Szlezak et al. [216] used SAXS to confirm the successful incorporation of hydrophilic and hydrophobic magnetic NPs within cubosomes for magnetically-guided drug delivery, occurring with full preservation of the cubic lipid structure.

Investigating the interaction of LNPs with polymers [172,217–220] as LNPs stabilizing agents, represents another field of intensive research. LNPs generally require steric stabilizers to improve colloidal stability in aqueous media and to enhance their pharmacokinetics and biodistribution profile in living organisms [221]. Poly(ethylene glycol) (PEG)-conjugated lipids are among the most common stabilizers for LNPs, recently also employed in the BioNTech/Pfizer and Moderna SARS-CoV-2 mRNA-LNPs vaccines [222]. The PEG moiety prevents LNPs aggregation and opsonin targeting, for prolonged LNPs circulation time in the blood. Alternatively, commercially available non-ionic triblock copolymers, such as Pluronics® or Poloxamers, are frequently used to stabilize non-lamellar LNPs, e.g., cubosomes and hexosomes, due to their high stabilization ability and low cost. The nature and concentration of the steric stabilizer deeply affects LNPs size, shape and phase behavior, which can be conveniently studied through SAXS. For instance, SAXS investigations showed that the stabilization of GMO cubosomes with the widely used Pluronic F127 produces well-dispersed particles, which, however, exhibit a different internal structure than the corresponding bulk assemblies in excess water (i.e., an Im3m cubic phase instead of the Pn3m cubic structure observed in bulk systems) [66,223]. Conversely, the Pn3m structure is preserved in Pluronic F127-stabilized phytantriol cubosomes [223] or in GMO cubosomes stabilized with Pluronic F108 [224]. Further studies investigated Tween 80 as potential stabilizing agent for LNPs, potentially providing enhanced LNPs penetration across the blood–brain barrier [156,225]. This stabilization strategy yields cubosomes with internal Im3m cubic phase and high colloidal stability, achieved at higher concentrations of Tween 80 than conventional Pluronics. More recently, Yu et al. [226] extended this investigation to phytantriol-based LNPs formulation, including two of the most popular ionizable lipids (ALC-0315 and SM-102) used in mRNA delivery [62]. In this study, the authors investigated the impact of different stabilizers (Pluronic F127, Pluronic F108 and Tween 80) in the pH-dependent phase behavior of LNPs. Incorporating Pluronic F108 and Tween 80 within the LNP formulation instead of the conventional F127 resulted in slightly larger LNPs, whereas the impact of stabilizers appeared to be only marginal in the phase behavior of LNPs, primarily governed by the lipid composition. This was attributed to the spatial distribution of stabilizers, predominantly localizing at the outer surface of LNPs rather than within their internal core.

In addition to conventional stabilizers, the latest years have witnessed an increasing interest in developing customized stabilizing agents, offering enhanced biosafety and/or specific functionalities [221]. The work of Balestri et al. [172] represents a relevant example in the field, where SAXS was employed to assess the structure of novel cubosomal formulations stabilized with the copolymer poly(*N*,*N*-dimethylacrylamide)-*block*-poly (N-isopropylacrylamide), introducing thermo-responsivity for advanced drug-delivery applications.

In the context of LNPs formulation for drug delivery, anomalous small-angle X-ray scattering (ASAXS) represents a significant advancement in the Synchrotron technology, which opens new opportunities for the characterization of LNPs interactions with stabilizers and guest active principles. In this technique, selecting a single wavelength (and corresponding energy) of the X-ray beam and working near the X-ray absorption edge of an element of interest results in a contrast variation method [64,227]. Consequently, this approach allows to highlight specific elements in the sample under investigation and gain insight into the spatial distribution of different components within LNPs, such as the lipid bilayer, guest molecules (e.g., metal ions or drugs often containing heavy metals) and stabilizing agents [125,228–230]. In combination with SAXS, it is also possible to perform X-ray absorption near-edge structure (XANES) spectroscopy, which can be exploited to monitor the chemical state of metal ions (e.g., as components of guest drugs) entrapped within LNPs, which can be connected to drug release processes [206,231]. For instance, Henriksen et al. recently employed XANES to investigate the molecular coordination of the positron emitter $^{64}Cu^{2+}$ loaded within several liposome formulations containing a specific chelator for copper, for application in in vivo positron emission tomography (PET) imaging [232].

Further SAXS investigations focused on the integration of LNPs into organic matrices, such as and hydrogels [233,234]. Among recent examples, Villalva et al. [234] prepared phytantriol cubosomes immobilized in chemically cross-linked hydrogels of partially oxidized hyaluronic acid, as biocompatible and biodegradable hybrids for sustained drug release. SAXS analysis confirmed the structural integrity of cubosomes when incorporated into hydrogels with varying degrees of chemical cross-linking. SAXS was also recently used to elucidate structural transformations of PC vesicles when exposed to synthetic and natural hydrogels, mimicking the extracellular matrix [235]. In this study, Bandara et al. demonstrated that the hydrogels cause a transition from unilamellar vesicles to multilamellar vesicles aggregates, due to an osmotic driving force from the hydrogel environment. This restructuring effect, which was less pronounced in the case of PC liposomes with a PEG corona, might have significant implications in the properties and fate of vesicles in biological tissues.

3. SANS applied to the investigation of lipid-based NPs

3.1. SANS for the characterization of the molecular structure of LNPs

SANS is the method of election to investigate the structure of LNPs at a molecular level [75,76], providing information not accessible with SAXS or, in several cases, any other technique. In the last decades, SANS has been widely employed to study the bilayer's structure in single-component phospholipid vesicles, e.g., made of phosphatidylcholines (PC) [236–239], phosphatidylglycerols (PG) [240,241], phosphatidylethanolamines (PE) [240], phosphatidylserines (PS) [242], cardiolipin [243] or sphingomyelins [244]. These investigations unveiled information such as bilayer thickness, area per lipid molecule and intra-bilayer structural parameters under different experimental conditions, e.g., as a function of temperature [243,245–247] or ionic strength [248,249]. SANS has been also applied to synthetic systems of higher complexity, e.g., vesicles with a heterogeneous bilayer composition to mimic bacterial membranes [250]. Many other studies employed SANS to address the effect of cholesterol on the molecular packing of synthetic phospholipid bilayers [251–256], providing insights on its biological role in natural membranes.

In addition, SANS represents an ideal method to characterize some structural fingerprints of lipid membranes, such as lateral heterogeneities (i.e., "lipid rafts") occurring in multicomponent synthetic and natural bilayers [257–259]. In this context, contrast variation (Section 1.2), combined with the selective deuteration of molecular components, enables to systematically highlight, or hide, micro- or nanodomains with different lipid composition [260–262]. Heberle et al. [263] provided a proof of concept of this approach, employing four-component vesicle models, containing cholesterol and a mixture of saturated and unsaturated PC. By contrast-matching the solvent, headgroups and hydrophobic chains of the lipids, they isolated the scattering contribution arising from lateral segregations in the acyl chain region, induced upon domain formation. Through systematic variations in lipid composition, authors correlated variation in the SANS signals with domain size and structure. Later studies further extended this strategy [264–267], e.g., applying it to determine the bending modulus of lipid nanodomains in synthetic vesicles [268].

In addition to lateral heterogeneity, SANS also proved as a powerful tool to study the asymmetric distribution of lipids across the bilayer (commonly encountered in natural plasma membranes) and related

inter-leaflet coupling phenomena, by introducing isotopic differences between inner and outer membrane leaflets [136,269–272].

3.2. SANS for the investigation of the interactions with biomolecules

SANS offers unique possibilities to explore the interactions of LNPs with biological molecules, providing information on their partitioning into the lipid matrix and structural rearrangements occurring at the molecular length scale. This information is instrumental for fundamental studies employing LNPs as synthetic models for cell membranes and for the application of NPs in different technological fields, from food science to drug delivery.

3.2.1. Interaction with peptides

In recent years, SANS has been intensively applied to investigate the interaction of synthetic lipid vesicles with different classes of peptides [273], ranging from antimicrobial [195,274–276] to amyloid-forming [277–281] and fusion peptides [282,283]. In the context of antimicrobial peptides, Silva et al. [274] recently investigated bacteria-mimicking PG/PE unilamellar vesicles interacting with a cecropin A-melittin hybrid peptide. Through SANS, they showed that the peptide induces the formation of tightly packed onion-like multilamellar structures, held together by intercalated peptides. Analysis of the associated Bragg progression demonstrated that this process involves membrane condensation, occurring through a fluid to gel phase transition of the lipid bilayer. The effects of similar antimicrobial peptides (i.e., melittin

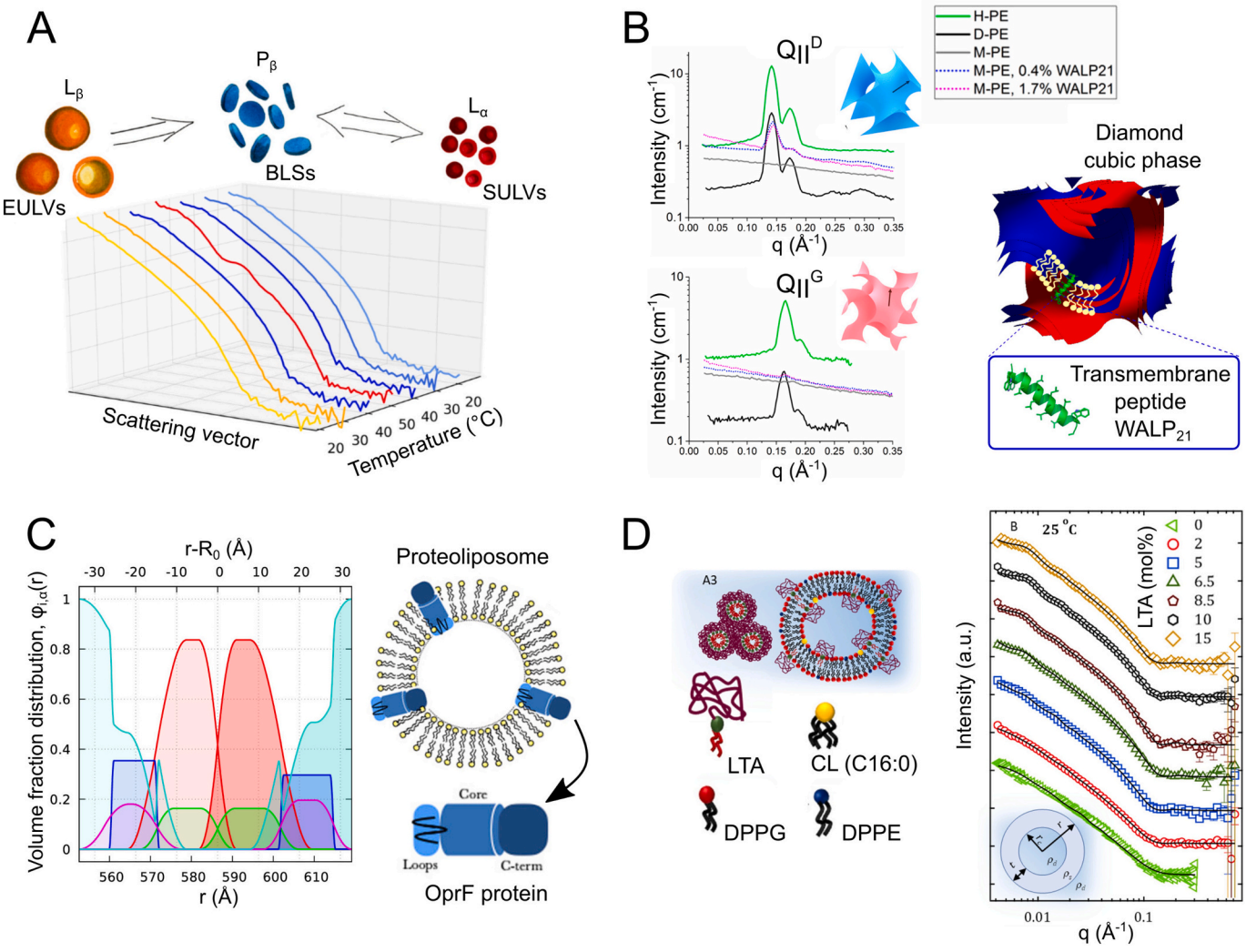

Fig. 5. (A) SANS data on 1,2-dipalmitoyl-sn-glycero-3-phosphocholine (DPPC)/Amyloid-Beta Peptide (25–35) (Aβ25–35) assemblies as a function of temperature. The best fit model to describe the SANS curves are indicated with colours corresponding to the structures schematically illustrated above. Reprinted from [279]; (B) SANS profiles for hydrogenated (H-), and deuterated (D-) phytanoyl monoethanolamide (PE), as well as for a proper H-PE/D-PE mixture to achieve fully contrast matched PE (M-PE), all at 25 °C. SANS curves of M-PE containing different amounts of the transmembrane peptide $WALP_{21}$ are also shown. Data for systems in excess D_2O, having a diamond cubic Q_{II}^D phase, are reported in the top graph, while the bottom graph collects SANS profiles systems featuring a gyroid cubic Q_{II}^G phase, at hydration 13% *w*/w D_2O. The right inset illustrates a diamond cubic Q_{II}^D phase with bilayer-embedded $WALP_{21}$. Reprinted with permission from [284]. Copyright 2022 American Chemical Society; (C) Volume fraction distributions calculated from the SANS data for proteoliposomes as a function of (i) the radial distance from the vesicle centre ((r), bottom horizontal axis) and (ii) the radial distance from the average vesicle radius ($r-R_0$, with R_0 average vesicle radius, top horizontal axis). Filled areas with lower transparencies refer to the inner monolayer, while higher intensities to the outer one. Red, blue, and light blue distributions represent the lipid hydrophobic group, lipid polar group and water, respectively. On the contrary, green and magenta distributions relate to the protein hydrophobic and polar groups, respectively. The right inset sketches a proteoliposome with embedded Oprf proteins. Reprinted with permission from [285]. Copyright 2022 American Chemical Society; (D) SANS profiles for liposomes containing 0–15 mol% Lipoteichoic acid (LTA) at 25 °C, fitted according to a spherical core-shell model, illustrated in the bottom inset. The left inset schematically illustrates mixed lipid/LTA vesicles (0–15 mol% LTA) and segregated LTA micelles at LTA >15 mol%. Readapted from [286]. (For interpretation of the references to colour in this figure legend, the reader is referred to the web version of this article.)

and alamethicin) on PC/PG mixed vesicles was also investigated by Quian et al [275]. Employing SANS coupled with selective deuterium labelling, they observed a peptide-induced recruitment of negatively charged PG into the outer leaflet of the bilayer, creating an asymmetric distribution of lipids across the membrane.

The interaction of lipid vesicles with amyloid-forming peptides represents another very active area of research, aimed at gaining insights on the onset of neurodegenerative pathologies. Among recent studies in this field, Ivankov et al. [279] investigated PC vesicles with incorporated amyloid-beta peptide, a key factor in Alzheimer's disease. By means of SANS, they found that the peptide triggered membrane damage, resulting in spontaneous reorganization of unilamellar vesicles to discoidal bicelle-like structures and small unilamellar vesicles (Fig. 5A), occurring during the thermodynamic phase transitions of lipids.

Other recent investigations employed SANS to address the effects of cell-penetrating [287] or fusion peptides [282,283] on model lipid vesicles. Santamaria et al. [282] investigated the process of membrane fusion for selected SARS-CoV-2 Spike fusion peptides, and how this is modulated by cholesterol and calcium ions. Complementing SANS with dynamic information from quasi-elastic and spin−echo neutron spectroscopy, they revealed different functions encoded in the Spike fusion domain and proposed a mechanism for the initiation of viral infection.

Despite most studies so far focused on vesicles, the application of SANS has been recently extended to investigate molecular interactions of non-lamellar lipid NPs. Van't Hag et al. [284] pioneered the field by developing a lipid deuteration strategy to obtain perfectly contrast-matched cubic phases in D_2O (Fig. 5B), having negligible effects on the phase behavior of cubic phase-forming lipids. This strategy potentially enables to determine the location and distribution host molecules (e.g., proteins and peptides) within non-lamellar lipid phases, crucial for their applications in technological fields, such as in *meso* crystallization and drug delivery. Additionally, Conn et al. [288] recently showed that contrast-matched bicontinuous cubic phases can also be successfully used to elucidate specific membrane protein conformations using SANS. This approach can be conveniently applied to characterize membrane structures of proteins that are typically too small for Cryogenic Electron Microscopy (Cryo-EM), or too large for Nuclear magnetic resonance (NMR) studies.

While the above studies [284,288] provided a proof of concept of the applicability of this method to bulk cubic mesophases, Yepuri et al. [289] extended it non-lamellar lipid NPs, i.e., phytantriol-based cubosomes. The work of Milogrodzka [202] represents the last advancement in this field, where authors investigated the interaction of monoolein cubosomes of high content of cholesterol and phospholipids, encapsulating a Coronavirus fusion peptide. The SANS investigation showed that cholesterol and phospholipids were essential to prompt the interaction with the peptide. Moreover, increasing concentrations of the fusion peptide enhanced membrane's negative curvature, due to the oblique insertion of the peptide, leading to an alteration of the bilayer structure and phase behavior.

3.2.2. Interaction with proteins

Beyond peptides, SANS has been widely used to characterize the interaction of LNPs with full-length proteins [59,285,290–294], vitamins [295] and hormones [254,296].

For instance, Spinozzi et al [285] focused on lipid vesicles with embedded outer membrane protein F (i.e., the main porin of *Pseudomonas aeruginosa*), recently identified as potential vaccines against antibiotic-resistant bacteria [297]. Employing a systematic variation of the solvent deuteration grade, coupled with a newly developed volume fraction-based approach for data analysis, they obtained quantitative structural information to optimize the design of this delivery system, such as the average amount and location of the protein in the lipid bilayer and effects of its incorporation on the bilayer's structure (Fig. 5C).

In another recent work, Holme et al. [293] investigated the interaction of PC vesicles with biologically relevant enzymes, i.e., the lipid-cleaving phospholipases C and D. Combining SANS with all-atom molecular dynamics simulations, they obtained a multi-scale structural information to guide the bottom-up design of sensitive liposome-based systems for therapy and diagnosis of phospholipases-dysregulating diseases.

Other studies applied SANS to sophisticated bacteria-mimicking vesicles, e.g., containing molecular components extracted from bacteria. In this context, Bharatiya et al. [286] focused on model lipid vesicles containing Lipoteichoic acid (LTA), a surface associated polymer tethered to the cytoplasmic membrane of Gram-positive bacteria. Here, SANS revealed the impact of increasing amount of LTA on the bilayer thickness and overall size of lipid vesicles (Fig. 5D); in addition, it pinpointed a threshold concentration for the incorporation of LTA after which self-aggregation occurs, which nicely correlates to LTA concentrations generally found in real bacterial membranes.

3.3. SANS applied to LNPs formulation

3.3.1. Drug loading

In the last decades, many investigations applied SANS to study the effects of host drug molecules on the structure of LNPs [64,298–302], aimed at guiding the rational design of lipid carriers for drug delivery.

Recent advances in this field include the work of Truzzi et al. [303], where the authors developed multilamellar liposomes co-loaded with isoniazid and rifampicin, for inhaled anti-tubercular therapy. By means of SANS, they obtained information on the carrier-cargo structures and interactions, such as multi-lamellae number and spacings, particle stability and drug localization. In addition, they demonstrated that isoniazid/rifampicin co-loading stabilized the multilamellar liposome architecture, increasing the drug loading capacity.

In another recent study, Motlaq et al. [304] investigated the co-assembly of PC lipids with ricyclic antidepressant drug amitriptyline hydrochloride (AMT). SANS analysis highlighted the formation of different structures as a function of sample concentration, from rod-like micelles to bilayer disks and vesicles (Fig. 6A). Remarkably, they detected spontaneous formation of ultrasmall unilamellar mixed vesicles (i.e., with diameter $<$15 nm) at low concentrations, characterized by excellent colloidal stability in physiological saline solution. Such systems were proposed as promising candidates for applications in drug delivery, owing to their high drug solubilization capacity, biocompatibility and good transport properties.

3.3.2. Interaction with LNPs stabilizing agents

Other studies focused on the mutual interaction between LNPs and their stabilizing agents, to optimize LNPs formulations for application in Nanomedicine [289,308–311].

In this context, several recent works applied SANS to investigate the effects of PEGylation (i.e., a widely employed LNPs stabilization strategy) on the structure of LNPs. To name a few, Xiao et al. [310] employed SANS to validate a new preparation protocol of azide-functionalized PEGylated liposomes with encapsulated drug nanocrystals for anticancer targeted delivery. Similarly, Nele et al. [312] performed an in-depth SANS investigation to characterize the effects of PEGylation, as well as preparation method and lipid composition, on the lamellarity of PC liposomes for drug delivery.

Other recent investigations focused on different polymeric stabilizers for LNPs. For instance, Yepuri et al. [289] investigated non-lamellar LNPs dispersed by the non-ionic surfactants Tween 80 and Pluronic F-127. Through SANS, they found that the liquid-crystalline structure of LNPs controls the arrangement of these surfactant within phytantriol cubosomes. In addition, Tsengam et al. [313] recently investigated the interaction between PC vesicles and Tween 80, often found together in formulations for drug delivery. By combing SANS with a Cryo-TEM investigation, they observed a surfactant-induced transformation of

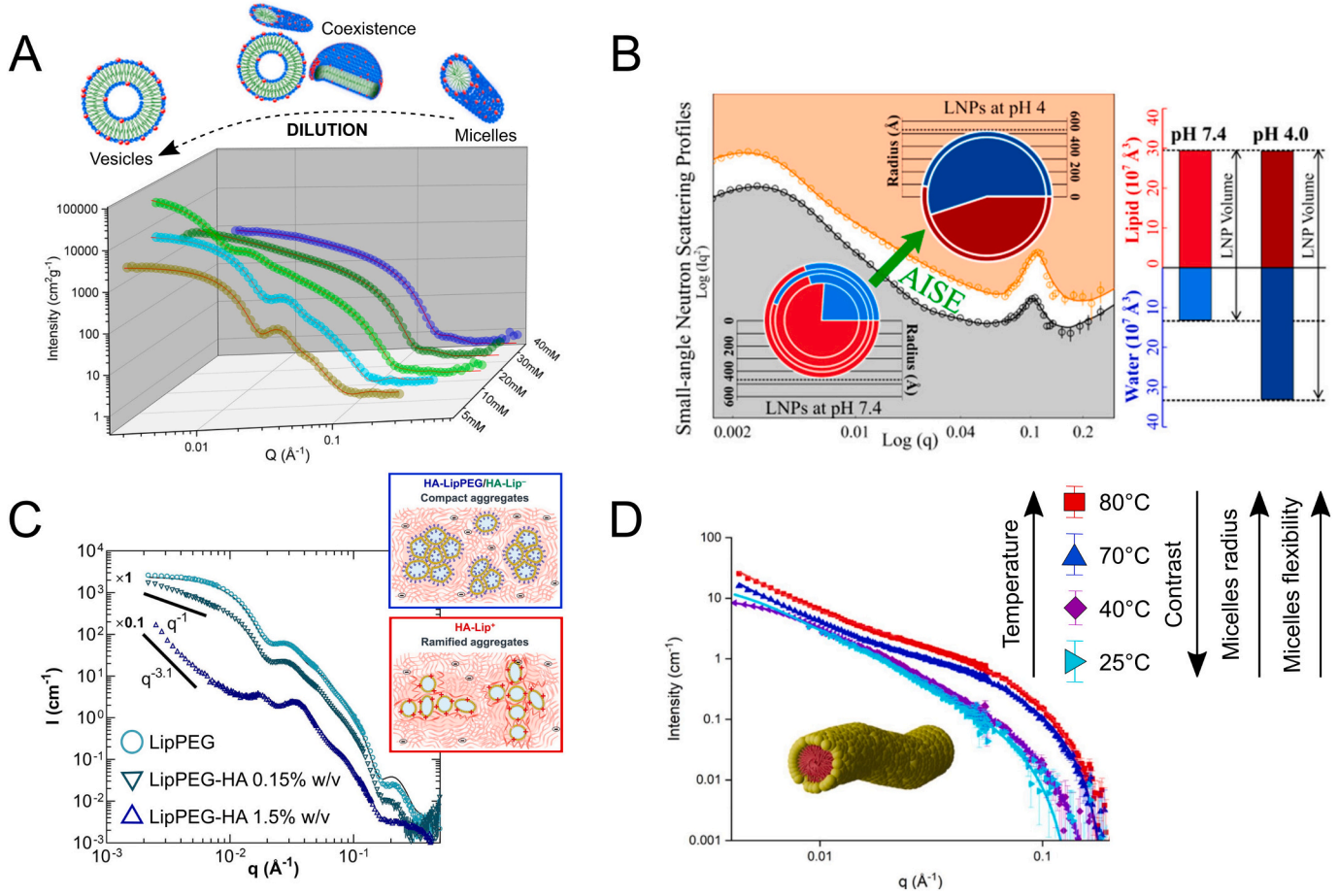

Fig. 6. (A) SANS profiles with best curve fits for 1,2-di-(9Z-octadecenoyl)-sn-glycero-3-phosphocholine (DOPC)/ amitriptyline hydrochloride (AMT), with fixed 0.25 DOPC mole fraction and total DOPC+AMT concentration in the range 5–40 mM. The top inset illustrates the different structures encountered upon dilution. Readapted from [304]; (B) SANS profiles and best fit curves for lipid nanoparticles (LNPs) in D_2O at pH 7.4 (black symbols and solid line) and 4.0 (orange symbols and solid line). The pie-charts show the changes of the lipid mixture (red) and water (blue) in the different regions of LNPs at pH 7.4 (gray area) and 4.0 (orange area), obtained from SANS analysis. The bar-charts show corresponding volume changes in the lipid mixture and water. Reprinted from [305]; (C) SANS profiles, together with best curve fits, for PEGylated liposomes (LipPEG) in suspensions, or in hyaluronic acid (HA) at 0.15% or 1.5% *w/v*, obtained in D_2O. The right insets sketch the structure of anionic and PEGylated liposomes (top) or cationic liposomes (bottom) in HA. Reprinted from [306] with permission from Elsevier; (D) SANS data and best curve fits for POPC in 99% *w*/w of D_3EAN in the temperature range 25–80 °C, fitted according to a flexible homogenous cylinder model. The increase in temperature determines an increase in the flexibility and radius of the micelles and a decrease in the contrast of the experiment. Reprinted from [307]. (For interpretation of the references to colour in this figure legend, the reader is referred to the web version of this article.)

vesicles into spherical micelles, and elucidated the structural aspects connected to it.

3.3.3. *Stimuli-responsive NPs formulations*

Recent studies applied SANS to investigate the structural responsivity to external *stimuli* in smart preparations of LNPs.

The work of Matviykiv et al. [314] represents a distinguished example, where authors prepared liposomes made of artificial phospholipids with a dedicated backbone chemistry and tail length, that form interdigitated bilayers. Such chemical features produce metastable non-spherical liposomes, endowed with mechanical and thermal responsivity for controlled-release applications. By means of SANS, the authors investigated temperature-induced structural changes of selected artificial liposomes and identified suitable preparations for use in the medically relevant temperature range (22–42 °C). Instead, Yuan et al. [315] focused on light-activatable PC liposomes, whose structure can be altered via plasmonic photothermal effect upon laser-irradiation to achieve a controlled release of cargoes. Through SANS, they highlighted that cholesterol inclusions play a key role in driving membrane destabilization and drug-release upon laser irradiation.

Moreover, Barriga et al. [316] recently investigated LNPs made of a mixture of cholesterol, phosphatidylcholines, phosphatidic acids and Pluronic F127. They used SANS to link LNPs composition with internal structure and to monitor the interaction with phospholipase D. The investigation highlighted a promising potential of such LNPs as enzyme-responsive structures to treat diseases involving phospholipase D dysregulation. Similarly, Li et al. [305] formulated LNPs with PC, cholesterol, PEGylated and ionizable lipids, incorporating plasmid DNA for gene-delivery. In this study SANS was used to investigate structural changes occurring upon acidification (from pH 7.4 to 4.0), faced by NPs while undergoing endocytosis in living organisms. Results detected structural responsivity, encompassing protonation of ionizable lipids, volume expansion and redistribution of aqueous and lipid domains (Fig. 6B). A good correlation between such structural variations and in-vitro expression efficiency was observed, disclosing promising application of pH-responsive LNPs in Nanomedicine.

3.3.4. *Novel formulation strategies*

SANS also represents a powerful tool to explore structural and morphological properties of novel LNPs formulations.

In this context, Liu et al. [317] recently developed a method to fabricate asymmetric lipid vesicles, which relies on lipid exchange

between lipid coated silica nanoparticles and originally symmetric vesicles. The efficiency of this approach was demonstrated through SANS, which detected asymmetry in vesicles composed of isotopically distinct PC lipids. The work of Jaudoin et al. [306] represents one of the first applications of SANS to hybrid vesicles-polymer systems, where authors investigated the microstructure of liposomes mixed with hyaluronic acid for drug delivery. Here, the SANS investigation aimed at assessing how the polymer affected the integrity and organization of liposomes, as well as the impact of hydrophilic drugs encapsulated within the hybrid system. Authors found that the integrity of liposomes was preserved in the polymer matrix and that liposomes surface (neutral, cationic, anionic, or anionic-PEGylated) is a key factor in controlling the overall microstructure of the hybrids (Fig. 6C).

Finally, recent studies pioneered the preparation and physicochemical characterization of lipid vesicles in ionic liquid [307,318–321]. Ionic liquids are a novel class of solvents of interest as a potential replacement of organic solvents in a vast range of chemical processes. In addition, they enable the self-assembly of a vast range of surfactants (including lipids) and, as such, represent a possible alternative to water in biotechnological applications. In this context, Bryant et al. [319] investigated the structure and properties of PC of varying composition in a library of different protic ionic liquids. Findings from SANS analysis showed that, as in water, longer acyl chain lengths determine increased bilayer melting temperatures and thicknesses. However, as a difference from the water phase behavior, the stability and structure of vesicles primarily depend on the underlying amphiphilic nanostructure of the ionic liquid, controlled by its anionic and cationic components. More recently, Manni et al. [307] detected a complex phase behavior of PC lipids in the ionic liquid ethylammonium nitrate, significantly different from the one in water. Specifically, SANS investigation showed that 1,2-distearoyl-sn-glycero-3-phosphocholine underwent a L_b-L_c phase transition upon heating, while 1-palmitoyl-2-oleoyl-sn-glycero-3-phosphocholine formed L_1 worm-like at high solvation (Fig. 6D). This was explained considering the larger solvation volume of the ionic liquid compared to water, inducing alterations in the lipid packing. In addition, recent investigations highlighted different membrane flexibility for PC vesicles when formed in ionic liquids [318,321]. In particular, Miao et al. [318] combined SANS with Neutron Spin-Echo to investigate egg PC vesicles in two different ionic liquids, and their water mixtures. They observed a decrease in the bilayer's bending modulus up to an order of magnitude compared to in water, while no significant changes in the structure of the vesicles' bilayer were detected.

4. Advances in SAXS and SANS methodologies to investigate lipid-based NPs

SAXS and SANS have been recently emerged as powerful techniques to probe dynamic processes involving LNPs. In particular, the high brilliance of Synchrotron X-ray sources allows for real-time monitoring of LNPs structural evolution, with resolution down to a few milliseconds. In addition, modern neutron sources enable the investigation of dynamic processes occurring at the molecular scale (i.e., within the lipid bilayer), through time-resolved SANS with smallest temporal step in the sub-second range. Such advancements in SAXS and SANS methods will be discussed in Sections 4.1 and 4.2, respectively. Finally, Section 4.3 will discuss innovative multi-techniques approaches recently introduced at Large Scale Facilities for X-rays and neutrons, enabling simultaneous in-situ combinations of SAXS and SANS with spectroscopic, calorimetric, and light scattering methods, as well as synchronized SAXS/SANS investigation.

4.1. Synchrotron TR-SAXS to probe the structural evolution of LNPs

With recent advances in Synchrotron radiation sources, TR-SAXS has emerged as an attractive approach for the real-time detection of dynamic structural transitions of LNPs, involving relatively fast processes within a few hundreds of milliseconds. The structural evolution of these lipid nano self-assemblies can be observed under different conditions: (i) upon exposure to *stimuli*, such as pH and ionic strength variations or application of light and electromagnetic fields (Section 4.1.1); (ii) upon interaction with biologically relevant molecules and engineered systems of interest for biomedical applications (Section 4.1.2). In this context, TR-SAXS is often combined with advanced set-ups [322,323] and dedicated microfluidic platforms [139,140,324,325], allowing for the continuous production and in situ structural characterization of LNPs, designed for drug delivery, diagnostic and theranostic applications.

4.1.1. Structural response to external stimuli

Nowadays, the advancements in time-resolved SAXS allows to characterize the dynamic structural response induced upon external *stimuli* [65,180,326] or *endogenous* stimuli, simulating specific processes and environments within the body [323,325,327,328]. Investigating such processes real-time is key for guiding the rational design of "smart" *stimuli*-responsive LNPs, as well as for gaining insights in the complex and dynamic transformations faced by LNPs in living organisms.

In this context, Hempt et al. [322] investigated the generation and evolution of lipid nanostructures during the process of milk digestion. To this purpose, they developed an experimental setup, shown in Fig. 7A, which enabled to combine flow-through TR-SAXS with an in vitro cell co-culture model simulating the small intestine. This set-up allowed to remotely trigger digestion by pumping pancreatic extract and monitor structural variations in the lipid phase of the milk emulsion droplets via Synchrotron TR-SAXS. Measurements revealed subsequent formation of different non-lamellar phases (i.e., from inverse micellar (L_2), to a lamellar (L_α), and inverse hexagonal (H_{II}) phase, coexisting with an Im3m cubic phase), possibly acting as carriers for poorly water-soluble milk components.

Similarly, Fong et al. [330] applied TR-SAXS to investigate the lipolysis of PC and PE vesicles, occurring during intestinal digestion. Results showed that lipid composition controls the structural transformation of lipid vesicles upon hydrolysis with the enzyme Phospholipase C, providing insights for the design of enzyme-responsive LNPs for drug delivery applications.

In addition, TR-SAXS has been applied to monitor pH-driven structural transition in LNPs in the physiological pH window. In this context, Yu et al. [62] recently combined TR-SAXS with rapid flow mixing to investigate the structural responsivity of LNPs containing two ionizable lipids widely employed for COVID-19 vaccine formulations, occurring upon gradual acidification as encountered in endosomes. TR-SAXS experiments provided direct evidence for the formation of structures with increasing membrane curvature (from inverse micellar, to inverse hexagonal and bicontinuous cubic, to lamellar phases) upon acidification, shedding lights on the link between the structure and endosomal escape of LNPs.

Moreover, recent investigations employed TR-SANS to elucidate the structural responsivity of LNPs to external *stimuli* (e.g., light or magnetic fields), aimed at developing lipid devices for controlled 'on-demand' drug release [65,180,326]. In this context, Caselli et al. [65] exploited real-time SAXS to monitor the structural changes in GMO cubosomes hybridized with superparamagnetic iron oxide nanoparticles (SPIONs) upon application of an alternating magnetic field (AMF). SAXS analysis revealed a transition from the cubic Pn3m to the inverse hexagonal phase within cubosomes, remotely triggered upon AMF application (Fig. 7B). This phase transformation, resulting from the local heat released by SPIONs upon AMF exposure, can be effectively applied to prompt the release of guest molecules from the water channels of cubosomes for controlled drug delivery applications.

4.1.2. Structural response to the interaction with molecules and engineered systems

TR-SAXS has been recently applied to shed light on the dynamic structural behavior of both lamellar and non-lamellar LNPs when

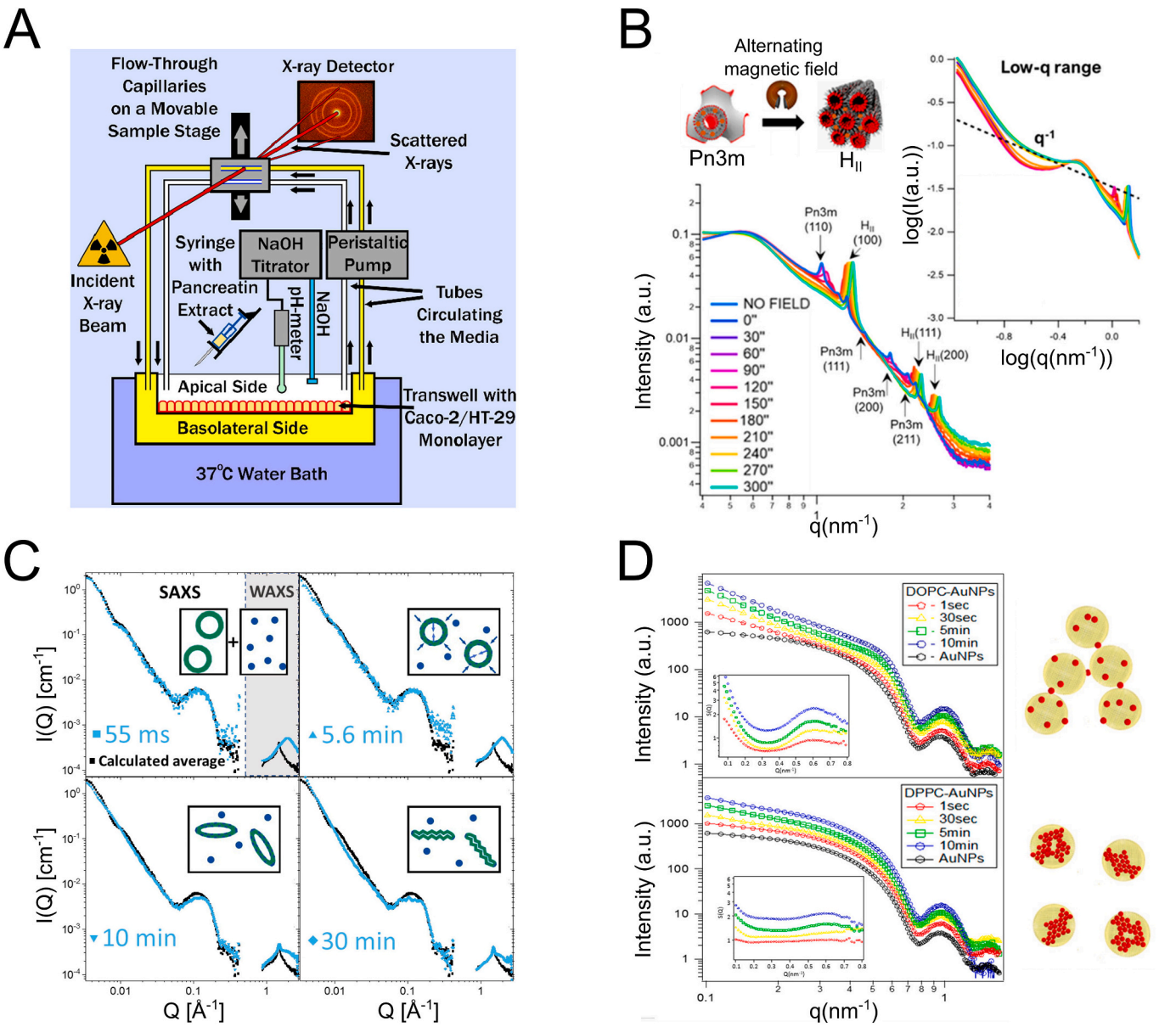

Fig. 7. (A) Experimental setup used for the in situ study of the milk digestion in the presence of a Caco-2/HT-29 co-colture. The formation of lipid nanostructures was simultaneously monitored through online SAXS on the apical and basolateral side of the cell layer. Reprinted from [322]; (B) SAXS profiles of monoolein cubosomes containing $9.5{\cdot}10^{-5}$ SPIONs per monoolein molecule, recorded at 25 °C under different times of exposure to the AMF. The Bragg reflexes of Pn3m and H_{II} phases are indexed in the graph with the corresponding Miller indices. The inset reports the detail of the low-q region of SAXS profiles, highlighting the rearrangement SPIONs into linear aggregates (identified by the emergence of a q^{-1} scattering feature) upon field exposure. Reprinted from [65]; (C) Time-resolved Small and Wide-Angle X-Ray Scattering (SAXS and WAXS, respectively) profiles of a 1:1 mass ratio mixture of DPPC and TX-100. Calculated average sum of the individual DPPC and TX-100 scattering patterns is also shown. The insets in the graphs illustrate the possible steps in the formation of the rippled bilamellar nanodiscs, involving increasing attraction between adjacent bilayers as TX-100 molecules insert into the vesicles, subsequently leading to a collapse of the spherical lipid vesicles into a flat doubled bilayer, followed by the formation of ordered ripples. Readapted from [329]; (D) TR-SAXS profiles of AuNPs-DOPC (top) and AuNPs-DPPC (bottom) hybrids collected at different times over 10 min of incubation. The inset shows the structure factor of the samples, with correlation peaks related to the center-to-center interparticle distances. Reprinted from [213].

interacting with biological and synthetic molecules, such as proteins [331,332], surfactants [329], and drug molecules [333].

In this context, Bjørnestad et al. [334] examined the interaction between unilamellar dipalmitoylphosphatidylcholine (DPPC) liposomes and Triton X-100 (TX-100, i.e., a non-ionic surfactant mostly used for biotechnological applications) at low temperatures, where the DPPC bilayer is resistant to solubilization. TR-SAXS investigation revealed the kinetics of collapse of DPPC vesicles upon addition of TX-100, leading to the formation of ordered rippled bilamellar disc structures (Fig. 7C), which prevent solubilization. Authors suggested that the bilayer ripple phase was adopted to counter-balance the packing constraints due to the insertion of TX-100 molecules, while the vesicles collapse was attributed to concomitant osmotic pressure and water structure destabilization effects. TR-SAXS also proved to be an effective tool to monitor interactions with more complex biomacromolecules, such as enzymes. In a recent work, Thorn et al. [332], explored GMO-based cubosomes as efficient bacterial-triggered drug delivery systems. They demonstrated that the release of different antibiotics from cubosomes can be triggered in the presence of bacteria by lipase-mediated digestion and disruption of the lipid nanocarriers. Specifically, TR-SAXS analysis showed that

non-regiospecific lipases induced the swelling and degradation of cubosomes via single-phase digestion kinetics, leading to the formation of lamellar structures with subsequent release of embedded drugs. Conversely, regiospecific lipases drove a two-phase digestion process, featuring a cubic to inverse hexagonal phase transition, which resulted in less effective drug release.

Further TR-SAXS investigations focused on the interaction of LNPs with engineered systems, from synthetic molecules to inorganic NPs, aimed at understanding relevant events at the nano-bio interface and inspiring the design of functional hybrid nanomaterials for biomedical applications.

The work of Cardellini et al. [213] represents a recent example, where authors investigated the temporal evolution of AuNPs adhesion and clustering onto fluid-phase and gel-phase PC target membranes, using TR-SAXS in combination with a stopped-flow apparatus. This investigation showed that AuNPs underwent fast aggregation onto fluid-phase PC vesicles, leading to fully AuNPs-decorated liposomes within few tens of seconds. In addition, the analysis of SAXS profiles over the

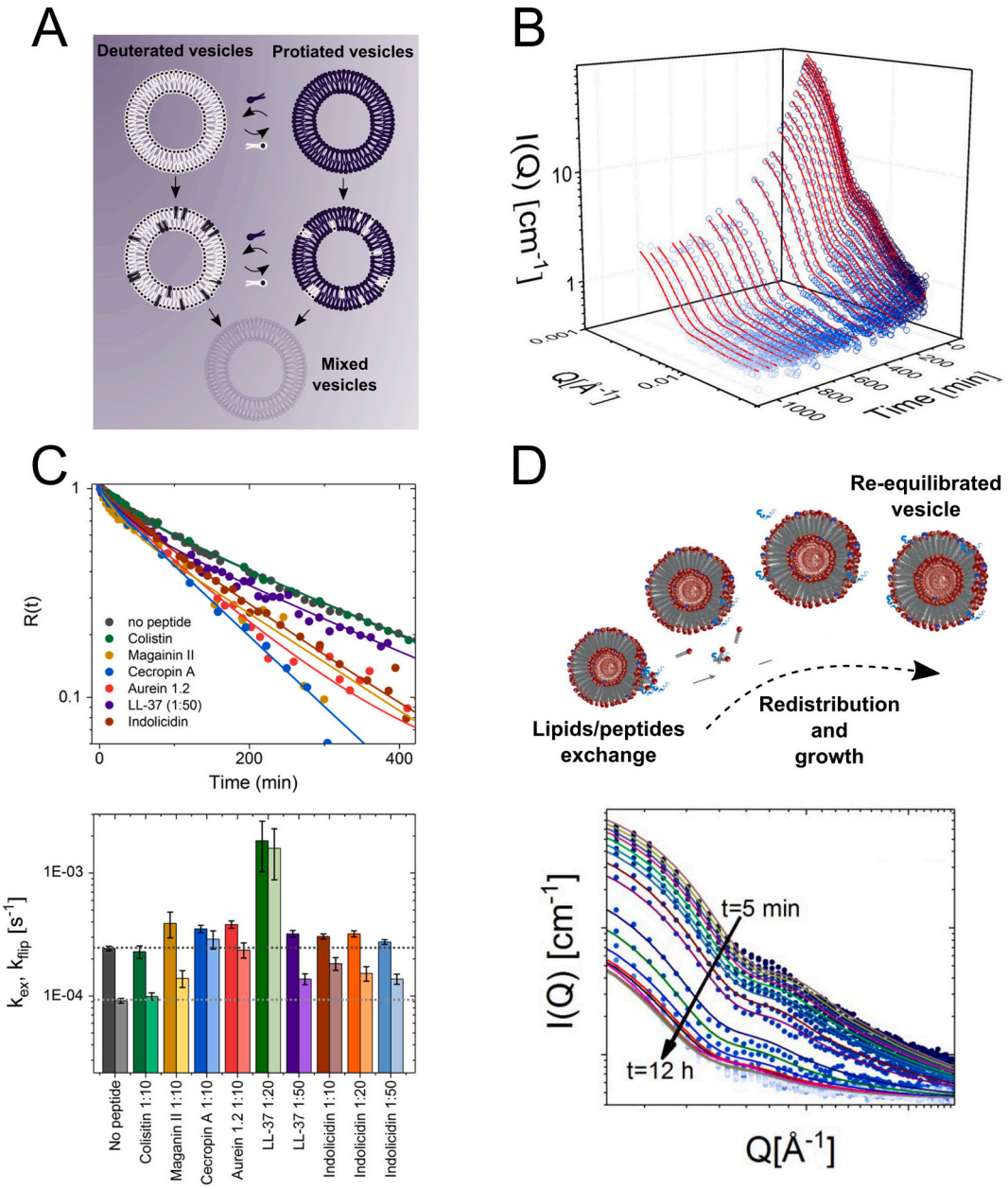

Fig. 8. (A) Conceptual scheme illustrating the methodology used to resolve intravesicle "flip−flop", and intervesicle exchange processes. This consists in mixing fully deuterated and hydrogenated vesicles in a 50/50% H_2O/D_2O mixture, which matches the average scattering length density of vesicles. Over time, contrast is lost due to molecular exchange processes, leading to a mixed population of vesicle and subsequent gradual decrease in neutron scattering intensity (as the one shown in Fig. 7B). Reprinted from [336]; (B) TR-SANS profiles with best curve fits for mixed 1,2-dimyristoyl-sn-glycero-3-phosphocholine (DMPC)/1,2-Dimyristoyl-sn-glycero-3-phosphoglycerol (DMPG) vesicles at 37 °C, obtained through the deuteration strategy described in Fig. 7A, showing a continuous decrease in the scattering intensity over time due to molecular rearrangements. Readapted from [336]; (C) Top: Rate of contrast decay (R(t)) and best curve fits for deuterated and hydrogenated vesicles, mixed in the absence and in the presence of different antimicrobial peptides. Bottom: Corresponding rate constants for intervesicle exchange (darker colours) and flip-flop (lighter colours) obtained from R(t) curve fittings (the top graph). Dotted lines indicate the intervesicle exchange and flip-flop constants for lipid vesicles without peptides. Reprinted from [334]; (D) TR-SANS profiles with best curve fits as a function of time obtained for deuterated and protiated DMPC/DMPG/1,2-Dimyristoyl-sn-glycero-3-phosphoethanolamine (DMPE)-PEG vesicles, mixed in the presence of indolicidin, at 37 °C. The top inset schematically illustrates the mechanism of size growth observed over time, induced by lipids/peptides molecular exchange and rearrangement. Reprinted from [336].

0–30s time-range (Fig. 7D), revealed a structural evolution of AuNPs aggregates from 1D to 2D clusters. In contrast, a slower and weaker interaction was observed onto gel-phase PC vesicles, suggesting partial NPs aggregation on the lipid membrane in the form of less densely packed AuNPs clusters. These TR-SAXS measurements highlighted that the physical state of vesicles controls the adhesion and aggregation of AuNPs onto the lipid shell, providing insights on the role of membrane physico-chemical features in nanobiointeractions.

4.2. TR-SANS to probe lipid diffusion in lipid-based NPs

In the last decade, TR-SANS has proved to be a powerful method to probe the dynamics of molecular diffusion in lipid vesicles (Section 4.2.1). In addition, it is label-free and non-headgroup specific, which represents a major advantage over other available methods for measuring kinetics of lipid exchange. Furthermore, recent investigations also applied TR-SANS to investigate how the dynamics of lipid exchange is affected upon interaction with relevant biological molecules, which will be discussed in Section 4.2.2.

4.2.1. Dynamics of transfer of lipids and sterols

TR-SANS can probe the diffusion of lipids in the bilayer, including transversal exchange across outer and inner bilayer leaflets (i.e., lipid flip-flop) or inter-vesicles lipid exchange.

This was proved for the first time by Nakano et al. [335], who applied TR-SANS to unilamellar PC vesicles. They demonstrated that the rates of inter-bilayer and trans-bilayer exchange can be independently determined with a single experiment, with a relatively simple approach. This relies on mixing two populations of vesicles with different isotopic composition, i.e., one with hydrogenated and the other with deuterated chain PC. While providing good contrast for fully hydrogenated or deuterated vesicles, the solvent D_2O/H_2O ratio is strategically set to match the SLD of vesicles with 50/50 hydrogenated/deuterated lipids (Fig. 8A). Upon mixing, lipid exchange and flip-flop induce a continuous decrease in the scattering intensity over time, as the SLD of vesicles approaches the contrast match point (Fig. 8B). The real-time monitoring of such intensity losses yields quantitative information on the kinetics of lipids transfer.

Later studies applied this strategy to other types of PC vesicles [337] or different environments [338]. For instance, Nguyen et al. [338] found that PC flip-flop is dramatically accelerated in methanol, a widely used solubilizing agent for lipid mixtures. Other groups extended the investigation to the transport of cholesterol in lipid membranes [114,339,340]. For instance, Breidigan et al. [340] applied TR-SANS to investigate the effects of different membrane environments on the inter- and intra-membrane movement of cholesterol. They found that the transport rate decreased with the degree of saturation of membrane lipids and by replacing PC with sphingomyelins.

4.2.2. Effects of the interaction with biomolecules

More recently, TR-SANS was applied to isolate and exclusively study the lipid flip-flop contribution and how this is affected by the interaction with different biological molecules, such as peptides or proteins [334,336,341–343]. This can be achieved by employing asymmetric vesicles with hydrogenated lipids in the inner leaflet and deuterated lipids in the outer. Among the examples, Nguyen et al. [341] investigated flip-flop exchange in asymmetric vesicles, made of hydrogenated (inner leaflet) and deuterated (outer leaflet) PC. They found that the interaction with different antimicrobial peptides (i.e., gramicidin, alamethicin, melittin) strongly enhances the rate of transversal lipid exchange. In addition, they highlighted that peptides adsorbed to the membrane surface might be more effective in eliminating asymmetry than when incorporated within the bilayer. A few years later, Nielsen et al. [334] investigated the effects of a wide library of natural antimicrobial peptides on bacteria-mimicking PC/PG/PE vesicles. Except for colistin, all the peptides accelerated phospholipid flip-flop (Fig. 8C), without involving membrane structural destabilization or pore-formation. These findings highlighted a common mechanism for the interaction of peptides with lipid membranes, possibly connected to their mode of action and in vivo antimicrobial activity. Marx et al. [344] extended the investigation to other antimicrobial peptides, namely frog peptides L18W-PGLa and magainin 2, and the lactoferricin derivative LF11–215. They found that the acceleration of lipid flip-flop in asymmetric PG/PE vesicles is highly peptide-specific, occurring at the fastest rate for L18W-PGLa.

In another recent study, Nielsen et al. [336] developed a new scattering model to analyze full Q-range TR-SANS profiles, allowing for simultaneous investigation of lipid flip-flop and vesicular growth. As a proof of concept, they applied this method to neat PC/PG/PE vesicles and to the same systems incubated with an accelerating substrate, i.e., indiolicine. They found that indiolicine increases the lipid flip-flop rate, while simultaneously prompting vesicles' size growth (Fig. 8D). This was explained in terms of peptide-induced lipid partial dissolution and reorganization, leading to larger and more polydisperse vesicles. In addition, TR-SANS experiments were performed on partially labelled lipid mixtures to isolate the dynamics of different lipid components. Thanks to this strategy, the authors pinpointed a faster exchange kinetics for PG than for PC lipids, while comparable increases in flip-flop rates were observed upon peptide addition.

Finally, recent works applied TR-SANS to investigate interactions with systems other than peptides, such as surfactans [329] or proteins [345]. In this context, Maric et al. [345] studied the kinetics of lipid exchange between PC vesicles and human lipoproteins. They discovered that lipid exchange occurs through two distinct mechanisms, i.e., particle collision and particle tethering to the lipid membrane. Moreover, they highlighted that these two modes of binding depend on the lipoprotein type and have different effects on lipid exchange.

4.3. Simultaneous multi-technique approaches

Recent technological advancements in neutron and synchrotron facilities enabled the combination of SANS or SAXS with complementary on-line techniques for a multi-method characterization occurring simultaneously on the same sample. These approaches offer unique possibilities to directly correlate the structural evolution occurring in a sample with modifications in its physical and chemical properties. Obtaining complementary data sets at the same time is vital for the study of processes with fast dynamics, for which ex-situ characterization of intermediates is not feasible and time-synchronization is required for a reliable integration of data from different techniques [346,347].

The high brilliance of Synchrotron sources offers a flexible environment for simultaneous characterization approaches, which were readily developed starting from the '90s [231,348,349]. Nowadays, these represent routine approaches at Synchrotron radiation facilities and include combinations of SAXS with Differential Scanning Calorimetry (DSC) [350], which allows for measuring heat exchanges within the samples during controlled temperature programs and relate them to specific structural transformations, e.g., bilayer melting transitions or mesoscale reorganizations in lipid systems [351]. In addition, SAXS can be integrated with on-line liquid chromatography [352,353]; this method is often employed to characterize polydisperse protein samples, allowing for isolating components of different size and collecting the scattering from homogeneous sub-populations, which strongly facilitates data analysis and interpretation. In addition, the concentration of specific protein subpopulations within the sample can be conveniently increased to enhance their scattering signal, which is particularly useful for weakly scattering samples or precious materials available in limited amounts. This approach could be potentially translated to the field of LNPs, e.g., to enable on-line purification and separation of vesicles of different size in polydisperse biological samples (e.g., of Extracellular Vesicles) or to identify different LNPs populations in synthetic formulations. Combinations of SAXS and TR-SAXS with spectroscopic

techniques, such as Raman [354,355], UV-Visible [356] and Fourier-transform infrared (FTIR) [357–359] spectroscopies, are also available, and can be used to simultaneously monitor the structure and the chemical state of a sample while undergoing transformations. While mostly applied to polymeric materials so far, integrated spectroscopic and scattering methods hold significant potential for the field of LPNs. This includes opportunities to investigate structural and conformational changes in lipid systems, monitor cargo encapsulation and elucidate specific interactions between lipid membranes and incorporated biomolecules or drugs.

SAXS can be also combined with Dynamic Light Scattering (DLS), for simultaneous investigation of nanoparticles structure and size. In this respect, the BioSAXS endstation of the EMBL beamline P12 at PETRA III (DESY, Hamburg, Germany) offers an advanced SAXS/DLS set-up featuring a multi-receiver four-channel DLS system to collect DLS data prior and during X-ray exposure [360]. This instrumentation provides an online screening of the hydrodynamic radius and polydispersity of particles, which can be readily combined with SAXS structural information for a multiscale investigation of particles properties. The combination of SAXS with rheology (Rheo-SAXS) represents another advancement in the field, which enables to monitor real-time structural deformations occurring in a sample in response to an applied shear stress [361]. This approach has been employed to probe the relationship between structure and rheological properties for a wide range of systems, including lamellar surfactant systems [362,363], colloidal suspensions [364,365] and polymer solutions [366].

Compared to X-ray, simultaneous multi-technique approaches involving neutrons have been only enabled in last years, thanks to recent technological advancements in high-intensity SANS instruments.

Among these, Jordan et al. [367] reported the first implementation of in situ size exclusion chromatography (SEC) on a SANS instrument, i.e., D22 (ILL, Grenoble, France). More recently, Johansen et al. [368] demonstrated that this dedicated SEC-SANS set-up is particularly useful to investigate complex soft matter systems, consisting in phospholipid nanodisc particles with embedded membrane proteins. Here, in situ SEC provided high sample homogeneity and purity, allowing for reducing the smearing of the scattering signal due to structural dispersity. This enabled a high-resolution structural analysis of originally polydisperse particles at a relatively low concentration, not achievable through a conventional SANS apparatus. Moreover, apparatus for simultaneous SANS and FTIR have been developed in recent years, and currently available at the instruments KWS2 [369] (Heinz Maier-Leibnitz Center (MLZ), Garching, Germany) and TAIKAN [370] (Material and Life Science Experimental Facility (MLF), Japan Proton Accelerator Research Complex (J-PARC), Tokai, Japan).

Similarly, SANS has been recently combined with Raman Spectroscopy at the NG7 30 m SANS instrument (NIST Center for Neutron Research (NCNR, Gaithersburg, MD) [371].

The integration of SANS with in situ DSC, a long-available feature in Synchrotron facilities, has faced several challenges connected to the lower flux of neutron sources, but also to scattering geometry and thermal control. These issues have been overcome only recently, with the development of a combined SANS/DCS system placed at Quokka instrument [372] (OPAL, ANSTO, Sydney, Australia), with accessible temperature range − 150-500 °C.

In addition, novel in situ DLS setups have been installed at SANS instruments in different Large Scale Facilities, including D11 [373] (ILL, Grenoble, France), ZOOM and LOQ [374] (ISIS Pulsed Neutron and Muon Source, Didcot, UK), SANS-I [375] (SINQ spallation source at Paul-Scherrer Institute (PSI) Villigen, Switzerland) and KWS2 [347] (MLZ), Garching, Germany). In this respect, Nawroth et al. [376] used synchronous time-resolved DLS and SANS at D11, combined with a stopped-flow device, to investigate the structural evolution of a bile salt-phospholipid micellar solution upon dilution, as model for the flow of bile secretion into the human digestive system. Crossed beam experiments of TR-DLS and TR-SANS revealed a stepwise formation of lipid vesicles, triggered upon digestion. The dynamics of the micelles to vesicles transition was characterized at a multiscale level, enabling direct correlation between particle size and molecular structure.

Analogously to Rheo-SAXS, combinations of SANS with rheology (Rheo-SANS) were made available at Large Scale Facilities, aimed at probing the microstructure–rheology relationship in soft matter samples [377,378]. In the context of surfactants, former SANS studies performed in-flow highlighted orientational transitions in lyotropic lamellar phases [379,380] or formation of multilamellar vesicles under shear stress [381]. Nowadays, TR-SANS in combination with rheology is widely used to investigate the dynamics of transformations and/or nonequilibrium microstructural transitions in surfactant systems under shear flow [382–384], which has relevant implications in the field of LNPs formulation. Recent advancements in this field feature the development of Capillary Rheo-SANS (CRSANS) [385], which uses pressure-driven flow through a long and flexible silica capillary to generate higher shear rates than in conventional Rheo-SANS experiments. The application of this method to LNPs would potentially enable to characterize their nanostructure and rheology at industrially-relevant shear rates, encountered under processing conditions such as extrusion, coating, spraying, or lubrication. Additionally, an in situ magnetorheological SANS setup has been recently installed at ILL [386], enabling simultaneous monitoring of the structural and rheological response of samples under magnetic field and shear flows. This new set-up offers intriguing possibilities for the investigation of hybrid LNPs containing magnetic inclusions, of relevance in the field of magnetically-guided drug delivery and/or magnetic fluid hyperthermia.

Finally, SAXS/SANS simultaneous analysis represents the latest frontier of in situ multi-technique characterization, recently introduced at D22 (ILL, Grenoble, France) [387,388]. Here, an advanced portable SAXS system, mounted on a standalone metal rack, has been successfully installed and tested in combination with SANS. Through this setup, SAXS and SANS data can be acquired from the same sample volume and fitted simultaneously using a common structural model. Remarkably, this novel instrumentation will allow in situ TR-SANS and SAXS, revealing complementary information on structural evolution occurring in the sample, i.e., from molecular to nanoscale rearrangements. Moreover, probing the same sample under different contrasts (i.e., provided by neutron and X-ray probes) will allow for accessing simultaneous information on different compartments in multicomponent systems. Overall, this SAXS/SANS combination represents a promising avenue to explore innovative LNPs of hybrid nature, and to investigate their molecular interactions with unprecedented accuracy.

5. Conclusions

LNPs represent the most promising class of nanocarriers for the delivery of hydrophobic and hydrophilic drugs, peptides, proteins, nucleic acids, and imaging agents. In addition, they offer opportunities for smart hybrid platforms engineering, where inorganic nanomaterials are incorporated within a structurally responsive lipid matrix.

Recent years have witnessed a tremendous growth in LNPs research, especially aimed at developing non-lamellar LNPs for next-generation Nanomedicine. Despite this, LNPs currently approved for clinical use are relatively few and primarily limited to liposome-based formulations. Understanding the structure-function relationship in LNPs, especially in physiological environments and upon interaction with biologically relevant molecules, represents a first step to overcome this translation bottleneck. *In this respect, more efforts should be devoted to couple biological investigation and performance studies on LNPs with a systematic screening of LNPs structure and transformations in biologically relevant conditions*. Small-angle X-ray and neutron scattering are robust and versatile techniques that serve perfectly to this purpose, offering ensemble-averaged and label-free structural information. The relevance of SAXS and SANS in this research field is increasingly recognized, as attested by the rapid broadening of users at Large Scale facilities,

including researchers from biomedical and pharmaceutical communities.

In this review, we discussed the state-of-the-art in SAXS and SANS applied to LNPs research, aimed at highlighting benefits and unique opportunities that these techniques bring to the field. A user-friendly description of small-angle scattering, including a basic introduction to data analysis, was also included (Section 1) to assist new users or researchers with diverse backgrounds. Throughout the review, a special focus was placed on structural information and interactions of LNPs with biomolecules and/or relevant physiological environments, of interest for their application in the medical field.

Overall, the spreading of SAXS and SANS across the biomedical community, along with the ongoing advancements in scattering technology, foretells a rapid evolution in LNPs research in the coming years. In addition, the emergence of new advanced approaches, outlined in Section 4, will open new avenues to explore dynamic transformations in LNPs within biological environments, possibly bridging the gap between conceptual design and clinical translation of LNPs.

CRediT authorship contribution statement

Lucrezia Caselli: Conceptualization, Methodology, Supervision, Writing – original draft, Writing – review & editing. **Laura Conti:** Writing – original draft. **Ilaria De Santis:** Writing – original draft. **Debora Berti:** Conceptualization, Funding acquisition, Methodology, Supervision, Writing – original draft, Writing – review & editing.

Declaration of competing interest

The authors declare that they have no known competing financial interests or personal relationships that could have appeared to influence the work reported in this paper.

Acknowledgments

This work has been supported by the European Community through the BOW project (H2020-EIC-FETPROACT2019, ID 952183) and by PRIN 2022 PNRR: "Lipid Nanovectors for the Delivery of Nucleic Acids: a Composition-Structure-Function Relationship Approach (Lancelot)" - P2022RBF5P - CUP B53D23025810001 - "Finanziato dall'Unione europea – Next Generation EU" - Missione 4, Componente 2, Investimento 1.1 - Avviso MUR D.D. 1409 del 14/09/2022. The authors also acknowledge MUR-Italy ("Progetto Dipartimenti di Eccellenza 2018–2022, ref B96C1700020008" and "Dipartimenti di Eccellenza 2023-2027 (DICUS 2.0)" allocated to the Department of Chemistry "Ugo Schiff") and the Center for Colloid and Surface Science (CSGI) for economic support.

Data availability

No data was used for the research described in the article.

References

[1] Aleandri S, Mezzenga R. The physics of Lipidic Mesophase delivery systems. Phys Today 2020;73(7):38–44. https://doi.org/10.1063/PT.3.4522.
[2] Blanco-Fernández G, Blanco-Fernandez B, Fernández-Ferreiro A, Otero-Espinar FJ. Lipidic Lyotropic liquid crystals: insights on biomedical applications. Adv Colloid Interface Sci 2023;313:102867. https://doi.org/10.1016/j.cis.2023.102867.
[3] Mezzenga R, Seddon JM, Drummond CJ, Boyd BJ, Schröder-Turk GE, Sagalowicz L. Nature-inspired design and application of Lipidic Lyotropic liquid crystals. Adv Mater 2019;31(35):1900818. https://doi.org/10.1002/adma.201900818.
[4] Seddon JM, Templer RH, Raynes EP, Boden N. Cubic phases of self-assembled amphiphilic aggregates. Philos Trans R Soc Lond Ser Phys Eng Sci 1997;344(1672):377–401. https://doi.org/10.1098/rsta.1993.0096.
[5] Shearman GC, Ces O, Templer RH, Seddon JM. Inverse Lyotropic phases of lipids and membrane curvature. J Phys Condens Matter 2006;18(28):S1105. https://doi.org/10.1088/0953-8984/18/28/S01.
[6] Tiddy GJT. Surfactant-water liquid crystal phases. Phys Rep 1980;57(1):1–46. https://doi.org/10.1016/0370-1573(80)90041-1.
[7] Barriga HMG, Holme MN, Stevens MM. Cubosomes: the next generation of smart lipid nanoparticles? Angew Chem Int Ed 2019;58(10):2958–78. https://doi.org/10.1002/anie.201804067.
[8] Larsson K. Aqueous dispersions of cubic lipid–water phases. Curr Opin Colloid Interface Sci 2000;5(1):64–9. https://doi.org/10.1016/S1359-0294(00)00040-6.
[9] Gustafsson J, Ljusberg-Wahren H, Almgren M, Larsson K. Submicron particles of reversed lipid phases in water stabilized by a nonionic amphiphilic polymer. Langmuir 1997;13(26):6964–71. https://doi.org/10.1021/la970566+.
[10] Chong JYT, et al. Steric stabilizers for cubic phase lyotropic liquid crystal nanodispersions (cubosomes). In: Advances in planar lipid bilayers and liposomes. 21. Academic Press; 2015. p. 131–87. https://doi.org/10.1016/bs.adplan.2014.11.001.
[11] Fong C, Le T, Drummond CJ. Lyotropic liquid crystal engineering–ordered nanostructured small molecule amphiphile self-assembly materials by design. Chem Soc Rev 2012;41(3):1297–322. https://doi.org/10.1039/C1CS15148G.
[12] Ridolfi A, Humphreys B, Caselli L, Montis C, Nylander T, Berti D, et al. Nanoscale structural and mechanical characterization of thin bicontinuous cubic phase lipid films. Colloids Surf B Biointerfaces 2022;210:112231. https://doi.org/10.1016/j.colsurfb.2021.112231.
[13] Larsson K. Cubic lipid-water phases: structures and biomembrane aspects. J Phys Chem 1989;93(21):7304–14. https://doi.org/10.1021/j100358a010.
[14] Seddon JM. Structure of the inverted hexagonal (HII) phase, and non-lamellar phase transitions of lipids. Biochim Biophys Acta BBA - Rev Biomembr 1990;1031(1):1–69. https://doi.org/10.1016/0304-4157(90)90002-T.
[15] Gilbert J, Valldeperas M, Dhayal SK, Barauskas J, Dicko C, Nylander T. Immobilisation of β-galactosidase within a lipid sponge phase: structure, stability and kinetics characterisation. Nanoscale 2019;11(44):21291–301. https://doi.org/10.1039/C9NR06675F.
[16] Valldeperas M, Wiśniewska M, Ram-On M, Kesselman E, Danino D, Nylander T, et al. Sponge phases and nanoparticle dispersions in aqueous mixtures of mono- and diglycerides. Langmuir 2016;32(34):8650–9. https://doi.org/10.1021/acs.langmuir.6b01356.
[17] Cárdenas M, Campbell RA, Yanez Arteta M, Lawrence MJ, Sebastiani F. Review of structural design guiding the development of lipid nanoparticles for nucleic acid delivery. Curr Opin Colloid Interface Sci 2023;66:101705. https://doi.org/10.1016/j.cocis.2023.101705.
[18] Hou X, Zaks T, Langer R, Dong Y. Lipid nanoparticles for mRNA delivery. Nat Rev Mater 2021;6(12):1078–94. https://doi.org/10.1038/s41578-021-00358-0.
[19] Liu P, Chen G, Zhang J. A review of liposomes as a drug delivery system: current status of approved products, regulatory environments, and future perspectives. Molecules 2022;27(4):1372. https://doi.org/10.3390/molecules27041372.
[20] Pattni BS, Chupin VV, Torchilin VP. New developments in liposomal drug delivery. Chem Rev 2015;115(19):10938–66. https://doi.org/10.1021/acs.chemrev.5b00046.
[21] Zhai J, Fong C, Tran N, Drummond CJ. Non-lamellar Lyotropic liquid crystalline lipid nanoparticles for the next generation of nanomedicine. ACS Nano 2019;13(6):6178–206. https://doi.org/10.1021/acsnano.8b07961.
[22] Salvi VR, Pawar P. Nanostructured lipid carriers (NLC) system: a novel drug targeting carrier. J Drug Deliv Sci Technol 2019;51:255–67. https://doi.org/10.1016/j.jddst.2019.02.017.
[23] Angelova A, Garamus VM, Angelov B, Tian Z, Li Y, Zou A. Advances in structural Design of Lipid-Based Nanoparticle Carriers for delivery of macromolecular drugs, phytochemicals and anti-tumor agents. Adv Colloid Interface Sci 2017;249:331–45. https://doi.org/10.1016/j.cis.2017.04.006.
[24] Fornasier M, Murgia S. Non-lamellar lipid liquid crystalline nanoparticles: a smart platform for nanomedicine applications. Front Soft Matter 2023;3:1109508. https://doi.org/10.3389/frsfm.2023.1109508.
[25] Karami Z, Hamidi M. Cubosomes: remarkable drug delivery potential. Drug Discov Today 2016;21(5):789–801. https://doi.org/10.1016/j.drudis.2016.01.004.
[26] Azmi IDM, Moghimi SM, Yaghmur A. Cubosomes and Hexosomes as versatile platforms for drug delivery. Ther Deliv 2015;6(12):1347–64. https://doi.org/10.4155/tde.15.81.
[27] Varghese R, Salvi S, Sood P, Kulkarni B, Kumar D. Cubosomes in Cancer drug delivery: a review. Colloid Interface Sci Commun 2022;46:100561. https://doi.org/10.1016/j.colcom.2021.100561.
[28] Mazur F, Bally M, Städler B, Chandrawati R. Liposomes and lipid bilayers in biosensors. Adv Colloid Interface Sci 2017;249:88–99. https://doi.org/10.1016/j.cis.2017.05.020.
[29] Liu Q, Boyd BJ. Liposomes in biosensors. Analyst 2012;138(2):391–409. https://doi.org/10.1039/C2AN36140J.
[30] Bulbake U, Doppalapudi S, Kommineni N, Khan W. Liposomal formulations in clinical use: an updated review. Pharmaceutics 2017;9(2):12. https://doi.org/10.3390/pharmaceutics9020012.
[31] Andra VVSNL, Pammi SVN, Bhatraju LVKP, Ruddaraju LK. A comprehensive review on novel liposomal methodologies, commercial formulations, clinical trials and patents. BioNanoScience 2022;12(1):274–91. https://doi.org/10.1007/s12668-022-00941-x.
[32] Caboi F, Amico GS, Pitzalis P, Monduzzi M, Nylander T, Larsson K. Addition of hydrophilic and lipophilic compounds of biological relevance to the Monoolein/water system. I Phase behavior. Chem Phys Lipids 2001;109(1):47–62. https://doi.org/10.1016/s0009-3084(00)00200-0.
[33] Tenchov R, Bird R, Curtze AE, Zhou Q. Lipid nanoparticles - from liposomes to mRNA vaccine delivery, a landscape of research diversity and advancement. ACS Nano 2021;15(11):16982–7015. https://doi.org/10.1021/acsnano.1c04996.

[34] Chang C, Meikle TG, Drummond CJ, Yang Y, Conn CE. Comparison of Cubosomes and liposomes for the encapsulation and delivery of curcumin. Soft Matter 2021; 17(12):3306–13. https://doi.org/10.1039/D0SM01655A.
[35] Vant Hag L, Li X, Meikle TG, Hoffmann SV, Jones NC, Pedersen JS, et al. How peptide molecular structure and charge influence the nanostructure of lipid Bicontinuous cubic Mesophases: model synthetic WALP peptides provide insights. Langmuir 2016;32(27):6882–94. https://doi.org/10.1021/acs.langmuir.6b01058.
[36] Nazaruk E, Majkowska-Pilip A, Bilewicz R. Lipidic cubic-phase nanoparticles—Cubosomes for efficient drug delivery to cancer cells. ChemPlusChem 2017;82(4):570–5. https://doi.org/10.1002/cplu.201600534.
[37] Phan S, Fong W-K, Kirby N, Hanley T, Boyd BJ. Evaluating the link between self-assembled Mesophase structure and drug release. Int J Pharm 2011;421(1): 176–82. https://doi.org/10.1016/j.ijpharm.2011.09.022.
[38] Boyd BJ, Whittaker DV, Khoo S-M, Davey G. Lyotropic liquid crystalline phases formed from Glycerate surfactants as sustained release drug delivery systems. Int J Pharm 2006;309(1):218–26. https://doi.org/10.1016/j.ijpharm.2005.11.033.
[39] Drummond CJ, Fong C. Surfactant self-assembly objects as novel drug delivery vehicles. Curr Opin Colloid Interface Sci 1999;4(6):449–56. https://doi.org/10.1016/S1359-0294(00)00020-0.
[40] Zabara A, Mezzenga R. Controlling molecular transport and sustained drug release in lipid-based liquid crystalline Mesophases. J Control Release 2014;188: 31–43. https://doi.org/10.1016/j.jconrel.2014.05.052.
[41] Negrini R, Mezzenga R. pH-responsive Lyotropic liquid crystals for controlled drug delivery. Langmuir 2011;27(9):5296–303. https://doi.org/10.1021/la200591u.
[42] Fong W-K, Hanley T, Boyd BJ. Stimuli responsive liquid crystals provide 'on-demand' drug delivery *in vitro* and *in vivo*. J Control Release 2009;135(3):218–26. https://doi.org/10.1016/j.jconrel.2009.01.009.
[43] Zhai J, Scoble JA, Li N, Lovrecz G, Waddington LJ, Tran N, et al. Epidermal growth factor receptor-targeted lipid nanoparticles retain self-assembled nanostructures and provide high specificity. Nanoscale 2015;7(7):2905–13. https://doi.org/10.1039/C4NR05200E.
[44] Deshpande S, Singh N. Influence of Cubosome surface architecture on its cellular uptake mechanism. Langmuir 2017;33(14):3509–16. https://doi.org/10.1021/acs.langmuir.6b04423.
[45] Conn CE, Mulet X, Moghaddam MJ, Darmanin C, Waddington LJ, Sagnella SM, et al. Enhanced uptake of an integral membrane protein, the dopamine D2L receptor, by cubic nanostructured lipid nanoparticles doped with Ni(II) chelated EDTA Amphiphiles. Soft Matter 2011;7(2):567–78. https://doi.org/10.1039/C0SM00790K.
[46] Zheng L, Bandara SR, Tan Z, Leal C. Lipid nanoparticle topology regulates endosomal escape and delivery of RNA to the cytoplasm. Proc Natl Acad Sci 2023; 120(27):e2301067120. https://doi.org/10.1073/pnas.2301067120.
[47] Tran N, Bye N, Moffat BA, Wright DK, Cuddihy A, Hinton TM, et al. Dual-modality NIRF-MRI Cubosomes and Hexosomes: high throughput formulation and in vivo biodistribution. Mater Sci Eng C Mater Biol Appl 2017;71:584–93. https://doi.org/10.1016/j.msec.2016.10.028.
[48] Strachan JB, Dyett BP, Nasa Z, Valery C, Conn CE. Toxicity and cellular uptake of lipid nanoparticles of different structure and composition. J Colloid Interface Sci 2020;576:241–51. https://doi.org/10.1016/j.jcis.2020.05.002.
[49] Pham AC, Clulow AJ, Boyd BJ. Formation of self-assembled Mesophases during lipid digestion. Front Cell Dev Biol 2021;9:657886. https://doi.org/10.3389/fcell.2021.657886.
[50] Ke PC, Lin S, Parak WJ, Davis TP, Caruso F. A decade of the protein Corona. ACS Nano 2017;11(12):11773–6. https://doi.org/10.1021/acsnano.7b08008.
[51] Cedervall T, Lynch I, Lindman S, Berggård T, Thulin E, Nilsson H, et al. Understanding the nanoparticle–protein corona using methods to quantify exchange rates and affinities of proteins for nanoparticles. Proc Natl Acad Sci 2007;104(7):2050–5. https://doi.org/10.1073/pnas.0608582104.
[52] Francia V, Schiffelers RM, Cullis PR, Witzigmann D. The biomolecular Corona of lipid nanoparticles for gene therapy. Bioconjug Chem 2020;31(9):2046–59. https://doi.org/10.1021/acs.bioconjchem.0c00366.
[53] Chen D, Ganesh S, Wang W, Amiji M. The role of surface chemistry in serum protein Corona-mediated cellular delivery and gene silencing with lipid nanoparticles. Nanoscale 2019;11(18):8760–75. https://doi.org/10.1039/C8NR09855G.
[54] Mirshafiee V, Kim R, Park S, Mahmoudi M, Kraft ML. Impact of protein pre-coating on the protein Corona composition and nanoparticle cellular uptake. Biomaterials 2016;75:295–304. https://doi.org/10.1016/j.biomaterials.2015.10.019.
[55] Aliakbarinodehi N, Gallud A, Mapar M, Wesén E, Heydari S, Jing Y, et al. Interaction kinetics of individual mRNA-containing lipid nanoparticles with an endosomal membrane mimic: dependence on pH, protein Corona formation, and lipoprotein depletion. ACS Nano 2022;16(12):20163–73. https://doi.org/10.1021/acsnano.2c04829.
[56] Richtering W, Alberg I, Zentel R. Nanoparticles in the biological context: surface morphology and protein Corona formation. Small 2020;16(39):2002162. https://doi.org/10.1002/smll.202002162.
[57] Madathiparambil Visalakshan R, González García LE, Benzigar MR, Ghazaryan A, Simon J, Mierczynska-Vasilev A, et al. The influence of nanoparticle shape on protein Corona formation. Small 2020;16(25):2000285. https://doi.org/10.1002/smll.202000285.
[58] El Mohamad M, Han Q, Clulow AJ, Cao C, Safdar A, Stenzel M, et al. Regulating the structural polymorphism and protein Corona composition of Phytantriol-based lipid nanoparticles using choline ionic liquids. J Colloid Interface Sci 2024; 657:841–52. https://doi.org/10.1016/j.jcis.2023.12.005.
[59] Sebastiani F, Yanez Arteta M, Lerche M, Porcar L, Lang C, Bragg RA, et al. Apolipoprotein E binding drives structural and compositional rearrangement of mRNA-containing lipid nanoparticles. ACS Nano 2021;15(4):6709–22. https://doi.org/10.1021/acsnano.0c10064.
[60] Fong W-K, Negrini R, Vallooran JJ, Mezzenga R, Boyd BJ. Responsive self-assembled nanostructured lipid Systems for Drug Delivery and Diagnostics. J Colloid Interface Sci 2016;484:320–39. https://doi.org/10.1016/j.jcis.2016.08.077.
[61] Xu Z, Seddon JM, Beales PA, Rappolt M, Tyler AII. Breaking isolation to form new networks: pH-triggered changes in connectivity inside lipid nanoparticles. J Am Chem Soc 2021;143(40):16556–65. https://doi.org/10.1021/jacs.1c06244.
[62] Yu H, Angelova A, Angelov B, Dyett B, Matthews L, Zhang Y, et al. Real-time pH-dependent self-assembly of Ionisable lipids from COVID-19 vaccines and in situ nucleic acid complexation. Angew Chem Int Ed 2023;62(35):e202304977. https://doi.org/10.1002/anie.202304977.
[63] Rajesh S, Zhai J, Drummond CJ, Tran N. Synthetic Ionizable Aminolipids induce a pH dependent inverse hexagonal to Bicontinuous cubic Lyotropic liquid crystalline phase transition in Monoolein nanoparticles. J Colloid Interface Sci 2021;589:85–95. https://doi.org/10.1016/j.jcis.2020.12.060.
[64] Di Cola E, Grillo I, Ristori S. Small angle X-Ray and Neutron Scattering: powerful tools for studying the structure of drug-loaded liposomes. Pharmaceutics 2016;8 (2):10. https://doi.org/10.3390/pharmaceutics8020010.
[65] Caselli L, Mendozza M, Muzzi B, Toti A, Montis C, Mello T, et al. Lipid cubic Mesophases combined with superparamagnetic Iron oxide nanoparticles: a hybrid multifunctional platform with tunable magnetic properties for Nanomedical applications. Int J Mol Sci 2021;22(17):9268. https://doi.org/10.3390/ijms22179268.
[66] Mendozza M, Montis C, Caselli L, Wolf M, Baglioni P, Berti D. On the Thermotropic and Magnetotropic phase behavior of lipid liquid crystals containing magnetic nanoparticles. Nanoscale 2018;10(7):3480–8. https://doi.org/10.1039/C7NR08478A.
[67] Montis C, Castroflorio B, Mendozza M, Salvatore A, Berti D, Baglioni P. Magnetocubosomes for the delivery and controlled release of therapeutics. J Colloid Interface Sci 2015;449:317–26. https://doi.org/10.1016/j.jcis.2014.11.056.
[68] Salvatore A, Montis C, Berti D, Baglioni P. Multifunctional Magnetoliposomes for sequential controlled release. ACS Nano 2016;10(8):7749–60. https://doi.org/10.1021/acsnano.6b03194.
[69] Mendozza M, Caselli L, Salvatore A, Montis C, Berti D. Nanoparticles and organized lipid assemblies: from interaction to Design of Hybrid Soft Devices. Soft Matter 2019;15(44):8951–70. https://doi.org/10.1039/C9SM01601E.
[70] Zhigaltsev IV, Tam YYC, Kulkarni JA, Cullis PR. Synthesis and characterization of hybrid lipid nanoparticles containing gold nanoparticles and a Weak Base drug. Langmuir 2022;38(25):7858–66. https://doi.org/10.1021/acs.langmuir.2c01221.
[71] Hollamby MJ. Practical applications of small-angle neutron scattering. Phys Chem Chem Phys 2013;15(26):10566–79. https://doi.org/10.1039/C3CP50293G.
[72] Gräwert M, Svergun D. A Beginner's guide to solution small-angle X-Ray Scattering (SAXS). Biochem 2020;42(1):36–42. https://doi.org/10.1042/BIO04201036.
[73] Svergun DI, Dmitriĭ I. Structure analysis by small-angle X-Ray and Neutron scattering. New York: Plenum press; 1987.
[74] Svergun DI. Small-angle X-Ray and Neutron Scattering as a tool for structural systems biology. Biol Chem 2010;391(7):737–43. https://doi.org/10.1515/BC.2010.093.
[75] Sivia D S. *Elementary scattering theory: for X-ray and neutron users*. Oxford University Press; 2011.
[76] Hamley Ian W. *Small-angle scattering: theory, instrumentation, data, and applications*. John Wiley & Sons; 2021.
[77] Jauncey GEM. The Scattering of X-rays and Bragg's Law. Proc Natl Acad Sci 1924; 10(2):57–60. https://doi.org/10.1073/pnas.10.2.57.
[78] Gommes CJ, Jaksch S, Frielinghaus H. Small-angle scattering for beginners. J Appl Cryst 2021;54(6):1832–43. https://doi.org/10.1107/S1600576721010293.
[79] Fritz G, Glatter O. Structure and interaction in dense colloidal systems: evaluation of scattering data by the generalized indirect Fourier transformation method. J Phys Condens Matter 2006;18(36):S2403. https://doi.org/10.1088/0953-8984/18/36/S14.
[80] Guinier A, Fournet G, Walker CB, Yudowitch KL. *Small-angle Scattering of X-rays*. New York: Wiley; 1955.
[81] Lang J, Zana R. Surfactant solutions: New methods of investigation. Surfactant science series 1987;22. 405-4.
[82] Doucet M, Cho JH, Alina G, Attala Z, Bakker J, Bouwman W, et al. SasView Version 5.0.3. 2020. https://doi.org/10.5281/zenodo.3930098.
[83] Breßler I, Kohlbrecher J, Thünemann AF. SASfit: a tool for small-angle Scattering data analysis using a library of analytical expressions. J Appl Cryst 2015;48(Pt 5): 1587–98. https://doi.org/10.1107/S1600576715016544.
[84] Kline SR. Reduction and analysis of SANS and USANS data using IGOR pro. J Appl Cryst 2006;39(6):895–900. https://doi.org/10.1107/S0021889806035059.
[85] Ilavsky J, Jemian PR. Irena: tool suite for modeling and analysis of small-angle Scattering. J Appl Cryst 2009;42(2):347–53. https://doi.org/10.1107/S0021889809002222.

[86] Shah RM, Mata JP, Bryant G, de Campo L, Ife A, Karpe AV, et al. Structure analysis of solid lipid nanoparticles for drug delivery: a combined USANS/SANS study. Part Part Syst Charact 2019;36(1):1800359. https://doi.org/10.1002/ppsc.201800359.

[87] Jeffries CM, et al. Small-angle X-ray and neutron scattering. Nature Reviews Methods Primers 2021;1(1):70.

[88] Narayanan T, Konovalov O. Synchrotron scattering methods for nanomaterials and soft matter research. Materials 2020;13(3):752. https://doi.org/10.3390/ma13030752.

[89] Narayanan T, Sztucki M, Zinn T, Kieffer J, Homs-Puron A, Gorini J, et al. Performance of the time-resolved ultra-small-angle X-Ray Scattering beamline with the extremely brilliant source. J Appl Cryst 2022;55(Pt 1):98–111. https://doi.org/10.1107/S1600576721012693.

[90] Bayrak M, Mata J, Conn C, Floury J, Logan A. Application of small angle Scattering (SAS) in structural characterisation of casein and casein-based products during digestion. Food Res Int 2023;169:112810. https://doi.org/10.1016/j.foodres.2023.112810.

[91] Hyde S, Ninham BW, Andersson S, Larsson K, Landh T, Blum Z, et al. Chapter 3 - Molecular forces and self-assembly. In: Hyde S, Ninham BW, Andersson S, Larsson K, Landh T, Blum Z, Lidin S, editors. The Language of Shape. Amsterdam: Elsevier Science B.V.; 1997. p. 87–140. https://doi.org/10.1016/B978-044481538-5/50004-6.

[92] Hyde S, Ninham BW, Andersson S, Larsson K, Landh T, Blum Z, et al. Chapter 4 - Beyond Flatland: the geometric forms due to self-assembly. In: Hyde S, Ninham BW, Andersson S, Larsson K, Landh T, Blum Z, Lidin S, editors. The Language of Shape. Amsterdam: Elsevier Science B.V.; 1997. p. 141–97. https://doi.org/10.1016/B978-044481538-5/50005-8.

[93] Hyde S, Ninham BW, Andersson S, Larsson K, Landh T, Blum Z, et al. Chapter 5 - Lipid self-assembly and function in biological systems. In: Hyde S, Ninham BW, Andersson S, Larsson K, Landh T, Blum Z, Lidin S, editors. The Language of Shape. Amsterdam: Elsevier Science B.V.; 1997. p. 199–235. https://doi.org/10.1016/B978-044481538-5/50006-X.

[94] Hyde S. Identification of Lyotropic liquid crystalline Mesophases. In: Handbook of applied surface and colloid chemistry. 2; 2001. p. 299–332.

[95] Tyler AII, Law RV, Seddon JM. X-ray diffraction of lipid model membranes. In: Owen DM, editor. Methods in Membrane Lipids. Methods in Molecular Biology. New York, NY: Springer; 2015. p. 199–225. https://doi.org/10.1007/978-1-4939-1752-5_16.

[96] Templer RH. Chapter 3 - Polymorphism of lipid-water systems. In: Seddon JM, Lipowsky R, Sackmann E, editors. Handbook of Biological Physics. 1. North-Holland: Structure and Dynamics of Membranes; 1995. p. 97–160. https://doi.org/10.1016/S1383-8121(06)80020-5.

[97] Reese W, Strango I, Dell R, Tristram-Nagle S, Harper P. Structural insights into the cubic–hexagonal phase transition kinetics of monoolein modulated by sucrose solutions. Phys Chem Chem Phys 2015;17(14):9194–204. https://doi.org/10.1039/C5CP00175G.

[98] Kulkarni CV, Wachter W, Iglesias-Salto G, Engelskirchen S, Ahualli S. Monoolein: a magic lipid? Phys Chem Chem Phys 2011;13(8):3004–21. https://doi.org/10.1039/C0CP01539C.

[99] Brooks NJ. Pressure effects on lipids and bio-membrane assemblies. IUCrJ 2014;1(Pt 6):470–7. https://doi.org/10.1107/S2052252514019551.

[100] Vacklin H, Khoo BJ, Madan KH, Seddon JM, Templer RH. The bending elasticity of 1-Monoolein upon relief of packing stress. Langmuir 2000;16(10):4741–8. https://doi.org/10.1021/la991408g.

[101] Hyde S, Ninham BW, Andersson S, Larsson K, Landh T, Blum Z, et al. Chapter 1 - The mathematics of curvature. In: Hyde S, Ninham BW, Andersson S, Larsson K, Landh T, Blum Z, Lidin S, editors. The Language of Shape. Amsterdam: Elsevier Science B.V.; 1997. p. 1–42. https://doi.org/10.1016/B978-044481538-5/50002-2.

[102] Hyde ST. Bicontinuous structures in Lyotropic liquid crystals and crystalline hyperbolic surfaces. Curr Opin Solid State Mater Sci 1996;1(5):653–62. https://doi.org/10.1016/S1359-0286(96)80047-7.

[103] Larsson K, Tiberg F. Periodic minimal surface structures in bicontinuous lipid–water phases and nanoparticles. Curr Opin Colloid Interface Sci 2005;9(6):365–9. https://doi.org/10.1016/j.cocis.2004.12.002.

[104] Förster S, Fischer S, Zielske K, Schellbach C, Sztucki M, Lindner P, et al. Calculation of scattering-patterns of ordered Nano- and Mesoscale materials. Adv Colloid Interface Sci 2011;163(1):53–83. https://doi.org/10.1016/j.cis.2010.12.003.

[105] Fong C, Zhai J, Drummond CJ, Tran N. Micellar Fd3m Cubosomes from Monoolein – long chain unsaturated fatty acid mixtures: stability on temperature and pH response. J Colloid Interface Sci 2020;566:98–106. https://doi.org/10.1016/j.jcis.2020.01.041.

[106] Mohammady SZ, Pouzot M, Mezzenga R. Oleoylethanolamide-based Lyotropic liquid crystals as vehicles for delivery of amino acids in aqueous environment. Biophys J 2009;96(4):1537–46. https://doi.org/10.1016/j.bpj.2008.10.057.

[107] Yaghmur A, de Campo L, Salentinig S, Sagalowicz L, Leser ME, Glatter O. Oil-loaded Monolinolein-based particles with confined inverse discontinuous cubic structure (Fd3m). Langmuir 2006;22(2):517–21. https://doi.org/10.1021/la052109w.

[108] Tassler S, Pawlowska D, Janich C, Giselbrecht J, Drescher S, Langner A, et al. Lysine-based amino-functionalized lipids for gene transfection: 3D phase behaviour and transfection performance. Phys Chem Chem Phys 2018;20(25):17393–405. https://doi.org/10.1039/C8CP01922C.

[109] Ren Y, Zuo X. Synchrotron X-Ray and neutron diffraction, total scattering, and small-angle scattering techniques for rechargeable battery research. Small Methods 2018;2(8):1800064. https://doi.org/10.1002/smtd.201800064.

[110] Lovesey SW, Lovesey SW. Theory of neutron Scattering from condensed matter. In: Volume II: Polarization effects and magnetic Scattering; international series of monographs on physics. Oxford, New York: Oxford University Press; 1986.

[111] Bée M. Quasielastic neutron Scattering, principles and applications in solid state chemistry. Biology and Materials Science; Taylor & Francis; 1988.

[112] Castellanos MM, McAuley A, Curtis JE. Investigating structure and dynamics of proteins in amorphous phases using neutron scattering. Comput Struct Biotechnol J 2017;15:117–30. https://doi.org/10.1016/j.csbj.2016.12.004.

[113] Gilbert EP. Small-angle X-Ray and neutron scattering in food colloids. Curr Opin Colloid Interface Sci 2019;42:55–72. https://doi.org/10.1016/j.cocis.2019.03.005.

[114] Perez-Salas U, Garg S, Gerelli Y, Porcar L. Deciphering lipid transfer between and within membranes with time-resolved small-angle neutron scattering. In: Current Topics in Membranes. 88. Elsevier; 2021. p. 359–412. https://doi.org/10.1016/bs.ctm.2021.10.004.

[115] Ashkar R, Bilheux HZ, Bordallo H, Briber R, Callaway DJE, Cheng X, et al. Neutron scattering in the biological sciences: progress and prospects. NIST 2018;D74(12).

[116] Pynn Roger. Neutron scattering: a primer. Los Alamos Science 1990;19:1–31.

[117] Arai M, Crawford K. Neutron sources and facilities. In: Bilheux HZ, McGreevy R, Anderson IS, editors. Neutron Imaging and Applications: A Reference for the Imaging Community. Neutron Scattering Applications and Techniques. Boston, MA: Springer US; 2009. p. 13–30. https://doi.org/10.1007/978-0-387-78693-3_2.

[118] Carlile C, Petrillo C, Carpineti M, Donzelli M. Neutron scattering facilities in Europe: present status and future perspectives. ESFRI Report. European Landscape of Research Infrastructures-ESFRI 2016;123.

[119] Andersen KH, Argyriou DN, Jackson AJ, Houston J, Henry PF, Deen PP, et al. The instrument suite of the European spallation source. In: Nucl Instrum Methods Phys Res Sect Accel Spectrometers Detect Assoc Equip. 957; 2020, 163402. https://doi.org/10.1016/j.nima.2020.163402.

[121] Heberle FA, Pan J, Standaert RF, Drazba P, Kučerka N, Katsaras J. Model-based approaches for the determination of lipid bilayer structure from small-angle neutron and X-Ray Scattering data. Eur Biophys J 2012;41(10):875–90. https://doi.org/10.1007/s00249-012-0817-5.

[122] Kiselev MA, Zemlyanaya EV, Gruzinov AYu, Zhabitskaya EI, Ipatova OM, Aksenov VL. Analysis of the vesicular structure of nanoparticles in the phospholipid-based drug delivery system using SAXS data. J Surf Investig X-Ray Synchrotron Neutron Tech 2019;13(1):111–6. https://doi.org/10.1134/S1027451019010257.

[123] Chappa V, Smirnova Y, Komorowski K, Müller M, Salditt T. The effect of polydispersity, shape fluctuations and curvature on small Unilamellar vesicle small-angle X-Ray Scattering curves. J Appl Cryst 2021;54(2):557–68. https://doi.org/10.1107/S1600576721001461.

[124] Fernandez RM, Riske KA, Amaral LQ, Itri R, Lamy MT. Influence of salt on the structure of DMPG studied by SAXS and optical microscopy. Biochim Biophys Acta BBA - Biomembr 2008;1778(4):907–16. https://doi.org/10.1016/j.bbamem.2007.12.005.

[125] Varga Z, Berényi S, Szokol B, Őrfi L, Kéri G, Peták I, et al. A closer look at the structure of sterically stabilized liposomes: a small-angle X-Ray Scattering study. J Phys Chem B 2010;114(20):6850–4. https://doi.org/10.1021/jp9109207.

[126] Angelov B, Angelova A, Filippov S, Karlsson G, Terrill N, Lesieur S, et al. SAXS study of sterically stabilized lipid Nanocarriers functionalized by DNA. J Phys Conf Ser 2012;351(1):012004. https://doi.org/10.1088/1742-6596/351/1/012004.

[127] Li Y, Zhang J, Song P, Miao X, Liu G, Yang C, et al. Small-angle X-Ray Scattering for PEGylated liposomal doxorubicin drugs: an analytical model comparison study. Mol Pharm 2023;20(9):4654–63. https://doi.org/10.1021/acs.molpharmaceut.3c00396.

[128] Castelletto V, Cheng G, Stain C, Connon CJ, Hamley IW. Self-assembly of a peptide Amphiphile containing l-carnosine and its mixtures with a multilamellar vesicle forming lipid. Langmuir 2012;28(31):11599–608. https://doi.org/10.1021/la302210b.

[129] Yaghmur A, Paasonen L, Yliperttula M, Urtti A, Rappolt M. Structural elucidation of light activated vesicles. J Phys Chem Lett 2010;1(6):962–6. https://doi.org/10.1021/jz100226v.

[130] De Mel JU, Gupta S, Willner L, Allgaier J, Stingaciu LR, Bleuel M, et al. Manipulating phospholipid vesicles at the nanoscale: a transformation from Unilamellar to multilamellar by an n-alkyl-poly(ethylene oxide). Langmuir 2021;37(7):2362–75. https://doi.org/10.1021/acs.langmuir.0c03302.

[131] Heftberger P, Kollmitzer B, Heberle FA, Pan J, Rappolt M, Amenitsch H, et al. Global small-angle X-Ray Scattering data analysis for multilamellar vesicles: the evolution of the Scattering density profile model. J Appl Cryst 2014;47(1):173–80. https://doi.org/10.1107/S1600576713029798.

[132] Frielinghaus H. Small-Angle Scattering Model for Multilamellar Vesicles. Phys Rev E 2007;76(5):051603. https://doi.org/10.1103/PhysRevE.76.051603.

[133] Konarev PV, Gruzinov AYu, Mertens HDT, Svergun DI. Restoring structural parameters of lipid mixtures from small-angle X-Ray Scattering data. J Appl Cryst 2021;54(Pt 1):169–79. https://doi.org/10.1107/S1600576720015368.

[134] Pabst G, Kučerka N, Nieh M-P, Rheinstädter MC, Katsaras J. Applications of neutron and X-Ray Scattering to the study of biologically relevant model membranes. Chem Phys Lipids 2010;163(6):460–79. https://doi.org/10.1016/j.chemphyslip.2010.03.010.

[135] Brzustowicz MR, Brunger AT. X-Ray Scattering from Unilamellar lipid vesicles. J Appl Cryst 2005;38(1):126–31. https://doi.org/10.1107/S0021889804029206.
[136] Eicher B, Heberle FA, Marquardt D, Rechberger GN, Katsaras J, Pabst G. Joint small-angle X-Ray and Neutron Scattering data analysis of asymmetric lipid vesicles. J Appl Cryst 2017;50(2):419–29. https://doi.org/10.1107/S1600576717000656.
[137] Marquardt D, Heberle FA, Nickels JD, Pabst G, Katsaras J. On scattered waves and lipid domains: detecting membrane rafts with X-rays and neutrons. Soft Matter 2015;11(47):9055–72. https://doi.org/10.1039/C5SM01807B.
[138] Spinozzi F, Barbosa LRS, Corucci G, Mariani P, Itri R. Small-angle Scattering from flat bilayers containing correlated Scattering length density Inhomogeneities. J Appl Cryst 2023;56(5):1348–60. https://doi.org/10.1107/S1600576723006143.
[139] Ghazal A, Gontsarik M, Kutter JP, Lafleur JP, Ahmadvand D, Labrador A, et al. Microfluidic platform for the continuous production and characterization of multilamellar vesicles: a synchrotron small-angle X-Ray Scattering (SAXS) study. J Phys Chem Lett 2017;8(1):73–9. https://doi.org/10.1021/acs.jpclett.6b02468.
[140] Ilhan-Ayisigi E, Yaldiz B, Bor G, Yaghmur A, Yesil-Celiktas O. Advances in microfluidic synthesis and coupling with synchrotron SAXS for continuous production and real-time structural characterization of Nano-self-assemblies. Colloids Surf B Biointerfaces 2021;201:111633. https://doi.org/10.1016/j.colsurfb.2021.111633.
[141] Yaghmur A, Hamad I. Microfluidic nanomaterial synthesis and in situ SAXS, WAXS, or SANS characterization: manipulation of size characteristics and online elucidation of dynamic structural transitions. Molecules 2022;27(14):4602. https://doi.org/10.3390/molecules27144602.
[142] Buscema M, Deyhle H, Pfohl T, Zumbuehl A, Müller B. Spatially resolved small-angle X-Ray Scattering for characterizing Mechanoresponsive liposomes using microfluidics. Mater Today Bio 2019;1:100003. https://doi.org/10.1016/j.mtbio.2019.100003.
[143] Eş I, Montebugnoli LJ, Filippi MFP, Malfatti-Gasperini AA, Radaic A, de Jesus MB, et al. High-throughput conventional and stealth cationic liposome synthesis using a chaotic advection-based microfluidic device combined with a centrifugal vacuum concentrator. Chem Eng J 2020;382:122821. https://doi.org/10.1016/j.cej.2019.122821.
[144] Castorph S, Riedel D, Arleth L, Sztucki M, Jahn R, Holt M, et al. Structure parameters of synaptic vesicles quantified by small-angle X-Ray Scattering. Biophys J 2010;98(7):1200–8. https://doi.org/10.1016/j.bpj.2009.12.4278.
[145] Castorph S, Arleth L, Sztucki M, Vainio U, Ghosh SK, Holt M, et al. Synaptic vesicles studied by SAXS: derivation and validation of a model form factor. J Phys Conf Ser 2010;247(1):012015. https://doi.org/10.1088/1742-6596/247/1/012015.
[146] Varga Z, Yuana Y, Grootemaat AE, van der Pol E, Gollwitzer C, Krumrey M, et al. Towards traceable size determination of extracellular vesicles. J Extracell Vesicles 2014;3. https://doi.org/10.3402/jev.v3.23298.
[147] Perissinotto F, Rondelli V, Senigagliesi B, Brocca P, Almásy L, Bottyán L, et al. Structural insights into fusion mechanisms of small extracellular vesicles with model plasma membranes. Nanoscale 2021;13(10):5224–33. https://doi.org/10.1039/D0NR09075A.
[148] Romancino DP, Buffa V, Caruso S, Ferrara I, Raccosta S, Notaro A, et al. Palmitoylation is a post-translational modification of Alix regulating the membrane organization of exosome-like small extracellular vesicles. Biochim Biophys Acta Gen Subj 2018;1862(12):2879–87. https://doi.org/10.1016/j.bbagen.2018.09.004.
[149] Palanisamy V, Sharma S, Deshpande A, Zhou H, Gimzewski J, Wong DT. Nanostructural and transcriptomic analyses of human saliva derived exosomes. PloS One 2010;5(1):e8577. https://doi.org/10.1371/journal.pone.0008577.
[150] Sarra A, Celluzzi A, Bruno SP, Ricci C, Sennato S, Ortore MG, et al. Biophysical characterization of membrane phase transition profiles for the discrimination of outer membrane vesicles (OMVs) from *Escherichia Coli* grown at different temperatures. Front Microbiol 2020;11:290. https://doi.org/10.3389/fmicb.2020.00290.
[151] Shen H-H, Crowston JG, Huber F, Saubern S, McLean KM, Hartley PG. The influence of Dipalmitoyl phosphatidylserine on phase behaviour of and cellular response to Lyotropic liquid crystalline dispersions. Biomaterials 2010;31(36):9473–81. https://doi.org/10.1016/j.biomaterials.2010.08.030.
[152] Tran N, Hawley AM, Zhai J, Muir BW, Fong C, Drummond CJ, et al. High-throughput screening of saturated fatty acid influence on nanostructure of Lyotropic liquid crystalline lipid nanoparticles. Langmuir 2016;32(18):4509–20. https://doi.org/10.1021/acs.langmuir.5b03769.
[153] Tran N, Hocquet M, Eon B, Sangwan P, Ratcliffe J, Hinton TM, et al. Non-lamellar Lyotropic liquid crystalline nanoparticles enhance the antibacterial effects of rifampicin against *Staphylococcus aureus*. J Colloid Interface Sci 2018;519:107–18. https://doi.org/10.1016/j.jcis.2018.02.048.
[154] Malheiros B, De Castro RD, Lotierzo MC, Casadei BR, Mariani P, Barbosa LRS. Influence of Hexadecylphosphocholine (Miltefosine) in Phytantriol-based Cubosomes: a structural investigation. Colloids Surf A Physicochem Eng Asp 2022;632:127720. https://doi.org/10.1016/j.colsurfa.2021.127720.
[155] Muller F, Salonen A, Glatter O. Phase behavior of Phytantriol/water Bicontinuous cubic Pn3m Cubosomes stabilized by Laponite disc-like particles. J Colloid Interface Sci 2010;342(2):392–8. https://doi.org/10.1016/j.jcis.2009.10.054.
[156] Azhari H, Strauss M, Hook S, Boyd BJ, Rizwan SB. Stabilising cubosomes with tween 80 as a step towards targeting lipid nanocarriers to the blood–brain barrier. Eur J Pharm Biopharm 2016;104:148–55. https://doi.org/10.1016/j.ejpb.2016.05.001.
[157] Boge L, Västberg A, Umerska A, Bysell H, Eriksson J, Edwards K, et al. Freeze-dried and re-hydrated liquid crystalline nanoparticles stabilized with disaccharides for drug-delivery of the Plectasin derivative AP114 antimicrobial peptide. J Colloid Interface Sci 2018;522:126–35. https://doi.org/10.1016/j.jcis.2018.03.062.
[158] Naidjonoka P, Fornasier M, Pålsson D, Rudolph G, Al-Rudainy B, Murgia S, et al. Bicontinuous cubic liquid crystalline phase nanoparticles stabilized by softwood hemicellulose. Colloids Surf B Biointerfaces 2021;203:111753. https://doi.org/10.1016/j.colsurfb.2021.111753.
[159] Meikle TG, Zabara A, Waddington LJ, Separovic F, Drummond CJ, Conn CE. Incorporation of antimicrobial peptides in nanostructured lipid membrane mimetic bilayer Cubosomes. Colloids Surf B Biointerfaces 2017;152:143–51. https://doi.org/10.1016/j.colsurfb.2017.01.004.
[160] Mohammad Y, Prentice RN, Boyd BJ, Rizwan SB. Comparison of Cubosomes and Hexosomes for the delivery of phenytoin to the brain. J Colloid Interface Sci 2022;605:146–54. https://doi.org/10.1016/j.jcis.2021.07.070.
[161] Serieye S, Méducin F, Tidu A, Guillot S. Incorporation of aromas in nanostructured Monolinolein-based Miniemulsions: a structural investigation. Colloids Surf A Physicochem Eng Asp 2018;555:802–8. https://doi.org/10.1016/j.colsurfa.2018.07.032.
[162] Victorelli FD, Salvati Manni L, Biffi S, Bortot B, Buzzá HH, Lutz-Bueno V, et al. Potential of curcumin-loaded Cubosomes for topical treatment of cervical cancer. J Colloid Interface Sci 2022;620:419–30. https://doi.org/10.1016/j.jcis.2022.04.031.
[163] Cai X, Fan B, Thang H, Drummond C, Tran N, Zhai J. Paclitaxel-loaded Cubosome lipid Nanocarriers stabilised with pH and hydrogen peroxide-responsive steric Stabilisers as drug delivery vehicles. J Mater Chem B 2023;11(2):403–14. https://doi.org/10.1039/D2TB01530G.
[164] Kulkarni CV, Yaghmur A, Steinhart M, Kriechbaum M, Rappolt M. Effects of high pressure on internally self-assembled lipid nanoparticles: a synchrotron small-angle X-Ray Scattering (SAXS) study. Langmuir 2016;32(45):11907–17. https://doi.org/10.1021/acs.langmuir.6b03300.
[165] Gontsarik M, Yaghmur A, Salentinig S. Dispersed liquid crystals as pH-adjustable antimicrobial peptide Nanocarriers. J Colloid Interface Sci 2021;583:672–82. https://doi.org/10.1016/j.jcis.2020.09.081.
[166] Caselli L, Ridolfi A, Cardellini J, Sharpnack L, Paolini L, Brucale M, et al. A Plasmon-based Nanoruler to probe the mechanical properties of synthetic and biogenic Nanosized lipid vesicles. Nanoscale Horiz 2021;6(7):543–50. https://doi.org/10.1039/D1NH00012H.
[167] Mertins O, Mathews PD, Angelova A. Advances in the design of pH-sensitive Cubosome liquid crystalline Nanocarriers for drug delivery applications. Nanomaterials 2020;10(5):963. https://doi.org/10.3390/nano10050963.
[168] Li Y, Angelova A, Hu F, Garamus VM, Peng C, Li N, et al. pH responsiveness of Hexosomes and Cubosomes for combined delivery of *Brucea Javanica* oil and doxorubicin. Langmuir 2019;35(45):14532–42. https://doi.org/10.1021/acs.langmuir.9b02257.
[169] Zhai J, Yap SL, Drummond CJ, Tran N. Controlling the pH dependent transition between Monoolein Fd3m micellar Cubosomes and Hexosomes using fatty acetate and fatty acid additive mixtures. J Colloid Interface Sci 2022;607:848–56. https://doi.org/10.1016/j.jcis.2021.08.173.
[170] Liu Q, Dong Y-D, Hanley TL, Boyd BJ. Sensitivity of nanostructure in charged Cubosomes to phase changes triggered by ionic species in solution. Langmuir 2013;29(46):14265–73. https://doi.org/10.1021/la402426y.
[171] Lotierzo MCG, Casadei BR, De Castro RD, Malheiros B, Barbosa LRS. Cubic-to-inverted micellar and the cubic-to-hexagonal-to-micellar transitions on Phytantriol-based Cubosomes induced by solvents. Drug Deliv Transl Res 2020;10(6):1571–83. https://doi.org/10.1007/s13346-020-00828-y.
[172] Balestri A, Lonetti B, Harrisson S, Farias-Mancilla B, Zhang J, Amenitsch H, et al. Thermo-responsive lipophilic NIPAM-based block copolymers as stabilizers for lipid-based cubic nanoparticles. Colloids Surf B Biointerfaces 2022;220:112884. https://doi.org/10.1016/j.colsurfb.2022.112884.
[173] Yaghmur A, Laggner P, Almgren M, Rappolt M. Self-assembly in Monoelaidin aqueous dispersions: direct vesicles to Cubosomes transition. PloS One 2008;3(11):e3747. https://doi.org/10.1371/journal.pone.0003747.
[174] Dong Y-D, Larson I, Hanley T, Boyd BJ. Bulk and dispersed aqueous phase behavior of Phytantriol: effect of vitamin E acetate and F127 polymer on liquid crystal nanostructure. Langmuir 2006;22(23):9512–8. https://doi.org/10.1021/la061706v.
[175] Akhlaghi SP, Ribeiro IR, Boyd BJ, Loh W. Impact of preparation method and variables on the internal structure, morphology, and presence of liposomes in Phytantriol-Pluronic® F127 Cubosomes. Colloids Surf B Biointerfaces 2016;145:845–53. https://doi.org/10.1016/j.colsurfb.2016.05.091.
[176] Yu H, Dyett BP, Zhai J, Strachan JB, Drummond CJ, Conn CE. Formation of particulate lipid Lyotropic liquid crystalline Nanocarriers using a microfluidic platform. J Colloid Interface Sci 2023;634:279–89. https://doi.org/10.1016/j.jcis.2022.12.028.
[177] Kim H, Sung J, Chang Y, Alfeche A, Leal C. Microfluidics synthesis of gene silencing Cubosomes. ACS Nano 2018;12(9):9196–205. https://doi.org/10.1021/acsnano.8b03770.
[178] Hong L, Dong Y-D, Boyd BJ. Preparation of nanostructured lipid drug delivery particles using microfluidic mixing. Pharm Nanotechnol 2019;7(6):484–95. https://doi.org/10.2174/2211738507666191004123545.
[179] Tajik-Ahmadabad B, Chollet L, White J, Separovic F, Polyzos A. Metallo-Cubosomes: zinc-functionalized cubic nanoparticles for therapeutic nucleotide delivery. Mol Pharm 2019;16(3):978–86. https://doi.org/10.1021/acs.molpharmaceut.8b00890.

[180] Jones BE, Kelly EA, Cowieson N, Divitini G, Evans RC. Light-responsive molecular release from Cubosomes using swell-squeeze lattice control. J Am Chem Soc 2022; 144(42):19532–41. https://doi.org/10.1021/jacs.2c08583.
[181] Bazylińska U, Wawrzyńczyk D, Kulbacka J, Picci G, Manni LS, Handschin S, et al. Hybrid Theranostic Cubosomes for efficient NIR-induced photodynamic therapy. ACS Nano 2022;16(4):5427–38. https://doi.org/10.1021/acsnano.1c09367.
[182] Patel R, Kaki M, Potluri VS, Kahar P, Khanna D. A comprehensive review of SARS-CoV-2 vaccines: Pfizer, Moderna & Johnson & Johnson. Hum Vaccin Immunother 2022;18(1):2002083. https://doi.org/10.1080/21645515.2021.2002083.
[183] Ziller A, Nogueira SS, Hühn E, Funari SS, Brezesinski G, Hartmann H, et al. Incorporation of mRNA in lamellar lipid matrices for parenteral administration. Mol Pharm 2018;15(2):642–51. https://doi.org/10.1021/acs.molpharmaceut.7b01022.
[184] Uebbing L, Ziller A, Siewert C, Schroer MA, Blanchet CE, Svergun DI, et al. Investigation of pH-responsiveness inside lipid nanoparticles for parenteral mRNA application using small-angle X-Ray Scattering. Langmuir 2020;36(44): 13331–41. https://doi.org/10.1021/acs.langmuir.0c02446.
[185] Sartori B, Marmiroli B. Tailoring lipid-based drug delivery Nanosystems by synchrotron small angle X-Ray Scattering. Pharmaceutics 2022;14(12):2704. https://doi.org/10.3390/pharmaceutics14122704.
[186] Montis C, Sostegni S, Milani S, Baglioni P, Berti D. Biocompatible cationic lipids for the formulation of liposomal DNA vectors. Soft Matter 2014;10(24):4287–97. https://doi.org/10.1039/C4SM00142G.
[187] Mamusa M, Barbero F, Montis C, Cutillo L, Gonzalez-Paredes A, Berti D. Inclusion of oligonucleotide antimicrobials in biocompatible cationic liposomes: a structural study. J Colloid Interface Sci 2017;508:476–87. https://doi.org/10.1016/j.jcis.2017.08.080.
[188] Montis C, Milani S, Berti D, Baglioni P. Complexes of Nucleolipid liposomes with single-stranded and double-stranded nucleic acids. J Colloid Interface Sci 2012; 373(1):57–68. https://doi.org/10.1016/j.jcis.2011.10.058.
[189] Sarkar S, Tran N, Soni SK, Nasa Z, Drummond CJ, Conn CE. Cuboplex-mediated nonviral delivery of functional siRNA to Chinese Hamster ovary (CHO) cells. ACS Appl Mater Interfaces 2021;13(2):2336–45. https://doi.org/10.1021/acsami.0c20956.
[190] Kim H, Leal C. Cuboplexes: topologically active siRNA delivery. ACS Nano 2015;9 (10):10214–26. https://doi.org/10.1021/acsnano.5b03902.
[191] Sarkar S, Tran N, Soni SK, Conn CE, Drummond CJ. Size-dependent encapsulation and release of dsDNA from cationic Lyotropic liquid crystalline cubic phases. ACS Biomater Sci Eng 2020;6(8):4401–13. https://doi.org/10.1021/acsbiomaterials.0c00085.
[192] Taratula O, Kuzmov A, Shah M, Garbuzenko OB, Minko T. Nanostructured lipid carriers as multifunctional nanomedicine platform for pulmonary co-delivery of anticancer drugs and siRNA. J Control Release Off J Control Release Soc 2013;171 (3):349–57. https://doi.org/10.1016/j.jconrel.2013.04.018.
[193] Freire RVM, Pillco-Valencia Y, da Hora GCA, Ramstedt M, Sandblad L, Soares TA, et al. Antimicrobial peptide induced colloidal transformations in Bacteria-mimetic vesicles: combining in silico tools and experimental methods. J Colloid Interface Sci 2021;596:352–63. https://doi.org/10.1016/j.jcis.2021.03.060.
[194] Utterström J, Barriga HMG, Holme MN, Selegård R, Stevens MM, Aili D. Peptide-folding triggered phase separation and lipid membrane destabilization in cholesterol-rich lipid vesicles. Bioconjug Chem 2022;33(4):736–46. https://doi.org/10.1021/acs.bioconjchem.2c00115.
[195] Nielsen JE, Bjørnestad VA, Lund R. Resolving the structural interactions between antimicrobial peptides and lipid membranes using small-angle Scattering methods: the case of Indolicidin. Soft Matter 2018;14(43):8750–63. https://doi.org/10.1039/C8SM01888J.
[196] Malanovic N, Leber R, Schmuck M, Kriechbaum M, Cordfunke RA, Drijfhout JW, et al. Phospholipid-driven differences determine the action of the synthetic antimicrobial peptide OP-145 on gram-positive bacterial and mammalian membrane model systems. Biochim Biophys Acta BBA - Biomembr 2015;1848(10, Part A):2437–47. https://doi.org/10.1016/j.bbamem.2015.07.010.
[197] Gontsarik M, Mohammadtaheri M, Yaghmur A, Salentinig S. pH-triggered Nanostructural transformations in antimicrobial peptide/oleic acid self-assemblies. Biomater Sci 2018;6(4):803–12. https://doi.org/10.1039/C7BM00929A.
[198] Boge L, Hallstensson K, Ringstad L, Johansson J, Andersson T, Davoudi M, et al. Cubosomes for topical delivery of the antimicrobial peptide LL-37. Eur J Pharm Biopharm 2019;134:60–7. https://doi.org/10.1016/j.ejpb.2018.11.009.
[199] Boge L, Umerska A, Matougui N, Bysell H, Ringstad L, Davoudi M, et al. Cubosomes post-loaded with antimicrobial peptides: characterization, bactericidal effect and proteolytic stability. Int J Pharm 2017;526(1):400–12. https://doi.org/10.1016/j.ijpharm.2017.04.082.
[200] Gontsarik M, Buhmann MT, Yaghmur A, Ren Q, Maniura-Weber K, Salentinig S. Antimicrobial peptide-driven colloidal transformations in liquid-crystalline nanocarriers. J Phys Chem Lett 2016;7(17):3482–6. https://doi.org/10.1021/acs.jpclett.6b01622.
[201] Boge L, Bysell H, Ringstad L, Wennman D, Umerska A, Cassisa V, et al. Lipid-based liquid crystals as carriers for antimicrobial peptides: phase behavior and antimicrobial effect. Langmuir 2016;32(17):4217–28. https://doi.org/10.1021/acs.langmuir.6b00338.
[202] Milogrodzka I, Nguyen Pham DT, Sama GR, Samadian H, Zhai J, De Campo L, et al. Effect of cholesterol on biomimetic membrane curvature and coronavirus fusion peptide encapsulation. ACS Nano 2023;17(9):8598–612. https://doi.org/10.1021/acsnano.3c01095.
[203] Zabara M, Senturk B, Gontsarik M, Ren Q, Rottmar M, Maniura-Weber K, et al. Multifunctional nano-biointerfaces: Cytocompatible antimicrobial Nanocarriers from stabilizer-free Cubosomes. Adv Funct Mater 2019;29(35):1904007. https://doi.org/10.1002/adfm.201904007.
[204] Caselli L, Ridolfi A, Mangiapia G, Maltoni P, Moulin J-F, Berti D, et al. Interaction of nanoparticles with lipid films: the role of symmetry and shape anisotropy. Phys Chem Chem Phys 2022;24(5):2762–76. https://doi.org/10.1039/D1CP03201A.
[205] Hameed S, Baimanov D, Li X, Liu K, Wang L. Synchrotron radiation-based analysis of interactions at the nano–bio interface. Environ Sci Nano 2022;9(9):3152–67. https://doi.org/10.1039/D2EN00408A.
[206] Sanchez-Cano C, Alvarez-Puebla RA, Abendroth JM, Beck T, Blick R, Cao Y, et al. X-ray-based techniques to study the nano–bio interface. ACS Nano 2021;15(3): 3754–807. https://doi.org/10.1021/acsnano.0c09563.
[207] Salassi S, Caselli L, Cardellini J, Lavagna E, Montis C, Berti D, et al. A martini coarse grained model of citrate-capped gold nanoparticles interacting with lipid bilayers. J Chem Theory Comput 2021;17(10):6597–609. https://doi.org/10.1021/acs.jctc.1c00627.
[208] Montis C, Caselli L, Valle F, Zendrini A, Carlà F, Schweins R, et al. Shedding light on membrane-templated clustering of gold nanoparticles. J Colloid Interface Sci 2020;573:204–14. https://doi.org/10.1016/j.jcis.2020.03.123.
[209] Ridolfi A, Caselli L, Montis C, Mangiapia G, Berti D, Brucale M, et al. Gold nanoparticles interacting with synthetic lipid rafts: an AFM investigation. J Microsc 2020;280(3):194–203. https://doi.org/10.1111/jmi.12910.
[210] Kariuki R, Penman R, Bryant SJ, Orrell-Trigg R, Meftahi N, Crawford RJ, et al. Behavior of citrate-capped Ultrasmall gold nanoparticles on a supported lipid bilayer Interface at atomic resolution. ACS Nano 2022;16(10):17179–96. https://doi.org/10.1021/acsnano.2c07751.
[211] Mendozza M, Caselli L, Montis C, Orazzini S, Carretti E, Baglioni P, et al. Inorganic nanoparticles modify the phase behavior and viscoelastic properties of non-lamellar lipid Mesophases. J Colloid Interface Sci 2019;541:329–38. https://doi.org/10.1016/j.jcis.2019.01.091.
[212] Cardellini J, Montis C, Barbero F, De Santis I, Caselli L, Berti D. Interaction of metallic nanoparticles with biomimetic lipid liquid crystalline cubic interfaces. Front Bioeng Biotechnol 2022;10:848687. https://doi.org/10.3389/fbioe.2022.848687.
[213] Cardellini J, Caselli L, Lavagna E, Salassi S, Amenitsch H, Calamai M, et al. Membrane phase drives the assembly of gold nanoparticles on biomimetic lipid bilayers. J Phys Chem C 2022;126(9):4483–94. https://doi.org/10.1021/acs.jpcc.1c08914.
[214] Meikle TG, Dyett BP, Strachan JB, White J, Drummond CJ, Conn CE. Preparation, characterization, and antimicrobial activity of Cubosome encapsulated metal nanocrystals. ACS Appl Mater Interfaces 2020;12(6):6944–54. https://doi.org/10.1021/acsami.9b21783.
[215] Cardellini J, Ridolfi A, Donati M, Giampietro V, Severi M, Brucale M, et al. Probing the coverage of nanoparticles by biomimetic membranes through nanoplasmonics. J Colloid Interface Sci 2023;640:100–9. https://doi.org/10.1016/j.jcis.2023.02.073.
[216] Szlezak M, Nieciecka D, Joniec A, Pękała M, Gorecka E, Emo M, et al. Monoolein cubic phase gels and cubosomes doped with magnetic nanoparticles–hybrid materials for controlled drug release. ACS Appl Mater Interfaces 2017;9(3): 2796–805. https://doi.org/10.1021/acsami.6b12889.
[217] Wakaskar RR. General overview of lipid–polymer hybrid nanoparticles, Dendrimers, Micelles, Liposomes, Spongosomes and Cubosomes. J Drug Target 2018;26(4):311–8. https://doi.org/10.1080/1061186X.2017.1367006.
[218] Mathews PD, Mertins O, Angelov B, Angelova A. Cubosomal lipid Nanoassemblies with pH-sensitive shells created by biopolymer complexes: a synchrotron SAXS study. J Colloid Interface Sci 2022;607:440–50. https://doi.org/10.1016/j.jcis.2021.08.187.
[219] Madrid RRM, Mathews PD, Pimenta BV, Mertins O. Biopolymer–lipid hybrid cubosome for delivery of Acemannan. Mater Proc 2023;14(1):56. https://doi.org/10.3390/IOCN2023-14486.
[220] Balestri A, Gibot L, Amenitsch H, Cervelli L, Montis C, Lonetti B, et al. PNIPAM-stabilized Cubosomes as Fusogenic delivery nanovectors for anticancer applications. Colloids Surf B Biointerfaces 2023;231:113532. https://doi.org/10.1016/j.colsurfb.2023.113532.
[221] Cai X, Zhai J, Tran N, Mulet X, Drummond CJ. Chapter Three - Lipid nanoparticle steric stabilization roadmap. In: Iglič A, Rappolt M, Pérez PL, editors. Advances in Biomembranes and Lipid Self-Assembly. 35. Academic Press; 2022. p. 41–75. https://doi.org/10.1016/bs.abl.2022.05.003.
[222] Hatziantoniou S, Maltezou HC, Tsakris A, Poland GA, Anastassopoulou C. Anaphylactic reactions to mRNA COVID-19 vaccines: a call for further study. Vaccine 2021;39(19):2605–7. https://doi.org/10.1016/j.vaccine.2021.03.073.
[223] Lee KWY, Nguyen T-H, Hanley T, Boyd BJ. Nanostructure of liquid crystalline matrix determines *in vitro* sustained release and *in vivo* Oral absorption kinetics for hydrophilic model drugs. Int J Pharm 2009;365(1):190–9. https://doi.org/10.1016/j.ijpharm.2008.08.022.
[224] Chong JYT, Mulet X, Waddington LJ, Boyd BJ, Drummond CJ. Steric stabilisation of self-assembled cubic Lyotropic liquid crystalline nanoparticles: high throughput evaluation of triblock polyethylene oxide-polypropylene oxide-polyethylene oxide copolymers. Soft Matter 2011;7(10):4768–77. https://doi.org/10.1039/C1SM05181D.
[225] Mohammad Y, Fallah AB, Reynolds JNJ, Boyd BJ, Rizwan SB. Steric stabilisers govern the colloidal and chemical stability but not *in vitro* cellular toxicity of Linoleoylethanolamide Cubosomes. Colloids Surf B Biointerfaces 2020;192: 111063. https://doi.org/10.1016/j.colsurfb.2020.111063.
[226] Yu H, Dyett B, Kirby N, Cai X, Mohamad ME, Bozinovski S, et al. pH-dependent Lyotropic Liquid crystalline mesophase and ionization behavior of phytantriol-

based ionizable lipid nanoparticles. Small 2024:2309200. https://doi.org/10.1002/smll.202309200.
[227] Sztucki M, Di Cola E, Narayanan T. Anomalous small-angle X-Ray scattering from charged soft matter. Eur Phys J Spec Top 2012;208(1):319–31. https://doi.org/10.1140/epjst/e2012-01627-x.
[228] Varga Z, Bóta A, Goerigk G. Localization of Dibromophenol in DPPC/water liposomes studied by anomalous small-angle X-Ray Scattering. J Phys Chem B 2006;110(23):11029–32. https://doi.org/10.1021/jp061750j.
[229] Bóta A, Klumpp E. Effects of contaminants on biological model membranes: the advantage of the ASAXS method for the study of the location of copper ions and Dihalogenated phenol molecules. Colloids Surf A Physicochem Eng Asp 2005;265(1):124–30. https://doi.org/10.1016/j.colsurfa.2005.02.041.
[230] Manet S, Cuvier A-S, Valotteau C, Fadda GC, Perez J, Karakas E, et al. Structure of Bolaamphiphile Sophorolipid micelles characterized with SAXS, SANS, and MD simulations. J Phys Chem B 2015;119(41):13113–33. https://doi.org/10.1021/acs.jpcb.5b05374.
[231] Bras W, Koizumi S, Terrill NJ. Beyond simple small-angle X-Ray scattering: developments in online complementary techniques and sample environments. IUCrJ 2014;1(6):478–91. https://doi.org/10.1107/S2052252514019198.
[232] Henriksen JR, Petersen AL, Hansen AE, Frankær CG, Harris P, Elema DR, et al. Remote loading of 64Cu2+ into liposomes without the use of ion transport enhancers. ACS Appl Mater Interfaces 2015;7(41):22796–806. https://doi.org/10.1021/acsami.5b04612.
[233] Grijalvo S, Mayr J, Eritja R, Díaz DD. Biodegradable liposome-encapsulated hydrogels for biomedical applications: a marriage of convenience. Biomater Sci 2016;4(4):555–74. https://doi.org/10.1039/C5BM00481K.
[234] Villalva DG, França CG, Loh W. Characterization of Cubosomes immobilized in hydrogels of hyaluronic acid and their use for diclofenac controlled delivery. Colloids Surf B Biointerfaces 2022;212:112352. https://doi.org/10.1016/j.colsurfb.2022.112352.
[235] Bandara SR, Molley TG, Kim H, Bharath PA, Kilian KA, Leal C. The structural fate of lipid nanoparticles in the extracellular matrix. Mater Horiz 2020;7(1):125–34. https://doi.org/10.1039/C9MH00835G.
[236] Kucerka N, Tristram-Nagle S, Nagle JF. Structure of fully hydrated fluid phase lipid bilayers with monounsaturated chains. J Membr Biol 2005;208(3):193–202. https://doi.org/10.1007/s00232-005-7006-8.
[237] Balgavý P, Dubničková M, Kučerka N, Kiselev MA, Yaradaikin SP, Uhríková, D.. Bilayer thickness and lipid interface area in Unilamellar extruded 1,2-Diacylphosphatidylcholine liposomes: a small-angle neutron scattering study. Biochim Biophys Acta BBA - Biomembr 2001;1512(1):40–52. https://doi.org/10.1016/S0005-2736(01)00298-X.
[238] Kiselev MA, Zemlyanaya EV, Aswal VK, Neubert RHH. What can we learn about the lipid vesicle structure from the small-angle neutron Scattering experiment? Eur Biophys J EBJ 2006;35(6):477–93. https://doi.org/10.1007/s00249-006-0055-9.
[239] Kučerka N, Gallová J, Uhríková D, Balgavý P, Bulacu M, Marrink S-J, et al. Areas of monounsaturated Diacylphosphatidylcholines. Biophys J 2009;97(7):1926–32. https://doi.org/10.1016/j.bpj.2009.06.050.
[240] Pan J, Heberle FA, Tristram-Nagle S, Szymanski M, Koepfinger M, Katsaras J, et al. Molecular structures of fluid phase Phosphatidylglycerol bilayers as determined by small angle neutron and X-Ray scattering. Biochim Biophys Acta BBA - Biomembr 2012;1818(9):2135–48. https://doi.org/10.1016/j.bbamem.2012.05.007.
[241] Kučerka N, Holland BW, Gray CG, Tomberli B, Katsaras J. Scattering density profile model of POPG bilayers as determined by molecular dynamics simulations and small-angle neutron and X-Ray Scattering experiments. J Phys Chem B 2012;116(1):232–9. https://doi.org/10.1021/jp208920h.
[242] Pan J, Cheng X, Monticelli L, Heberle FA, Kučerka N, Tieleman DP, et al. The molecular structure of a phosphatidylserine bilayer determined by scattering and molecular dynamics simulations. Soft Matter 2014;10(21):3716–25. https://doi.org/10.1039/C4SM00066H.
[243] Pan J, Cheng X, Sharp M, Ho C-S, Khadka N, Katsaras J. Structural and mechanical properties of Cardiolipin lipid bilayers determined using neutron spin Echo, small angle neutron and X-Ray scattering, and molecular dynamics simulations. Soft Matter 2014;11(1):130–8. https://doi.org/10.1039/C4SM02227K.
[244] Doktorova M, Kučerka N, Kinnun JJ, Pan J, Marquardt D, Scott HL, et al. Molecular structure of sphingomyelin in fluid phase bilayers determined by the joint analysis of small-angle neutron and X-Ray Scattering data. J Phys Chem B 2020;124(25):5186–200. https://doi.org/10.1021/acs.jpcb.0c03389.
[245] Kučerka N, Nieh M-P, Katsaras J. Fluid phase lipid areas and bilayer thicknesses of commonly used phosphatidylcholines as a function of temperature. Biochim Biophys Acta BBA - Biomembr 2011;1808(11):2761–71. https://doi.org/10.1016/j.bbamem.2011.07.022.
[246] Gordeliy VI, Cherezov V, Teixeira J. Strength of thermal undulations of phospholipid membranes. Phys Rev E Stat Nonlin Soft Matter Phys 2005;72(6 Pt 1):061913. https://doi.org/10.1103/PhysRevE.72.061913.
[247] Kuklin A, Zabelskii D, Gordeliy I, Teixeira J, Brûlet A, Chupin V, et al. On the origin of the anomalous behavior of lipid membrane properties in the vicinity of the chain-melting phase transition. Sci Rep 2020;10(1):5749. https://doi.org/10.1038/s41598-020-62577-9.
[248] De Mel JU, Gupta S, Perera RM, Ngo L, Zolnierczuk P, Bleuel M, et al. Influence of external NaCl salt on membrane rigidity of neutral DOPC vesicles. Langmuir 2020;36(32):9356–67. https://doi.org/10.1021/acs.langmuir.0c01004.
[249] Uhríková D, Kučerka N, Teixeira J, Gordeliy V, Balgavý P. Structural changes in Dipalmitoylphosphatidylcholine bilayer promoted by Ca2+ ions: a small-angle neutron scattering study. Chem Phys Lipids 2008;155(2):80–9. https://doi.org/10.1016/j.chemphyslip.2008.07.010.
[250] Luchini A, Cavasso D, Radulescu A, D'Errico G, Paduano L, Vitiello G. Structural organization of Cardiolipin-Containing vesicles as models of the bacterial cytoplasmic membrane. Langmuir 2021;37(28):8508–16. https://doi.org/10.1021/acs.langmuir.1c00981.
[251] Gallová J, Uhríková D, Hanulová M, Teixeira J, Balgavý P. Bilayer thickness in Unilamellar extruded 1,2-Dimyristoleoyl and 1,2-Dierucoyl phosphatidylcholine vesicles: SANS contrast variation study of cholesterol effect. Colloids Surf B Biointerfaces 2004;38(1–2):11–4. https://doi.org/10.1016/j.colsurfb.2004.07.012.
[252] Gallová J, Uhríková D, Kučerka N, Doktorovová S, Funari SS, Teixeira J, et al. The effects of cholesterol and β-Sitosterol on the structure of saturated Diacylphosphatidylcholine bilayers. Eur Biophys J EBJ 2011;40(2):153–63. https://doi.org/10.1007/s00249-010-0635-6.
[253] Knoll W, Schmidt G, Ibel K, Sackmann E. Small-angle neutron Scattering study of lateral phase separation in Dimyristoylphosphatidylcholine-cholesterol mixed membranes. Biochemistry 1985;24(19):5240–6. https://doi.org/10.1021/bi00340a043.
[254] Drolle E, Kučerka N, Hoopes MI, Choi Y, Katsaras J, Karttunen M, et al. Effect of melatonin and cholesterol on the structure of DOPC and DPPC membranes. Biochim Biophys Acta 2013;1828(9):2247–54. https://doi.org/10.1016/j.bbamem.2013.05.015.
[255] Krivanek R, Jeworrek C, Czeslik C, Winter R. Composition fluctuations in phospholipid-sterol vesicles – a small-angle neutron Scattering study. Z Für Phys Chem 2008;222(12):1679–92. https://doi.org/10.1524/zpch.2008.5433.
[256] Murugova T, Ivankov O, Ermakova E, Kondela T, Hrubovčák P, Skoi V, et al. Structural changes introduced by cholesterol and melatonin to the model membranes mimicking preclinical conformational diseases. Gen Physiol Biophys 2020;39(2):135–44. https://doi.org/10.4149/gpb_2019054.
[257] Kinnun JJ, Bolmatov D, Lavrentovich MO, Katsaras J. Lateral heterogeneity and domain formation in cellular membranes. Chem Phys Lipids 2020;232:104976. https://doi.org/10.1016/j.chemphyslip.2020.104976.
[258] Cebecauer M, Amaro M, Jurkiewicz P, Sarmento MJ, Šachl R, Cwiklik L, et al. Membrane Lipid Nanodomains. Chem Rev 2018;118(23):11259–97. https://doi.org/10.1021/acs.chemrev.8b00322.
[259] Lingwood D, Simons K. Lipid rafts as a membrane-organizing principle. Science 2010;327(5961):46–50. https://doi.org/10.1126/science.1174621.
[260] Kinnun JJ, Scott HL, Bolmatov D, Collier CP, Charlton TR, Katsaras J. Biophysical studies of lipid Nanodomains using different physical characterization techniques. Biophys J 2023;122(6):931–49. https://doi.org/10.1016/j.bpj.2023.01.024.
[261] Kinnun JJ, Scott HL, Ashkar R, Katsaras J. Biomembrane structure and material properties studied with neutron Scattering. Front Chem 2021;9:642851. https://doi.org/10.3389/fchem.2021.642851.
[262] Nickels JD, Smith JC, Cheng X. Lateral organization, bilayer asymmetry, and inter-leaflet coupling of biological membranes. Chem Phys Lipids 2015;192:87–99. https://doi.org/10.1016/j.chemphyslip.2015.07.012.
[263] Heberle FA, Petruzielo RS, Pan J, Drazba P, Kučerka N, Standaert RF, et al. Bilayer thickness mismatch controls domain size in model membranes. J Am Chem Soc 2013;135(18):6853–9. https://doi.org/10.1021/ja3113615.
[264] DiPasquale M, Deering TG, Desai D, Sharma AK, Amin S, Fox TE, et al. Influence of ceramide on lipid domain stability studied with small-angle neutron Scattering: the role of acyl chain length and unsaturation. Chem Phys Lipids 2022;245:105205. https://doi.org/10.1016/j.chemphyslip.2022.105205.
[265] Ahmadi D, Thompson KC, García Sakai V, Schweins R, Moulin M, Haertlein M, et al. Nanoscale structure and dynamics of model membrane lipid raft systems, studied by neutron scattering methods. Front Physiol 2022;10:864746. https://doi.org/10.3389/fphy.2022.864746.
[266] Heberle FA, Doktorova M, Goh SL, Standaert RF, Katsaras J, Feigenson GW. Hybrid and nonhybrid lipids exert common effects on membrane raft size and morphology. J Am Chem Soc 2013;135(40):14932–5. https://doi.org/10.1021/ja407624c.
[267] Krzyzanowski N, Porcar L, Perez-Salas U. A small-angle neutron Scattering, calorimetry and densitometry study to detect phase boundaries and nanoscale domain structure in a binary lipid mixture. Membranes 2023;13(3):323. https://doi.org/10.3390/membranes13030323.
[268] Nickels JD, Cheng X, Mostofian B, Stanley C, Lindner B, Heberle FA, et al. Mechanical properties of Nanoscopic lipid domains. J Am Chem Soc 2015;137(50):15772–80. https://doi.org/10.1021/jacs.5b08894.
[269] Frewein MPK, Piller P, Semeraro EF, Czakkel O, Gerelli Y, Porcar L, et al. Distributing Aminophospholipids asymmetrically across leaflets causes anomalous membrane stiffening. Biophys J 2023;122(12):2445–55. https://doi.org/10.1016/j.bpj.2023.04.025.
[270] Eicher B, Marquardt D, Heberle FA, Letofsky-Papst I, Rechberger GN, Appavou M-S, et al. Intrinsic curvature-mediated Transbilayer coupling in asymmetric lipid vesicles. Biophys J 2018;114(1):146–57. https://doi.org/10.1016/j.bpj.2017.11.009.
[271] Heberle FA, Marquardt D, Doktorova M, Geier B, Standaert RF, Heftberger P, et al. Subnanometer structure of an asymmetric model membrane: Interleaflet coupling influences domain properties. Langmuir 2016;32(20):5195–200. https://doi.org/10.1021/acs.langmuir.5b04562.
[272] Sarmento MJ, Hof M, Šachl R. Interleaflet coupling of lipid Nanodomains – insights from in vitro systems. Front Cell Dev Biol 2020;8:284. https://doi.org/10.3389/fcell.2020.00284.
[273] Nielsen JE, Koynarev VR, Lund R. Peptide meets membrane: investigating peptide-lipid interactions using small-angle Scattering techniques. Curr Opin

Colloid Interface Sci 2023;66:101709. https://doi.org/10.1016/j.cocis.2023.101709.
[274] Silva T, Claro B, Silva BFB, Vale N, Gomes P, Gomes MS, et al. Unravelling a mechanism of action for a Cecropin A-Melittin hybrid antimicrobial peptide: the induced formation of multilamellar lipid stacks. Langmuir 2018;34(5):2158–70. https://doi.org/10.1021/acs.langmuir.7b03639.
[275] Qian S, Heller WT. Peptide-induced asymmetric distribution of charged lipids in a vesicle bilayer revealed by small-angle neutron Scattering. J Phys Chem B 2011;115(32):9831–7. https://doi.org/10.1021/jp204045t.
[276] Pachler M, Kabelka I, Appavou M-S, Lohner K, Vácha R, Pabst G. Magainin 2 and PGLa in bacterial membrane mimics I: peptide-peptide and lipid-peptide interactions. Biophys J 2019;117(10):1858–69. https://doi.org/10.1016/j.bpj.2019.10.022.
[277] Rai DK, Sharma VK, Anunciado D, O'Neill H, Mamontov E, Urban V, et al. Neutron Scattering studies of the interplay of amyloid β peptide(1–40) and an anionic lipid 1,2-Dimyristoyl-Sn-Glycero-3-Phosphoglycerol. Sci Rep 2016;6(1):30983. https://doi.org/10.1038/srep30983.
[278] Martel A, Antony L, Gerelli Y, Porcar L, Fluitt A, Hoffmann K, et al. Membrane permeation versus Amyloidogenicity: a multitechnique study of islet amyloid polypeptide interaction with model membranes. J Am Chem Soc 2017;139(1):137–48. https://doi.org/10.1021/jacs.6b06985.
[279] Ivankov O, Murugova TN, Ermakova EV, Kondela T, Badreeva DR, Hrubovčák P, et al. Amyloid-Beta peptide (25–35) triggers a reorganization of lipid membranes driven by temperature changes. Sci Rep 2021;11(1):21990. https://doi.org/10.1038/s41598-021-01347-7.
[280] Pallbo J, Imai M, Gentile L, Takata S, Olsson U, Sparr E. NACore amyloid formation in the presence of phospholipids. Front Physiol 2020;11:592117.
[281] Ricci C, Maccarini M, Falus P, Librizzi F, Mangione MR, Moran O, et al. Amyloid β-peptide interaction with membranes: can chaperones change the fate? J Phys Chem B 2019;123(3):631–8. https://doi.org/10.1021/acs.jpcb.8b11719.
[282] Santamaria A, Batchu KC, Matsarskaia O, Prévost SF, Russo D, Natali F, et al. Strikingly different roles of SARS-CoV-2 fusion peptides uncovered by neutron Scattering. J Am Chem Soc 2022;144(7):2968–79. https://doi.org/10.1021/jacs.1c09856.
[283] Heller WT, Zolnierczuk PA. The Helix-to-sheet transition of an HIV-1 fusion peptide derivative changes the mechanical properties of lipid bilayer membranes. Biochim Biophys Acta BBA - Biomembr 2019;1861(3):565–72. https://doi.org/10.1016/j.bbamem.2018.12.004.
[284] Vant Hag L, De Campo L, Garvey CJ, Feast GC, Leung AE, Yepuri NR, et al. Using SANS with contrast-matched lipid Bicontinuous cubic phases to determine the location of encapsulated peptides, proteins, and other biomolecules. J Phys Chem Lett 2016;7(14):2862–6. https://doi.org/10.1021/acs.jpclett.6b01173.
[285] Spinozzi F, Alcaraz J-P, Ortore MG, Gayet L, Radulescu A, Martin DK, et al. Small-angle neutron Scattering reveals the nanostructure of liposomes with embedded OprF Porins of *Pseudomonas aeruginosa*. Langmuir 2022;38(49):15026–37. https://doi.org/10.1021/acs.langmuir.2c01342.
[286] Bharatiya B, Wang G, Rogers SE, Pedersen JS, Mann S, Briscoe WH. Mixed liposomes containing gram-positive Bacteria lipids: Lipoteichoic acid (LTA) induced structural changes. Colloids Surf B Biointerfaces 2021;199:111551. https://doi.org/10.1016/j.colsurfb.2020.111551.
[287] Diedrichsen RG, Vetri V, Prévost S, Foderà V, Nielsen HM. Carrier peptide interactions with liposome membranes induce reversible clustering by surface adsorption and shape deformation. J Colloid Interface Sci 2023;650:1821–32. https://doi.org/10.1016/j.jcis.2023.07.078.
[288] Conn CE, De Campo L, Whitten AE, Garvey CJ, Krause-Heuer AM, Van 't Hag, L.. Membrane protein structures in lipid bilayers; small-angle neutron Scattering with contrast-matched Bicontinuous cubic phases. Front Chem 2021;8:619470. https://doi.org/10.3389/fchem.2020.619470.
[289] Yepuri NR, Clulow AJ, Prentice RN, Gilbert EP, Hawley A, Rizwan SB, et al. Deuterated Phytantriol – a versatile compound for probing material distribution in liquid crystalline lipid phases using neutron Scattering. J Colloid Interface Sci 2019;534:399–407. https://doi.org/10.1016/j.jcis.2018.09.022.
[290] Rubinson KA, Pokalsky C, Krueger S, Prochaska LJ. Structure determination of functional membrane proteins using small-angle neutron Scattering (SANS) with small, mixed-lipid liposomes: native beef heart mitochondrial cytochrome c oxidase forms dimers. Protein J 2013;32(1):27–38. https://doi.org/10.1007/s10930-012-9455-0.
[291] Doktorova M, Heberle FA, Kingston RL, Khelashvili G, Cuendet MA, Wen Y, et al. Cholesterol promotes protein binding by affecting membrane electrostatics and solvation properties. Biophys J 2017;113(9):2004–15. https://doi.org/10.1016/j.bpj.2017.08.055.
[292] Satsoura D, Kučerka N, Shivakumar S, Pencer J, Griffiths C, Leber B, et al. Interaction of the full-length Bax protein with biomimetic mitochondrial liposomes: a small-angle neutron Scattering and fluorescence study. Biochim Biophys Acta BBA - Biomembr 2012;1818(3):384–401. https://doi.org/10.1016/j.bbamem.2011.10.007.
[293] Holme MN, Rashid MH, Thomas MR, Barriga HMG, Herpoldt K, Heenan RK, et al. Fate of liposomes in the presence of phospholipase C and D: from atomic to supramolecular lipid arrangement. ACS Cent Sci 2018;4(8):1023–30. https://doi.org/10.1021/acscentsci.8b00286.
[294] Kumari A, Saha D, Bhattacharya J, Aswal VK, Moulick RG. Studying the structural Organization of non-Membranous Protein Hemoglobin in a lipid environment after reconstitution. Int J Biol Macromol 2023;243:125212. https://doi.org/10.1016/j.ijbiomac.2023.125212.
[295] DiPasquale M, Nguyen MHL, Rickeard BW, Cesca N, Tannous C, Castillo SR, et al. The antioxidant vitamin E as a membrane raft modulator: tocopherols Do not abolish lipid domains. Biochim Biophys Acta BBA - Biomembr 2020;1862(8):183189. https://doi.org/10.1016/j.bbamem.2020.183189.
[296] Bolmatov D, McClintic WT, Taylor G, Stanley CB, Do C, Collier CP, et al. Deciphering melatonin-stabilized phase separation in phospholipid bilayers. Langmuir 2019;35(37):12236–45. https://doi.org/10.1021/acs.langmuir.9b01534.
[297] Mayeux G, Gayet L, Liguori L, Odier M, Martin DK, Cortès S, et al. Cell-free expression of the outer membrane protein OprF of *Pseudomonas aeruginosa* for vaccine purposes. Life Sci Alliance 2021;4(6):e202000958. https://doi.org/10.26508/lsa.202000958.
[298] Boggara MB, Krishnamoorti R. Small-angle neutron scattering studies of phospholipid−NSAID adducts. Langmuir 2010;26(8):5734–45. https://doi.org/10.1021/la903854s.
[299] De Mel JU, Gupta S, Harmon S, Stingaciu L, Roth EW, Siebenbuerger M, et al. Acetaminophen interactions with phospholipid vesicles induced changes in morphology and lipid dynamics. Langmuir 2021;37(31):9560–70. https://doi.org/10.1021/acs.langmuir.1c01458.
[300] Sreij R, Prévost S, Dargel C, Dattani R, Hertle Y, Wrede O, et al. Interaction of the Saponin Aescin with ibuprofen in DMPC model membranes. Mol Pharm 2018;15(10):4446–61. https://doi.org/10.1021/acs.molpharmaceut.8b00421.
[301] Vitiello G, Luchini A, D'Errico G, Santamaria R, Capuozzo A, Irace C, et al. Cationic liposomes as efficient Nanocarriers for the drug delivery of an anticancer cholesterol-based ruthenium complex. J Mater Chem B 2015;3(15):3011–23. https://doi.org/10.1039/C4TB01807A.
[302] Truzzi E, Capocefalo A, Meneghetti F, Maretti E, Mori M, Iannuccelli V, et al. Design and physicochemical characterization of novel hybrid SLN-liposome nanocarriers for the smart co-delivery of two Antitubercular drugs. J Drug Deliv Sci Technol 2022;70:103206. https://doi.org/10.1016/j.jddst.2022.103206.
[303] Truzzi E, Meneghetti F, Mori M, Costantino L, Iannuccelli V, Maretti E, et al. Drugs/lamellae Interface influences the inner structure of double-loaded liposomes for inhaled anti-TB therapy: an in-depth small-angle neutron scattering investigation. J Colloid Interface Sci 2019;541:399–406. https://doi.org/10.1016/j.jcis.2019.01.094.
[304] Forooqi Motlaq V, Gedda L, Edwards K, Doutch J, Bergström LM. Spontaneous formation of Ultrasmall Unilamellar vesicles in mixtures of an amphiphilic drug and a phospholipid. Langmuir 2023;39(32):11337–44. https://doi.org/10.1021/acs.langmuir.3c01023.
[305] Li Z, Carter J, Santos L, Webster C, Van Der Walle CF, Li P, et al. Acidification-induced structure evolution of lipid nanoparticles correlates with their *in vitro* gene transfections. ACS Nano 2023;17(2):979–90. https://doi.org/10.1021/acsnano.2c06213.
[306] Jaudoin C, Grillo I, Cousin F, Gehrke M, Ouldali M, Arteni A-A, et al. Hybrid systems combining liposomes and entangled hyaluronic acid chains: influence of liposome surface and drug encapsulation on the microstructure. J Colloid Interface Sci 2022;628:995–1007. https://doi.org/10.1016/j.jcis.2022.07.146.
[307] Salvati Manni L, Davies C, Wood K, Assenza S, Atkin R, Warr GG. Unusual phosphatidylcholine lipid phase behavior in the ionic liquid Ethylammonium nitrate. J Colloid Interface Sci 2023;643:276–81. https://doi.org/10.1016/j.jcis.2023.03.161.
[308] Yanez Arteta M, Kjellman T, Bartesaghi S, Wallin S, Wu X, Kvist AJ, et al. Successful reprogramming of cellular protein production through mRNA delivered by functionalized lipid nanoparticles. Proc Natl Acad Sci 2018;115(15). https://doi.org/10.1073/pnas.1720542115.
[309] Dao TPT, Fernandes F, Er-Rafik M, Salva R, Schmutz M, Brûlet A, et al. Phase separation and Nanodomain formation in hybrid polymer/lipid vesicles. ACS Macro Lett 2015;4(2):182–6. https://doi.org/10.1021/mz500748f.
[310] Xiao Y, Liu Q, Clulow AJ, Li T, Manohar M, Gilbert EP, et al. PEGylation and surface functionalization of liposomes containing drug nanocrystals for cell-targeted delivery. Colloids Surf B Biointerfaces 2019;182:110362. https://doi.org/10.1016/j.colsurfb.2019.110362.
[311] Moiseev RV, Kaldybekov DB, Filippov SK, Radulescu A, Khutoryanskiy VV. Maleimide-decorated PEGylated Mucoadhesive liposomes for ocular drug delivery. Langmuir 2022;38(45):13870–9. https://doi.org/10.1021/acs.langmuir.2c02086.
[312] Nele V, Holme MN, Kauscher U, Thomas MR, Doutch JJ, Stevens MM. Effect of formulation method, lipid composition, and PEGylation on vesicle Lamellarity: a small-angle neutron Scattering study. Langmuir 2019;35(18):6064–74. https://doi.org/10.1021/acs.langmuir.8b04256.
[313] Mkam Tsengam IK, Omarova M, Kelley EG, McCormick A, Bothun GD, Raghavan SR, et al. Transformation of lipid vesicles into micelles by adding nonionic surfactants: elucidating the structural pathway and the intermediate structures. J Phys Chem B 2022;126(11):2208–16. https://doi.org/10.1021/acs.jpcb.1c09685.
[314] Matviykiv S, Deyhle H, Kohlbrecher J, Neuhaus F, Zumbuehl A, Müller B. Small-angle neutron scattering study of temperature-induced structural changes in liposomes. Langmuir 2019;35(34):11210–6. https://doi.org/10.1021/acs.langmuir.9b01603.
[315] Yuan Z, Das S, Do C, Park YC. Effect of cholesterol on nano-structural alteration of light-activatable liposomes via laser irradiation: small angle neutron scattering study. Colloids Surf A Physicochem Eng Asp 2022;641:128548. https://doi.org/10.1016/j.colsurfa.2022.128548.
[316] Barriga HMG, Pence IJ, Holme MN, Doutch JJ, Penders J, Nele V, et al. Coupling lipid nanoparticle structure and automated single-particle composition analysis to design phospholipase-responsive nanocarriers. Adv Mater 2022;34(26):2200839. https://doi.org/10.1002/adma.202200839.

[317] Liu Y, Kelley EG, Batchu KC, Porcar L, Perez-Salas U. Creating asymmetric phospholipid vesicles via exchange with lipid-coated silica nanoparticles. Langmuir 2020;36(30):8865–73. https://doi.org/10.1021/acs.langmuir.0c01188.
[318] Miao S, Hoffmann I, Gradzielski M, Warr GG. Lipid membrane flexibility in protic ionic liquids. J Phys Chem Lett 2022;13(23):5240–5. https://doi.org/10.1021/acs.jpclett.2c00980.
[319] Bryant SJ, Wood K, Atkin R, Warr GG. Effect of Protic ionic liquid nanostructure on phospholipid vesicle formation. Soft Matter 2017;13(7):1364–70. https://doi.org/10.1039/C6SM02652D.
[320] Mitra S, Ray D, Bhattacharya G, Gupta R, Sen D, Aswal VK, et al. Probing the effect of a room temperature ionic liquid on phospholipid membranes in multilamellar vesicles. Eur Biophys J 2019;48(2):119–29. https://doi.org/10.1007/s00249-018-1339-6.
[321] Kumari P, Faraone A, Kelley EG, Benedetto A. Stiffening effect of the [Bmim][Cl] ionic liquid on the bending dynamics of DMPC lipid vesicles. J Phys Chem B 2021;125(26):7241–50. https://doi.org/10.1021/acs.jpcb.1c01347.
[322] Hempt C, Gontsarik M, Buerki-Thurnherr T, Hirsch C, Salentinig S. Nanostructure generation during milk digestion in presence of a cell culture model simulating the small intestine. J Colloid Interface Sci 2020;574:430–40. https://doi.org/10.1016/j.jcis.2020.04.059.
[323] Yaghmur A, Rappolt M, Jonassen ALU, Schmitt M, Larsen SW. In situ monitoring of the formation of Lipidic non-lamellar liquid crystalline depot formulations in synovial fluid. J Colloid Interface Sci 2021;582:773–81. https://doi.org/10.1016/j.jcis.2020.08.084.
[324] He V, Cadarso VJ, Seibt S, Boyd BJ, Neild A. A novel droplet-based approach to study phase transformations in Lyotropic liquid crystalline systems. J Colloid Interface Sci 2023;641:459–69. https://doi.org/10.1016/j.jcis.2023.03.011.
[325] Ghazal A, Gontsarik M, Kutter JP, Lafleur JP, Labrador A, Mortensen K, et al. Direct monitoring of calcium-triggered phase transitions in Cubosomes using small-angle X-Ray Scattering combined with microfluidics. J Appl Cryst 2016;49(6):2005–14. https://doi.org/10.1107/S1600576716014199.
[326] Sun X, Alcaraz N, Qiao R, Hawley A, Tan A, Boyd BJ. Magnetically-stimulated transformations in nanostructure of lipid Mesophases: effect of structure of Iron oxide nanoparticles. Colloids Surf B Biointerfaces 2020;191:110965. https://doi.org/10.1016/j.colsurfb.2020.110965.
[327] Khan NF, Salim M, Binte Abu Bakar SY, Ristroph K, Prud'homme RK, Hawley A, et al. Small-volume in vitro lipid digestion measurements for assessing drug dissolution in lipid-based formulations using SAXS. Int J Pharm X 2022;4:100113. https://doi.org/10.1016/j.ijpx.2022.100113.
[328] Hong L, Sesen M, Hawley A, Neild A, Spicer PT, Boyd BJ. Comparison of bulk and microfluidic methods to monitor the phase behaviour of nanoparticles during digestion of lipid-based drug formulations using *in situ* X-Ray scattering. Soft Matter 2019;15(46):9565–78. https://doi.org/10.1039/C9SM01440C.
[329] Bjørnestad VA, Soto-Bustamante F, Tria G, Laurati M, Lund R. Beyond the standard model of solubilization: non-ionic surfactants induce collapse of lipid vesicles into rippled Bilamellar Nanodiscs. J Colloid Interface Sci 2023;641:553–67. https://doi.org/10.1016/j.jcis.2023.03.037.
[330] Fong W-K, Sánchez-Ferrer A, Rappolt M, Boyd BJ, Mezzenga R. Structural transformation in vesicles upon hydrolysis of phosphatidylethanolamine and phosphatidylcholine with phospholipase C. Langmuir 2019;35(46):14949–58. https://doi.org/10.1021/acs.langmuir.9b02288.
[331] Angelov B, Angelova A, Filippov SK, Drechsler M, Štěpánek P, Lesieur S. Multicompartment lipid cubic nanoparticles with high protein upload: millisecond dynamics of formation. ACS Nano 2014;8(5):5216–26. https://doi.org/10.1021/nn5012946.
[332] Thorn CR, Clulow AJ, Boyd BJ, Prestidge CA, Thomas N. Bacterial lipase triggers the release of antibiotics from digestible liquid crystal nanoparticles. J Control Release 2020;319:168–82. https://doi.org/10.1016/j.jconrel.2019.12.037.
[333] Mertz N, Bock F, Østergaard J, Yaghmur A, Weng Larsen S. Investigation of diclofenac release and dynamic structural behavior of non-lamellar liquid crystal formulations during in situ formation by UV–vis imaging and SAXS. Int J Pharm 2022;623:121880. https://doi.org/10.1016/j.ijpharm.2022.121880.
[334] Nielsen JE, Bjørnestad VA, Pipich V, Jenssen H, Lund R. Beyond structural models for the mode of action: how natural antimicrobial peptides affect lipid transport. J Colloid Interface Sci 2021;582:793–802. https://doi.org/10.1016/j.jcis.2020.08.094.
[335] Nakano M, Fukuda M, Kudo T, Endo H, Handa T. Determination of Interbilayer and Transbilayer lipid transfers by time-resolved small-angle neutron scattering. Phys Rev Lett 2007;98(23):238101. https://doi.org/10.1103/PhysRevLett.98.238101.
[336] Nielsen JE, Lund R. Molecular transport and growth of lipid vesicles exposed to antimicrobial peptides. Langmuir 2022;38(1):374–84. https://doi.org/10.1021/acs.langmuir.1c02736.
[337] Nakano M, Fukuda M, Kudo T, Matsuzaki N, Azuma T, Sekine K, et al. Flip-flop of phospholipids in vesicles: kinetic analysis with time-resolved small-angle neutron scattering. J Phys Chem B 2009;113(19):6745–8. https://doi.org/10.1021/jp900913w.
[338] Nguyen MHL, DiPasquale M, Rickeard BW, Stanley CB, Kelley EG, Marquardt D. Methanol accelerates DMPC Flip-flop and transfer: a SANS study on lipid dynamics. Biophys J 2019;116(5):755–9. https://doi.org/10.1016/j.bpj.2019.01.021.
[339] Garg S, Porcar L, Woodka AC, Butler PD, Perez-Salas U. Noninvasive neutron scattering measurements reveal slower cholesterol transport in model lipid membranes. Biophys J 2011;101(2):370–7. https://doi.org/10.1016/j.bpj.2011.06.014.
[340] Breidigan JM, Krzyzanowski N, Liu Y, Porcar L, Perez-Salas U. Influence of the membrane environment on cholesterol transfer [S]. J Lipid Res 2017;58(12):2255–63. https://doi.org/10.1194/jlr.M077909.
[341] Nguyen MHL, DiPasquale M, Rickeard BW, Doktorova M, Heberle FA, Scott HL, et al. Peptide-induced lipid flip-flop in asymmetric liposomes measured by small angle neutron scattering. Langmuir 2019;35(36):11735–44. https://doi.org/10.1021/acs.langmuir.9b01625.
[342] Nguyen MHL, DiPasquale M, Rickeard BW, Yip CG, Greco KN, Kelley EG, et al. Time-resolved SANS reveals pore-forming peptides cause rapid lipid reorganization. New J Chem 2021;45(1):447–56. https://doi.org/10.1039/D0NJ04717A.
[343] Nielsen JE, Prévost SF, Jenssen H, Lund R. Impact of antimicrobial peptides on *E. coli* -mimicking lipid model membranes: correlating structural and dynamic effects using scattering methods. Faraday Discuss 2021;232:203–17. https://doi.org/10.1039/D0FD00046A.
[344] Marx L, Frewein MPK, Semeraro EF, Rechberger GN, Lohner K, Porcar L, et al. Antimicrobial peptide activity in asymmetric bacterial membrane mimics. Faraday Discuss 2021;232(0):435–47. https://doi.org/10.1039/D1FD00039J.
[345] Maric S, Lind TK, Raida MR, Bengtsson E, Fredrikson GN, Rogers S, et al. Time-resolved small-angle neutron Scattering as a probe for the dynamics of lipid exchange between human lipoproteins and naturally derived membranes. Sci Rep 2019;9(1):7591. https://doi.org/10.1038/s41598-019-43713-6.
[346] Urban VS, Heller WT, Katsaras J, Bras W. Soft matter sample environments for time-resolved small angle neutron Scattering experiments: a review. Appl Sci 2021;11(12):5566. https://doi.org/10.3390/app11125566.
[347] Balacescu L, Brandl G, Kaneko F, Schrader TE, Radulescu A. Light Scattering and absorption complementarities to neutron Scattering: in situ FTIR and DLS techniques at the high-intensity and extended Q-range SANS diffractometer KWS-2. Appl Sci 2021;11(11):5135. https://doi.org/10.3390/app11115135.
[348] Bras W, Ryan AJ. Sample environments and techniques combined with small angle X-Ray Scattering. Adv Colloid Interface Sci 1998;75(1):1–43. https://doi.org/10.1016/S0001-8686(97)00032-8.
[349] Bras W, Ryan AJ. Small-angle X-Ray Scattering and wide-angle X-Ray Scattering experiments combined with thermal and spectroscopic analysis techniques. J Mol Struct 1996;383(1–3):309–14. https://doi.org/10.1016/S0022-2860(96)09303-9.
[350] Bras W, Derbyshire GE, Devine A, Clark SM, Cooke J, Komanschek BE, et al. The combination of thermal analysis and time-resolved X-Ray techniques: a powerful method for materials characterization. J Appl Cryst 1995;28(1):26–32. https://doi.org/10.1107/S0021889894008320.
[351] Bunjes H, Unruh T. Characterization of lipid nanoparticles by differential scanning calorimetry, X-Ray and Neutron Scattering. Adv Drug Deliv Rev 2007;59(6):379–402. https://doi.org/10.1016/j.addr.2007.04.013.
[352] Mathew E, Mirza A, Menhart N. Liquid-chromatography-coupled SAXS for accurate sizing of aggregating proteins. J Synchrotron Radiat 2004;11(4):314–8. https://doi.org/10.1107/S0909049504014086.
[353] Graewert MA, Franke D, Jeffries CM, Blanchet CE, Ruskule D, Kuhle K, et al. Automated pipeline for purification, biophysical and X-Ray analysis of biomacromolecular solutions. Sci Rep 2015;5(1):10734. https://doi.org/10.1038/srep10734.
[354] Bryant GK, Gleeson HF, Ryan AJ, Fairclough JPA, Bogg D, Goossens JGP, et al. Raman spectroscopy combined with small angle X-Ray Scattering and wide angle x-Ray Scattering as a tool for the study of phase transitions in polymers. Rev Sci Instrum 1998;69(5):2114–7. https://doi.org/10.1063/1.1148907.
[355] Hirose R, Yoshioka T, Yamamoto H, Reddy KR, Tahara D, Hamada K, et al. In-house simultaneous collection of small-angle X-Ray Scattering, wide-angle X-Ray diffraction and Raman Scattering data from polymeric materials. J Appl Cryst 2014;47(3):922–30. https://doi.org/10.1107/S1600576714006724.
[356] Chen X, Schröder J, Hauschild S, Rosenfeldt S, Dulle M, Förster S. Simultaneous SAXS/WAXS/UV–vis study of the nucleation and growth of nanoparticles: a test of classical nucleation theory. Langmuir 2015;31(42):11678–91. https://doi.org/10.1021/acs.langmuir.5b02759.
[357] Bras W, Derbyshire GE, Bogg D, Cooke J, Elwell MJ, Komanschek BU, et al. Simultaneous Studies of Reaction Kinetics and Structure Development in Polymer Processing. Science 1995;267(5200):996–9.
[358] Tashiro K, Yamamoto H. Structural evolution mechanism of crystalline polymers in the isothermal melt-crystallization process: a proposition based on simultaneous WAXD/SAXS/FTIR measurements. Polymers 2019;11(8):1316. https://doi.org/10.3390/polym11081316.
[359] Liu Y, Tian F, Zhou P, Zhu H, Zhong J, Chen M, et al. A novel in situ sample environment setup for combined small angle X-Ray Scattering (SAXS), wide-angle x-Ray Scattering (WAXS), and Fourier transform infrared spectrometer (FTIR) simultaneous measurement. Rev Sci Instrum 2023;94(3):033103. https://doi.org/10.1063/5.0128211.
[360] Falke S, Dierks K, Blanchet C, Graewert M, Cipriani F, Meijers R, et al. Multi-Channel in situ dynamic light Scattering instrumentation enhancing biological small-angle X-Ray Scattering experiments at the PETRA III beamline P12. J Synchrotron Radiat 2018;25(2):361–72. https://doi.org/10.1107/S1600577517017568.
[361] Narayanan T, Dattani R, Möller J, Kwaśniewski P. A microvolume shear cell for combined rheology and X-Ray Scattering experiments. Rev Sci Instrum 2020;91(8):085102. https://doi.org/10.1063/5.0012905.
[362] Mortensen K. Structural studies of lamellar surfactant systems under shear. Curr Opin Colloid Interface Sci 2001;6(2):140–5. https://doi.org/10.1016/S1359-0294(01)00071-1.

[363] Ito M, Kosaka Y, Kawabata Y, Kato T. Transition processes from the lamellar to the onion state with increasing temperature under shear flow in a nonionic surfactant/water system studied by Rheo-SAXS. Langmuir 2011;27(12):7400–9. https://doi.org/10.1021/la104826s.
[364] Panine P, Narayanan T, Vermant J, Mewis J. Structure and rheology during shear-induced crystallization of a latex suspension. Phys Rev E 2002;66(2):022401. https://doi.org/10.1103/PhysRevE.66.022401.
[365] Camerel F, Gabriel JCP, Batail P, Panine P, Davidson P. Combined SAXS−rheological studies of liquid-crystalline colloidal dispersions of mineral particles. Langmuir 2003;19(24):10028–35. https://doi.org/10.1021/la034626p.
[366] Di Cola E, Fleury C, Panine P, Cloitre M. Steady shear flow alignment and rheology of lamellae-forming ABC triblock copolymer solutions: orientation, defects, and disorder. Macromolecules 2008;41(10):3627–35. https://doi.org/10.1021/ma702876k.
[367] Jordan A, Jacques M, Merrick C, Devos J, Forsyth VT, Porcar L, et al. SEC-SANS: size exclusion chromatography combined in situ with small-angle neutron Scattering. J Appl Cryst 2016;49(6):2015–20. https://doi.org/10.1107/S1600576716016514.
[368] Johansen NT, Pedersen MC, Porcar L, Martel A, Arleth L. Introducing SEC–SANS for studies of complex self-organized biological systems. Acta Crystallogr Sect Struct Biol 2018;74(12):1178–91. https://doi.org/10.1107/S2059798318007180.
[369] Kaneko F, Seto N, Sato S, Radulescu A, Schiavone MM, Allgaier J, Ute K. Development of a simultaneous SANS/FTIR measuring system. Chemistry letters 2015;44(4):497–9.
[370] Kaneko F, Kawaguchi T, Radulescu A, Iwase H, Morikawa T, Takata S, et al. A new simultaneous measurement system of wide Q-range small angle neutron Scattering combined with polarized Fourier transform infrared spectroscopy. Rev Sci Instrum 2019;90(9):093906. https://doi.org/10.1063/1.5112054.
[371] López-Barrón CR, Zeng Y, Schaefer JJ, Eberle APR, Lodge TP, Bates FS. Molecular alignment in polyethylene during cold drawing using in-situ SANS and Raman spectroscopy. Macromolecules 2017;50(9):3627–36. https://doi.org/10.1021/acs.macromol.7b00504.
[372] Pullen SA, Booth N, Olsen SR, Day B, Franceschini F, Mannicke D, et al. Design and implementation of a differential scanning calorimeter for the simultaneous measurement of small angle neutron Scattering. Meas Sci Technol 2014;25(5):055606. https://doi.org/10.1088/0957-0233/25/5/055606.
[373] Heigl RJ, Longo M, Stellbrink J, Radulescu A, Schweins R, Schrader TE. Crossover from a Linear to a Branched Growth Regime in the Crystallization of Lysozyme. Crystal growth & design 2018;18(3):1483–94.
[374] Nigro V, Angelini R, King S, Franco S, Buratti E, Bomboi F, et al. Apparatus for simultaneous dynamic light scattering–small angle neutron scattering investigations of dynamics and structure in soft matter. Rev Sci Instrum 2021;92(2):023907. https://doi.org/10.1063/5.0035529.
[375] Kohlbrecher J, Bollhalder A, Vavrin R, Meier G. A high pressure cell for small angle neutron Scattering up to 500MPa in combination with light Scattering to investigate liquid samples. Rev Sci Instrum 2007;78(12):125101. https://doi.org/10.1063/1.2817632.
[376] Nawroth T, Buch P, Buch K, Langguth P, Schweins R. Liposome formation from bile salt–lipid micelles in the digestion and drug delivery model fassifmod estimated by combined time-resolved neutron and dynamic light scattering. Mol Pharm 2011;8(6):2162–72. https://doi.org/10.1021/mp100296w.
[377] Eberle APR, Porcar L. Flow-SANS and Rheo-SANS applied to soft matter. Curr Opin Colloid Interface Sci 2012;17(1):33–43. https://doi.org/10.1016/j.cocis.2011.12.001.
[378] Narayanan T, Wacklin H, Konovalov O, Lund R. Recent applications of synchrotron radiation and neutrons in the study of soft matter. Crystallogr Rev 2017;23(3):160–226. https://doi.org/10.1080/0889311X.2016.1277212.
[379] Penfold J, Staples E, Lodhi AK, Tucker I, Tiddy GJT. Shear-induced transformations in the lamellar phase of Hexaethylene glycol Monohexadecyl ether. J Phys Chem B 1997;101(1):66–72. https://doi.org/10.1021/jp9622851.
[380] Zipfel J, Berghausen J, Lindner P, Richtering W. Influence of shear on Lyotropic lamellar phases with different membrane defects. J Phys Chem B 1999;103(15):2841–9. https://doi.org/10.1021/jp983917h.
[381] Diat O, Roux D, Nallet F. Effect of shear on a Lyotropic lamellar phase. J Phys II 1993;3(9):1427–52. https://doi.org/10.1051/jp2:1993211.
[382] Gentile L, Behrens MA, Porcar L, Butler P, Wagner NJ, Olsson U. Multilamellar vesicle formation from a planar lamellar phase under shear flow. Langmuir 2014;30(28):8316–25. https://doi.org/10.1021/la501071s.
[383] Gentile L, Silva BFB, Lages S, Mortensen K, Kohlbrecher J, Olsson U. Rheochaos and flow instability phenomena in a nonionic lamellar phase. Soft Matter 2012;9(4):1133–40. https://doi.org/10.1039/C2SM27101J.
[384] Heptner N, Chu F, Lu Y, Lindner P, Ballauff M, Dzubiella J. Nonequilibrium structure of colloidal dumbbells under oscillatory shear. Phys Rev E 2015;92(5):052311. https://doi.org/10.1103/PhysRevE.92.052311.
[385] Murphy RP, Riedel ZW, Nakatani MA, Salipante PF, Weston JS, Hudson SD, et al. Capillary RheoSANS: measuring the rheology and nanostructure of complex fluids at high shear rates. Soft Matter 2020;16(27):6285–93. https://doi.org/10.1039/D0SM00941E.
[386] Zákutná D, Graef K, Dresen D, Porcar L, Honecker D, Disch S. In situ magnetorheological SANS setup at Institut Laue-Langevin. Colloid Polym Sci 2021;299(2):281–8. https://doi.org/10.1007/s00396-020-04713-5.
[387] Metwalli E, Götz K, Lages S, Bär C, Zech T, Noll DM, et al. A novel experimental approach for nanostructure analysis: simultaneous small-angle X-Ray and Neutron Scattering. J Appl Cryst 2020;53(3):722–33. https://doi.org/10.1107/S1600576720005208.
[388] Metwalli E, Götz K, Zech T, Bär C, Schuldes I, Martel A, et al. Simultaneous SAXS/SANS method at D22 of ILL: instrument upgrade. Appl Sci 2021;11(13):5925. https://doi.org/10.3390/app11135925.